Rubén A. García Ruiz

Estudio de la distribución de temperatura de aire en un invernadero tipo en Almería ("raspa y amagado")

TESIS DOCTORAL

FEB
2020

UNIVERSIDAD
DE ALMERÍA

DEPARTAMENTO DE INGENIERÍA

TESIS DOCTORAL

Estudio de la distribución de temperatura de aire en un invernadero tipo en Almería ("raspa y amagado")

Rubén A. García Ruiz

Doctorado en Tecnología de Invernaderos e
Ingeniería Industrial y Ambiental

Dirigida por:
Prof, Dr. Javier López Martínez
Prof, Dr. José Luis Blanco Claraco

Almería, Febrero de 2020

UNIVERSIDAD
DE ALMERÍA

UNIVERSIDAD DE ALMERÍA
DEPARTAMENTO DE INGENIERÍA

TESIS DOCTORAL

Estudio de la distribución de temperatura de aire en un invernadero tipo en Almería ("raspa y amagado")

AUTOR: Rubén A. García Ruiz

Tesis Doctoral presentada dentro del Programa de Doctorado en Tecnología de Invernaderos e Ingeniería Industrial y Ambiental (RD 99/11), en la línea de investigación de Agricultura de Precisión, Agroingeniería, Energías Renovables, Fotogrametría, SIG, Teledetección.

DIRECTORES:
Prof. Dr. Javier López Martínez
Prof. Dr. José Luis Blanco Claraco

Almería, Febrero de 2020

Dedicado a mi familia y a mi novia.

Índice general

Resumen **VII**

Abstract **IX**

1. Introducción **1**
1.1. Antecedentes 1
1.2. Justificación 2
1.3. Hipótesis 2
1.4. Objetivos 3

2. Publicaciones científicas **5**
2.1. Publicación científica 1 6
2.2. Publicación científica 2 19
2.3. Publicación científica 3 30

3. Resumen de las publicaciones científicas **49**
3.1. Publicación científica 1 49
3.2. Publicación científica 2 53
3.3. Publicación científica 3 60

4. Conclusiones generales **69**
4.1. Publicación científica 1: On air temperature distribution and ISO 7726-defined heterogeneity inside a typical greenhouse in Almería 69
4.2. Publicación científica 2: Uncertainty-Aware Calibration of a Hot-Wire Anemometer With Gaussian Process Regression . . 70
4.3. Publicación científica 3: Ultraviolet Index (UVI) inside an Almería-Type Greenhouse (Southeastern Spain) 71

Abreviaturas **73**

Bibliografía **75**

Resumen

La Tesis Doctoral nace con el objetivo de estudiar el ambiente térmico en el interior de invernaderos y especialmente la influencia que tiene sobre el trabajador, ya que la mayoría de estudios similares en invernaderos están centrados en el cultivo. En este trabajo se estudian las condiciones de temperatura de aire con respecto a los trabajadores, específicamente se analiza la heterogeneidad de temperatura de aire en el interior de un invernadero siguiendo los métodos recogidos en la norma ISO 7726. Para ello, se utiliza una red de sensores inalámbrica y se lleva a cabo una campaña experimental de un año de duración en un invernadero típico en Almería. Los resultados permiten caracterizar la distribución de temperatura de aire en el interior de un invernadero y confirma la existencia de heterogeneidad en la temperatura de aire conforme a la norma ISO 7726, así como identificar patrones en su distribución.

Derivado de este estudio, se encontraron dificultades en medir con precisión y bajo coste la velocidad del viento en el interior de un invernadero, lo que lleva a realizar una calibración de un anemómetro de bajo coste. La calibración se centra en un anemómetro de hilo caliente, en el que se intenta solventar su principal inconveniente, que es la perdida de precisión causada por los cambios en la temperatura de aire o temperatura ambiente. Dicha calibración se realiza por medio de un Proceso de Regresión Gaussiana y se valida con datos reales, alcanzándose el objetivo de conseguir un dispositivo de bajo coste y capaz de realizar medidas con precisión de velocidad de aire en un rango típico de temperatura de aire.

Finalmente, y también como consecuencia del estudio del ambiente térmico, se observó que los trabajadores de invernadero, a pesar de la cubierta plástica que cubre dichos invernaderos, pueden ser susceptibles de riesgos asociados a la radiación ultravioleta en piel y ojos. Por ello, mediante una red de sensores, se realiza una campaña de medida de la radiación ultravioleta durante un año de duración en el interior de un invernadero típico en Almería. Los resultados indican que se supera el límite de riesgo establecido por la Organización Mundial de la Salud, por lo que se confirma que exis-

te riesgo sobre la salud de los trabajadores de invernaderos por radiación ultravioleta.

PALABRAS CLAVE: invernadero, seguridad y salud, ambiente térmico, distribución de temperatura de aire, calibración de sensor, riesgo UV.

Abstract

This Doctoral Thesis was born with the aim of studying the thermal environment inside greenhouses and especially the influence it has on the worker, since most similar studies in greenhouses are focused on the crop. In this work the air temperature conditions with respect to the workers are studied, specifically the heterogeneity of air temperature inside a greenhouse is analysed following the methods gathered in ISO 7726. To achieve this goal, a network of wireless sensors and a year-long experimental campaign is carried out in a typical greenhouse in Almería. The results allow the characterization of the air temperature distribution inside a greenhouse and confirms the existence of heterogeneity in air temperature according to the norm ISO 7726, as well identifying patterns in its distribution.

Derived from this study, difficulties were found in accurately measuring and with low cost the wind speed inside a greenhouse, which leads to a calibration of a low cost anemometer. The calibration focuses on a hot-wire anemometer, which attempts to solve its main drawback, namely its loss of accuracy when air temperature or ambient temperature changes. This calibration is carried out by means of a Gaussian Regression Process and is validated with real data, reaching the goal of achieving a low-cost device capable of accurately measuring air velocity in a typical air temperature range.

Finally, and also as a consequence of the study of the thermal environment, it was observed that greenhouse workers, despite the plastic cover covering such greenhouses, may be susceptible to risks associated to ultraviolet radiation on skin and eyes. For this reason, through a network of sensors, a measurement campaign of ultraviolet radiation is carried out for a year inside a typical greenhouse in Almería. The results indicate that the risk limit established by the World Health Organization is exceeded, so it is confirmed that there exist risk to the health of greenhouse workers by ultraviolet radiation.

KEYWORDS: greenhouse, occupational safety and health, thermal environment, air temperature distribution, sensor calibration, UV risk.

Capítulo 1

Introducción

1.1. Antecedentes

En los últimos tiempos, el mercado demanda alimentos saludables y obtenidos respetando al medio ambiente, de forma que satisfaga las necesidades de las generaciones presentes y futuras, garantizando al mismo tiempo la rentabilidad y el uso responsable y eficiente de los recursos. La agricultura biológica o sostenible, por tanto, no está referida sólo a los alimentos sino también a la forma de obtenerlos [1]. Por lo que, para obtener producciones agrícolas sostenibles, es tan necesaria la protección de la seguridad y salud de los trabajadores como la obtención de recursos y la mejora de los parámetros ambientales que intervienen en la forma de obtención de estos productos.

En el sur de Europa y especialmente en zonas costeras mediterráneas se cumplen los requisitos medioambientales óptimos para el cultivo de vegetales en invernaderos [2]. En Almería, los invernaderos ocupan alrededor de 30000 ha, la mayor extensión de invernaderos en todo el mundo, lo que hace que empleen alrededor de 55000 trabajadores cada año [3]. Los invernaderos son edificaciones agrícolas destinadas a mantener unas condiciones climáticas adecuadas para el cultivo. Están compuestos de cubiertas de plástico, sujetas por estructuras metálicas ligeras, con ventilación a través de ventanas en techo y paredes. Estas cubiertas plásticas filtran la radiación solar, de forma que en el interior de un invernadero se recibe casi exclusivamente radiación solar difusa. Además, según la norma UNE-EN 13031-1 [4], las dimensiones del recinto deben permitir a las personas trabajar cómodamente en su interior. Los invernaderos típicos en Almería son de bajo coste y gracias al clima de la región, no son necesarios sistemas de calefacción o enfriamiento.

Los cultivos de invernadero en Almería se realizan mayoritariamente desde finales de julio (trasplante) hasta mediados de junio (arranque de planta-

ción), habitualmente con dos ciclos de cultivo al año [5]. Sin embargo, este periodo de trabajo se extiende hasta el año completo, ya que tareas de mantenimiento se realizan en periodos sin cosecha [6, 7, 8].

La estructura de esta tesis es la siguiente: en primer lugar, se incluyen las publicaciones científicas asociadas a la presente Tesis Doctoral en el Capítulo 2. A continuación, se hace un resumen de cada una de ellas en el Capítulo 3. Finalmente, en el Capítulo 4 se exponen las conclusiones generales, indicando de qué publicación se desprenden.

1.2. Justificación

- Los trabajadores de invernaderos están expuestos a condiciones de trabajo que pueden no ser favorables y afectar a su salud. Sin embargo, los datos experimentales obtenidos en invernaderos suelen utilizarse para el estudio y mejora del cultivo, siendo escasos los datos experimentales relativos al estudio del estrés térmico de trabajadores. Indicios de heterogeneidad del ambiente térmico en el interior de dichas instalaciones agrícolas también justifican este estudio.

- Adicionalmente, el alto coste de anemómetros que permitan medir la temperatura de aire en el interior de invernaderos con precisión justifica el estudio de calibración de un anemómetro de bajo coste.

- Por otro lado, existen indicios de radiación ultravioleta (UV) mayor a los límites a partir de los cuales existe riesgo para la salud. También por la relación de la exposición a la radiación solar UV y la salud de las personas trabajadoras. Además, se justifica la elaboración, si procede, de una pequeña guía de recomendaciones ante el riesgo por radiación UV.

1.3. Hipótesis

Esta investigación pretende:

- Estudiar la temperatura de aire en un invernadero típico de Almería ("raspa y amagado") durante un año completo y demostrar la heterogeneidad del ambiente térmico según la norma ISO 7726, en diferentes puntos del interior de un invernadero y en diferentes alturas antropométricas (cabeza, cintura y pies).

- Adicionalmente, calibrar un anemómetro de bajo coste para realizar medidas con una mayor precisión en el interior de invernaderos.
- Demostrar la existencia o no, durante un año completo, de riesgos para la salud de la población trabajadora por exposición prolongada a radiación solar UV en la superficie de trabajo del interior de los invernaderos tipo Almería (raspa y amagado).

1.4. Objetivos

Los objetivos de la presente tesis doctoral son los siguientes:

- Monitorizar la temperatura de aire en tiempo real durante un año completo en diferentes puntos del interior de un invernadero típico de Almería y en el exterior, por medio de una red inalámbrica de sensores (o WSN, por sus siglas en inglés, Wireless Sensor Network) distribuida equitativamente en horizontal y vertical. Los datos recogidos permiten analizar la posible heterogeneidad de la temperatura de aire dentro de un invernadero de acuerdo a la norma ISO 7726, algo a tener en cuenta, ya que tiene incidencia sobre el estrés térmico de los trabajadores y también sobre el cultivo. Este análisis además permite caracterizar la distribución de la temperatura de aire del invernadero y sus variaciones a lo largo de las cuatro estaciones del año.
- Adicionalmente, calibrar un anemómetro de hilo térmico de bajo coste mediante Regresión de Procesos Gaussianos.
- Como extensión al objetivo inicial, analizar el posible riesgo sobre la salud de los trabajadores de invernaderos debido a la radiación ultravioleta en un invernadero típico de Almería, además de proponer recomendaciones y medidas de protección en caso de que se confirme que exista dicho riesgo.

Capítulo 2

Publicaciones científicas

La presente tesis doctoral pretende monitorizar diferentes parámetros climáticos en el interior de un invernadero, con especial atención a la temperatura de aire y a estudiar su posible heterogeneidad dentro de un invernadero de acuerdo a la norma ISO 7726. Este objetivo se materializó en la 1ª publicación científica [9]. Sin embargo, en este estudió se encontraron problemas para medir correctamente la velocidad del viento en el interior de un invernadero, ya que para medirla adecuadamente y con precisión, es necesario un anemómetro ultrasónico, con un coste alto. Debido al elevado número de sensores necesarios (13) y a los recursos disponibles, se decidió emplear anemómetros de hilo térmico de bajo coste. Para su correcto funcionamiento, estos dispositivos se deben calibrar previamente, y aun así tienen un gran inconveniente, que es la pérdida de precisión cuando varía la temperatura ambiente. Para solventar este inconveniente se realizó una calibración de un anemómetro de hilo térmico mediante Regresión de Procesos Gaussianos. Este trabajo ha dado como fruto la 2ª publicación científica de esta tesis doctoral [10]. Finalmente y también derivado de los trabajos realizados, se observó que en el interior de un invernadero existía la posibilidad de riesgo sobre la salud de los trabajadores debido a la radiación ultravioleta. Bajo esta hipótesis, se abordó un análisis de la incidencia de radiación UV en los trabajadores en el interior de un invernadero típico de Almería, dando como resultado la publicación de un tercer artículo científico [11].

2.1. Publicación científica 1

Título: On air temperature distribution and ISO 7726-defined heterogeneity inside a typical greenhouse in Almería.

Autores: Rubén A. García-Ruiz, Javier López-Martínez, José L. Blanco-Claraco, José Pérez-Alonso y Ángel J. Callejón-Ferre.

Revista científica: Computers and Electronics in Agriculture.

Volumen: 151.

Páginas: 264-275.

Año: 2018.

doi: 10.1016/j.compag.2018.06.001

Datos JCR (Journal Citation Reports):

Factor de impacto (2018): 3.171.

Categoría: AGRICULTURE, MULTIDISCIPLINARY.

Ranking categoría: 5/56.

Cuartil: Q1.

Editor: ELSEVIER SCI LTD.

País: Reino Unido.

Computers and Electronics in Agriculture 151 (2018) 264–275

Contents lists available at ScienceDirect

Computers and Electronics in Agriculture

journal homepage: www.elsevier.com/locate/compag

Original papers

On air temperature distribution and ISO 7726-defined heterogeneity inside a typical greenhouse in Almería

Rubén A. García-Ruiz[a,*], Javier López-Martínez[a], José L. Blanco-Claraco[a], José Pérez-Alonso[a], Ángel J. Callejón-Ferre[a,b]

[a] Department of Engineering, University of Almería, Agrifood Campus of International Excellence (ceiA3), Ctra. de Sacramento s/n, 04120, Almería, Spain
[b] Laboratory-Observatory Andalusian Working Conditions in the Agricultural Sector (LASA), C/ Albert Einstein s/n, 2ªplanta, Isla de la Cartuja, 41092, Sevilla, Spain

ARTICLE INFO

Keywords:
Greenhouse
Thermal environment
Heat stress
Air temperature distribution
Heterogeneous environment

ABSTRACT

Studies about the air temperature inside greenhouses are usually focused on the crop growth. However, the thermal environment inside greenhouses can affect the safety of the workers and also their productivity. This work focuses on the study of air temperature conditions with respect to workers following the requirements and methods gathered in ISO 7726, which indicates that measurements should be taken at different points in both, horizontal and vertical directions in order to study heterogeneous thermal environments. For the present work, data were gathered by the Wireless Sensor Network (WSN) designed in our previous work, hereby extended by an experimental campaign carried out during a complete year in a typical greenhouse in Almeriía. The aim is performing a long-term study of air temperature inside a greenhouse as well as the assessment of air temperature heterogeneity. The results, which allow characterizing air temperature inside the greenhouse, prove the existence of patterns of heterogeneity as a function of the incidence of sunlight and time of day. During the analysed period, air temperature heterogeneity is mainly present in the central hours of the day and it is higher in the horizontal dimension rather than vertically. In addition, it has been observed that the vast majority of homogeneous days correlate with cloudy days. Finally, based on the results obtained some recommendations are presented for assessing the thermal environment of greenhouses.

1. Introduction

Areas of the South of Europe and specially Mediterranean coastal areas meet the optimum environmental conditions for growing vegetables in plastic-covered greenhouses (Hernández et al., 2017). Specifically, in Almeriía (Spain) they cover approximately 30,000 ha, the largest extension of greenhouses worldwide. Consequently, around 55,000 workers are employed each year in Almeriía (Cabrera et al., 2016). Greenhouses are agricultural buildings that consist of light metal structures covered with transparent plastic, with ventilation through the walls and ceiling, and diffuse solar radiation. These buildings maintain an adequate temperature and humidity allowing to extend the crops for almost the complete year (from the end of July to the beginning of June of the following year). However, these conditions are not the better for the wellbeing of the greenhouse workers, whose working period lasts practically the complete year, since maintenance work is also carried in non-crop periods (Pérez-Alonso et al., 2011; Callejón-Ferre et al., 2009; Callejón-Ferre et al., 2011b).

Despite greenhouses soften the outdoor climate environment, large variations in air temperature and humidity do still occur throughout the day. Humidity and specially air temperature are the main parameters that affect workers and crops inside of greenhouses (Vox et al., 2010; Zhao et al., 2001). In greenhouses of Almeriía, air temperature vary from around 50 °C in the middle of the day in summer to near 0 °C at night in winter.

Several authors (Callejón-Ferre et al., 2011a; Riemer and Bechar, 2016; Cecchini et al., 2010; Marucci et al., 2012; Diano et al., 2016; Okushima et al., 2001) have reported heat stress risk fundamentally during the warmer months (spring and summer). Environments with high temperatures and humidity can affect the safety of the workers, causing severe problems to the cardiovascular system and the thermoregulatory system of workers (Chad and Brown, 1995; Zhao et al., 2009). Moreover, these environments also have a negative impact in the productivity of workers. Additionally, Risk of cold in winter have been also pointed out (Callejón-Ferre et al., 2011a).

To assess the thermal environment and its influence to the workers,

* Corresponding author.
E-mail addresses: rgr051@ual.es (R.A. García-Ruiz), javier.lopez@ual.es (J. López-Martínez), jlblanco@ual.es (J.L. Blanco-Claraco), jpalonso@ual.es (J. Pérez-Alonso), acallejo@ual.es (Á.J. Callejón-Ferre).

https://doi.org/10.1016/j.compag.2018.06.001
Received 3 April 2018; Received in revised form 21 May 2018; Accepted 2 June 2018

we need to follow several rules (Parsons, 2013). According to the International Standard Organization (ISO), the environment is classified in moderate or extreme. Depending on the category, a different index and ISO Standard must be used. To calculate these indexes, in any case, the measurement of several climatic parameters are required and in some cases also the metabolic rate of the activity carried out by the workers, based in ISO 8996 (ISO 8996:2004,), and the clothing insulation and sweat rate, ISO 9920 (ISO 9920:2007, 2007). Moreover, the ISO 7726 Standard (ISO 7726:1998, 1998) defines the specifications and methods that must to be fulfilled to asses the thermal environment. The specifications address the expected parameters of measuring instruments such as measurement range, accuracy, and response time. Regarding the methods, physical magnitudes may vary with the space as much horizontally as vertically and the environment can be considered homogeneous or heterogeneous. An environment will be considered as homogeneous if the physical magnitude under consideration is practically uniform in the analysed area. On the other hand, an environment will be heterogeneous if there are significant variations in the physical magnitude. The limits for each climatic parameters that define the environment as heterogeneous or not, with respect that parameter, are established in the ISO 7726. In case of heterogeneous environments, the rule states that the physical magnitudes need to be measured at different points both horizontally and vertically. In the latter, ISO 7726 specifically establishes three heights where the measurements must to be carried out: ankle, abdomen, and head.

Related to the thermal assessment inside a greenhouse and the heat stress in workers, only the work presented by Marucci et al. (2012) comply with the requirements for the measuring instruments described in the ISO 7726. However, these work only perform measurements in one position inside the greenhouse and in one height. Recent work carried out by López-Martínez et al. (2018), fulfilling with ISO 7726, reveals heterogeneity conditions of the greenhouse analysed. In this work, twelve measuring stations were distributed along the greenhouse, each one measuring climatic parameters at the three heights specified by the rule. According to that results obtained, it is pointed out that greenhouses are environment where the heterogeneity conditions can be achieved.

Others works, focused in the crop growth conditions, have shown large air temperature differences in vertical and also in horizontal direction inside greenhouses. Zhao et al. (2001), Soni et al. (2005) and Zorzeto and Leal (2017) measured vertical differences of around 7 °C, 10 °C and 14 °C, respectively. López et al. (2013) and Kittas et al. (2003) obtained horizontal differences of around 6 °C and 8 °C, respectively. Granados et al. (2016) measured the average temperature during January to March in a greenhouse, observing temperature differences of up to 4.4 °C at 6 a.m. and up to 9.1 °C at 2 p.m. between 0.2 and 2.6 m in height. In three different greenhouses in Almeriía studied by López et al. (2012b), it was recorded maximum air temperature differences between 10 and 12 °C for different tests performed between 11:30 a.m. and 2:30 p.m.. In simulations with computational fluids dynamics (CFD), large variations of temperature inside the greenhouse have been also observed: Boulard et al. (2017) obtained vertical differences of up to 12 °C, Molina-Aiz et al. (2004) obtained variations of temperature of around 9 °C in a similar greenhouse and in a location very close to the greenhouse studied in this work, and Tong et al. (2009) obtained variations of temperature as large as 12 °C. All these results also suggest that greenhouses may be heterogeneous environments when are evaluated according the ISO 7726.

To carry out the measurements inside of a greenhouse at different points at the same time, a sensor network is required. In recent years, Wireless Sensor Networks (WSNs) have been used to carry out measurements in different points. This type of networks are composed of battery-powered nodes provided with sensors that supply the corresponding information in real time and transmit it to a central base-station (BS) where it will be stored and from where nodes can be monitored and controlled (Ferentinos et al., 2017). The main advantages of WSN are the capability of measuring multiple points avoiding the use of wires, which are usually damaged and wore out when exposed to aggressive environment (high variations of air temperature and humidity) and could hinder the cultivation practices. Furthermore, thanks to the advances in electronics and wireless communications, it is possible to develop WSNs with a low cost and low energy consumption.

In the present work we have used a WSN to overcome the scarcity of real measured air temperature data inside a greenhouse during a complete year, also allowing us to assess whether air temperature is heterogeneous or not (according to ISO 7726) inside a typical greenhouse. This work is a continuation of our previous one (López-Martínez et al., 2018), in which the WSN and twelve measurement stations where designed and put into operation in a greenhouse. The present work carries out a measurement campaign during a complete year with the objective of evaluating the heterogeneous conditions of a greenhouse with respect to the air temperature.

To sum up, the aim of the present work is twofold:

- Monitoring, using a WSN, the air temperature distribution inside a typical greenhouse during a complete year, at three different heights and multiple points equally distributed horizontally. These data will allow to characterize the air temperature distribution of the greenhouse and its variations along the four seasons of the year.
- To study the air temperature heterogeneity inside a typical greenhouse according to ISO 7726 and providing some recommendations for the assessing of the thermal environment of a greenhouse.

This paper is organized as follows: initially, the material and methods are explained in Section 2. The experimental results and their discussion are detailed in Section 3. Finally, we outline some conclusions in Section 4.

2. Material and Methods

2.1. Experimental setup

The experiment was carried out in a greenhouse located at 15 km east of Almeriía (36°52′*N* - 2°17′255 *W* and 98 m above sea level), in the southeastern Spain. The experimental campaign was performed during a complete year, since December 2016 to November 2017 and the time between measurements was 30 s. The greenhouse is raspa y amagado type, the most common in this region. Its surface area is 1024 m^2 (32 × 32 m) and the heights of the gutter and ridge are 3.4 m and 4.1 m, respectively. The drawing of the greenhouse is defined in Fig. 1. The structure is made of steel, with the resistant elements of wire mesh type and is covered by three polyethylene layers of 200 μm, with 81% visible light transmittance and 29% diffuse light transmittance. Inside the greenhouse, the soil is covered of gravel and sand, and tomato plants are cultivated. Ventilation is natural through lateral windows and roof vents. There are windows on all four sides of the greenhouse and 4 roof vents. The area of each window is specified in Fig. 2. Each window is opened and closed by means of an electric engine with a power of 0.5 hp, being all of them controlled by a central control station. The central control station closes the windows either air velocity is greater than 35 km/h or air temperature is lower than around 8 °C, since this temperature value is also related with relative air humidity. These values are selected in order to achieve the optimal physiologic and production conditions for the plants cultivated, in this case tomato plants.

The implemented WSN comprises 12 measurement stations distributed inside the greenhouse (Fig. 1). Each station consists of a structure with three heights where the sensors are installed. Air temperature (*ta*), globe temperature (*tg*), relative air humidity (*RH*) and air velocity (v_a) have been measured at the three heights, while UVI ultraviolet radiation (UVI) is measured only at the higher height of each

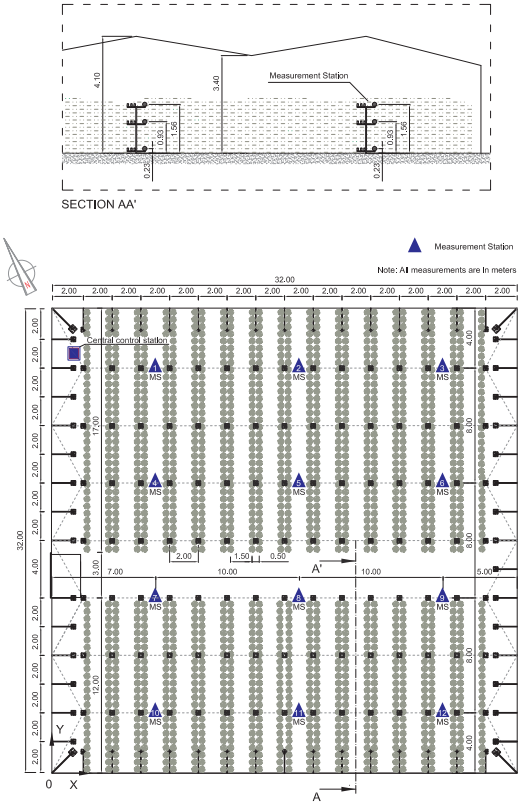

Fig. 1. Drawing of the greenhouse, where also are defined the locations of the measurement stations.

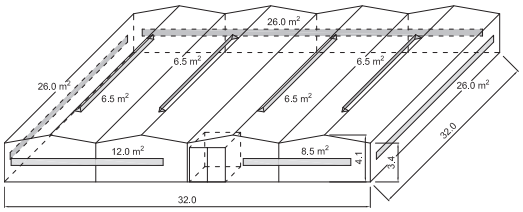

Fig. 2. 3D model of the greenhouse, where the dimensions of the windows are specified.

station. Therefore, the measurement stations are composed by four probes for each height (to measure air temperature, globe temperature, relative air humidity, and air velocity) and a UVI probe located at the top height, as it can be seen in Fig. 3. The heights were selected at 0.23 m, 0.93 m and 1.56 m according to the 50th percentile of Spanish population (Carmona-Benjumea, 2001). The characteristics of the measuring instruments fulfil with the specifications defined in ISO 7726 (except for UVI measurement that is not considered in the standard) and are presented in Table 1.

These climatic parameters have been measured using a WSN that employs IEEE 802.15.4 and ZigBee as communication protocol, and a smartphone to transmit the data by 4G to a server installed in the Data Processing Centre of the University of Almeriía (CPD-UAL) enabling access to these data by a web interface (HTTP) or by safe Secure Shell

Fig. 3. One of the 12 measurement stations located inside the greenhouse.

(SSH) links. Mesh topology is used (where nodes are connected directly to each other for peer-to-peer communication) at the communication low level, but it is modified by firmware and software so that communication follows a logical tree, generating routing tables which can be changed at any time via the Internet. Network architecture is explained in detail in López-Martínez et al. (2018).

Table 2 summarizes some related works regarding the use of WSNs (Pérez-Alonso et al., 2011; Marucci et al., 2012; Zorzeto and Leal, 2017; Molina-Aiz et al., 2004; Ferentinos et al., 2017; Balendonck et al., 2014; Vox et al., 2014; López et al., 2012a; Srbinovska et al., 2015; Bojacá et al., 2009; Kittas et al., 2008). The communication protocol used for most of them, and also in our present work, is IEEE 802.15.4 plus ZigBee. Regarding the network topology, some works (Ferentinos et al., 2017; Balendonck et al., 2014; Srbinovska et al., 2015) use a star topology (comprising a central node connected to all the sensing nodes) while others (Vox et al., 2014) use a tree topology (comprising a central node connected to the sensing nodes without loops).

2.2. ISO 7726 complying and heterogeneity assessment

The Standard ISO 7726 defines the basic physical magnitudes associated to the study of the thermal environment: air temperature (ta), mean radiant temperature ($\overline{ir}$), absolute air humidity (AH, expressed by the partial vapour pressure) and air velocity (v_a). An approximate value of mean radiant temperature can be obtained by measuring globe temperature (tg) and other basic parameters such as air temperature and air velocity. Globe temperature combines the effects of radiation, air temperature and air velocity and is measured by means of a black sphere with a temperature sensor at its centre. Thus, considering this method for calculating mean radiant temperature, the climate parameters that must be measured to assess the thermal environment are: air temperature (ta), globe temperature (tg), absolute air humidity (AH), and air velocity (v_a). By means of these parameters, other parameters required to obtain different thermal stress indices can be calculated, as operative temperature (t_o) for PMV index (ISO 7730:2005,)

Table 1
Characteristics of the measuring instruments used.

Climatic parameter	Measurement range	Accuracy	Model and manufacturer
Air temperature (*ta*)	−15 °C to 250 °C	±0.06 °C at 0 °C	Pt-100 515–725 (TC Direct)
Globe temperature (*tg*)	−15 °C to 250 °C	±0.06 °C at 0 °C	Pt-100 515–725 (TC Direct)
Relative air humidity (*RH*)	0 to 100% *HR*	±3% *HR*	Si7021-A20 (Silicon Labs)
Air velocity (v_a)	0.05 to 20 m s^{-1}	±10%	Rev. C (Modern Device)
UVI	0 to 15	±1	Si1145/46/47 (Silicon Labs)

and natural wet-bulb temperature (t_{nw}) for WTGB index (ISO 7243:2017,).

ISO 7726 also defines the specifications relatives to the spatial variation of physical magnitudes, which are different depending on the type of environment considered (comfort-class C or heat stress-class S). In this work heat stress is possible, so class S environment is selected. One of the specifications is three heights where physical magnitudes must to be measured in the case that environment is heterogeneous, corresponding to ankle, abdomen and head. To consider a thermal environment as heterogeneous, any parameter considered as basic for the ISO 7726 (air temperature, mean radiant temperature, air velocity or partial vapour pressure) must be out of a limit with respect to its mean value. The limits that define a heterogeneous environment are summarized in Table 3. To calculate the mean value of each basic parameter weighting factors must be applied to each measurement height, being 1 for ankle and head, and 2 for abdomen.

Despite there are four basic parameters and any of them show variations along the greenhouse, previous results of López-Martínez et al. (2018) suggest that the air temperature is the climatic parameter that may show larger variations. In fact, no mean radiant temperature heterogeneity was found in the period studied. In addition, air temperature may be the parameter with more influence over workers in the greenhouse. According to this, the present work has been focused in the air temperature variations. Additionally, the relationship between air temperature and globe temperature along the year has been obtained in order to show the influence of diffuse solar radiation inside the greenhouse. Ultraviolet Radiation Index (*UVI*) also has been measured to determine the presence of clouds. In total, more than two million of measurements have been studied in the year analysed from the 36 points of measurement (12 stations by 3 heights).

As described before, to consider an environment as heterogeneous, some measurement must be out of the range specified respect to the weighted mean value of all the measurements (of all the measurement stations). In this case for air temperature, the range defined in ISO 7726 is ± 2 °C. The time when no value is out of this range, the environment is considered as homogeneous. To assess heterogeneity, first, mean value and heterogeneity limits are calculated. For horizontal heterogeneity, the weighted mean of the 3 heights per each measurement station is calculated, resulting 12 values for each instant of time. These values are compared with the heterogeneity limits and if one of them exceeds the limits, horizontal heterogeneity exists. On the other hand, for vertical heterogeneity, the mean of the 12 measurement stations per each height is calculated, resulting 3 values for each instant of time, which are compared with respect the mean value in the same way that horizontal heterogeneity. The heterogeneity conditions of the greenhouse has been evaluated along a complete year, comparing the differences between the four seasons of the year.

2.3. Considerations and study limitations

An aspect to take into account for the results interpretation is that data have been analysed using time in UTC (Coordinated Universal Time). Local time in Almeriía is CET (Central European Time) with daylight saving time in summer.

Greenhouses environment is peculiar since it cannot be classified as indoors due to the existence of diffuse solar radiation, low wind speed, and high humidity. In addition, plastic covers are not fully waterproof and dusk and calcium carbonate (coming from paint the covers with whitewash) are present in the environment. Measurement stations have been exposed to these difficult operation conditions, making necessary weekly visits to clean and maintenances tasks. This facts have caused the loss of measurements of some station during short periods of time, specially during holiday periods.

3. Results and discussion

First, the results of the air temperature measurement campaign inside the greenhouse are presented and distribution of air temperature is analysed. Next, air temperature heterogeneity in the greenhouse, according to ISO 7726, is assessed during a complete year both horizontally and vertically. Finally, from the results obtained, some recommendations are exposed for assessing air temperature heterogeneity of the thermal environment in a greenhouse.

3.1. Variation of air temperature

Next we summarize the measurements of air temperature carried out during the experimental campaign. In Table 4, minimum and maximum values of air temperature for each month are gathered. As it is logical, its minimum values are measured at dawn and maximum values at midday. The maximum value for air temperature took place in August and is 55 °C, whereas the minimum value were measured in January is around 1 °C. It is striking that the vast majority of the maximum and minimum values were measured at the height 3 or top height of the measurement stations. This trend could be observed in Fig. 4, where the weighted mean of the measurements of each height for two different sunny days is represented (for January, 30th and July, 30th 2017). Temperature in height 3 is higher than the rest of heights during the day, but at night height 1 is the highest, whereas height 3 is the lowest. This is because the thermal gradient is reversed, as the floor works as thermal accumulator and at night it transfers heat to the environment.

It has been calculated the mean air temperature per seasons in each instant using the weighting factors for heights defined in ISO 7726, obtaining a average day per season. This is shown in Fig. 5, together with the standard deviation. As expected, in summer and winter air temperature inside the greenhouse is the highest and lowest, respectively. In spring it can be observed that the temperature is higher than autumn in the middle of the day whereas at night the temperature is a bit lower. Standard deviation is higher in the middle of the day than at night for all the seasons. In addition, standard deviation also seems to increase with air temperature as it is higher in warmer seasons. The presence of clouds has influence in air temperature inside the greenhouse. The percentage of cloudy days per season was 39%, 39%, 56% and 28% for autumn, winter, spring and summer, respectively.

Videos with a 3D representation of data showing how air temperature varies during the day have been included in this work.[1] In

[1] See: https://www.youtube.com/playlist?list=PLguxjVND_tkzeqU0prXUZXZzix9ZNIsyu.

Table 2
Summary of related works regarding the use of WSNs.

Work	Application	Stations			ISO 7726 application	Measurement campaign	Time between measurements	**Accuracy/range of measurement instruments**			
		Configuration (horizontal × vertical)	Heights (m)	Total measurements				Air temperature	Globe temperature	Relative humidity	Others
Balendonck et al. (2014)	Horizontal climatic heterogeneity and crop growth	100 × 1	Different at each trial	100	No	60 days (10 for each trial)	1 min.	SHT71 (±0.4 °C)		SHT71 ±5% RH	–
Bojacá et al. (2009)	Effect of temperature distribution on the crop growth	25x1	1.5	25	No	28 days	6 min	±0.01 °C			Solar radiation
Ferentinos et al. (2017)	Climatic heterogeneity and crop growth	5 × 1	1.8	1	No	4 months (3 different trials)	30 s.	SHT75 (±0.3 °C)		SHT75 ±2% RH	Solar radiation
Kittas et al. (2008)	Impact of insect screens and ventilation openings on the greenhouse climate	24 × 2 + 12 × 1 + 12 × 1	1.1–2 + 1.1 - + 2.85	72	No	2 months (during 10–17 h)	5 min	±0.1 °C		±2%.	Air velocity, solar radiation, vapor pressure
López et al. (2012a,b)	Characterize airflow and temperature distribution of greenhouses	12 × 2	1–2	24	No	–	–	±0.18 °C		±2.5%	Air velocity
Marucci et al. (2012)	Thermal stress by workers employed in vegetable grafting	1 × 1	1.5	1	Yes	10 months	–	Pt-100 1/3 DIN (±0.13 °C)	Pt-100 1/3 DIN (±0.13 °C)	±2%	Air velocity, damp bulb temperature, partial vapor pressure
Molina-Aiz et al. (2004)	Influence of wind speed on the ventilation performance	4 × 3 + 1 × 6 + 6ground- + 10top + 4windows	0.5–1.5–2.5 + 0.5-1–1.5-2–2.5–3 + ground + top + -windows	38	No	4 days (during different periods of time)	30 s.	NTC (±0.4 °C)		±3% RH	Air velocity, solar radiation
Pérez-Alonso et al. (2011)	Thermal stress in the greenhouse construction	12 × 1	-	12	No	4 months	5 min.	Pt-100 Class A (±0.25 °C)	Pt-100 1/3 DIN (±0.13 °C)	±2.5%	Dry air temperature, air velocity, solar radiation
Srbinovska et al. (2015)	Crop growth	5 × 1	–	5	No	7 days	30 min.	SHT11 (±0.5 °C)		SHT11 ±3% RH	
Vox et al. (2014)	Crop growth	2×1	–	2	No	20 days	60 s.	SHT75 (±0.4 °C)		SHT75 ±2% RH	Air pressure, solar radiation
Zorzeto and Leal (2017)	Vertical and horizontal climatic heterogeneity with evaporative cooling	21 × 2 + 3 × 1	1.2–2.4 + 4.5	45	No	30 days (3 different trials)	30 s	SHT75 (±0.4 °C)		SHT75 ±2% RH	Air velocity
López-Martínez et al. (2018) and this work	Thermal stress and climatic heterogeneity	13 × 3	0.23–0.93–1.5-6	39	Yes	1 year (01/12/16–31/11/17)	30 s	Pt-100 1/10 DIN (±0.07 °C)	Pt-100 1/3 DIN (±0.07 °C)	±3% RH	Air velocity, UVI

Table 3
Thresholds from which the environment is considered heterogeneous.

Basic parameters	Range (respect to mean value)
Air temperature (ta)	±2 °C (0–50 °C)
Mean radiant temperature ($\overline{tr}$)	±10 °C (0–50 °C)
Air velocity (v_a)	$\pm(0.3 + 0.15 \cdot v_a)$ m s^{-1}
Partial vapour pressure (P_a)	±0.45 kPa

Table 4
Minimum and maximum values of air temperature measured at any point of the greenhouse for each month.

	Air temperature (°C)	
	Min.	Max.
December 2016	3.9	34.0
January 2017	1.1	36.2
February 2017	2.3	37.5
March 2017	3.9	41.7
April 2017	6.5	41.7
May 2017	8.9	44.1
June 2017	14.0	53.6
July 2017	12.4	54.5
August 2017	18.8	55.0
September 2017	13.2	44.8
October 2017	10.6	41.9
November 2017	4.4	36.3

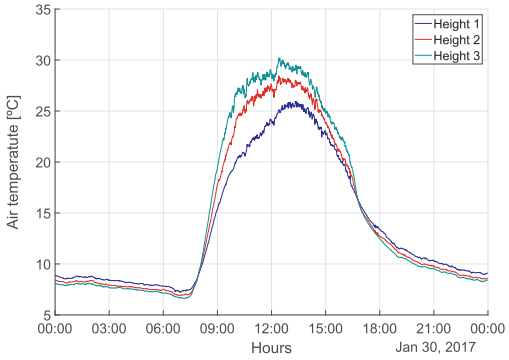

(a) January, 30th 2017

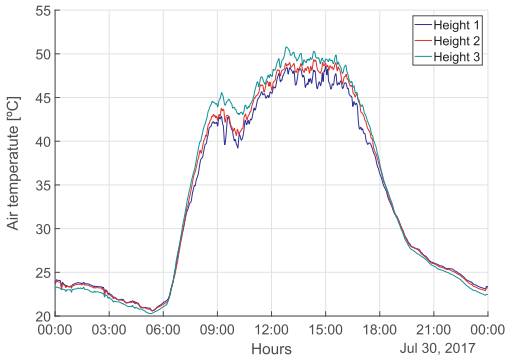

(b) July, 30th 2017

Fig. 4. Mean air temperature for each height for two different dates.

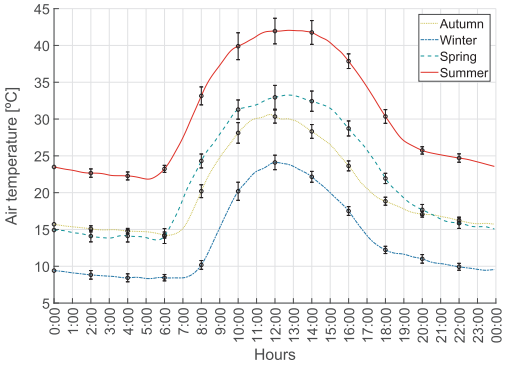

Fig. 5. Average day and confident intervals (± 1σ) of mean air temperature per season.

Fig. 6, a capture of a determined instant of the video is shown for air temperature. All the measurements recorded by the measurement stations are represented in the videos, that is 36 measurements (12 stations by 3 heights). The four images of Fig. 6 are different views of the same time. Each measurement is represented by a blue[2] marker and for each station, a label of the weighted mean value of this station is shown at the top of these markers. In a scale of colours, the weighted mean air temperature of each station also is visualized at the bottom of the z-axis. Markov Random Fields (MRF) has been used to interpolate the rest of points of the scale colour inside the greenhouse. It should be noted that the two images on the left have a scale of colours indicated in the bottom-left image and it is different to the two images on the right which have a scale of colours specified in the bottom-right image. At the bottom right, another valuable information is provided by the videos: the overall minimum and maximum values, and the maximum temperature difference among all the sensors installed. In addition, it is provided the partial minimum values, maximum values and maximum temperature differences for each of the three heights measured (that correspond to ankle, abdomen and head).

Finally, from the 3D videos, air temperature distribution inside the greenhouse is studied horizontally in different periods of the day. In Fig. 7, a top view of the greenhouse for four different moments of a day (January, 8th 2017) has been represented. At night (5:00 UTC), there is few difference of temperature (around 2.5 °C) and the west side of the greenhouse is a bit warmer. In the morning (10:40 UTC), the southeast side of the greenhouse is heated by the sun and consequently is warmer than the rest. Temperature variations are high reaching near 11 °C. In the early afternoon (15:40 UTC), temperature distribution changes due to the position of the sun and temperature differences decrease. The southeast side of the greenhouse gets cold at the same time that the west side gets hot. At 20:40 UTC, sun has gone down and variations of temperature are low as at 5:00 and as is usual at night. Results show that the patterns are similar in the rest of days of the year. When sun rays strike in the walls and lateral windows (where there is not plastic cover), it heats this side of the greenhouse producing higher temperature differences respect other areas in the greenhouse. Therefore, distribution of temperature inside the greenhouse is influenced by the position of the sun. Variations of temperature are high at midday and decrease as approach to night. In a nearby location and the same type of greenhouse, CFD simulations of Molina-Aiz et al. (2004) obtained variations of temperature close to these: 15 °C at 14:30 (July, 16th 2003), 5.3 °C at 19:30 (April, 18th 2003) and 4.8 °C at 20:15 (July, 13th 2003). It should be noted that this greenhouse has a larger area than the

[2] For interpretation of color in Fig. 6, the reader is referred to the web version of this article.

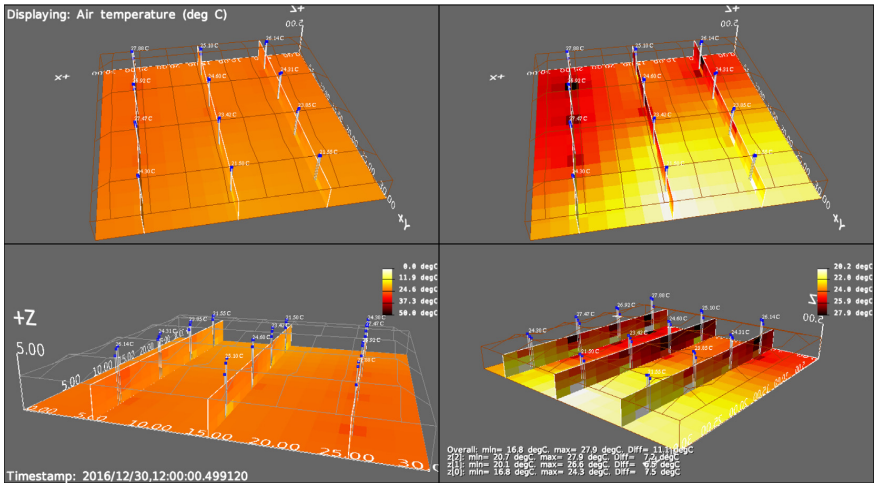

Fig. 6. Air temperature distribution inside the greenhouse (four different views). Image capture of the 3D video at 12:00 UTC, 30th Dec 2016.

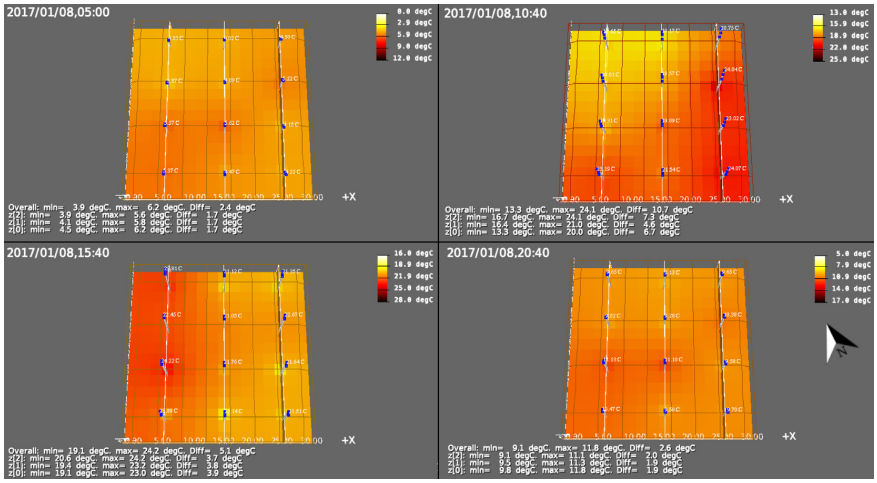

Fig. 7. Air temperature distribution inside the greenhouse at four different moments along a day (January, 8th 2017): 5:00 UTC, 10:40 UTC, 15:40 UTC and 20:40 UTC.

greenhouse studied in this work and temperature variations could be a bit higher for that reason.

3.2. Assess of air temperature heterogeneity

First, it has been studied the quantity of heterogeneous days per month and also per season (Figs. 8–11). So that, each day has been classified in one of the three categories: heterogeneous for more than 3 h, heterogeneous from 30 min to 3 h and homogeneous, where days with very shorts period of heterogeneity (less than 30 min of heterogeneity) have also been included in the group of homogeneous days. The intervals of categories have been defined in this way to avoid considering a day heterogeneous with very few time or some "peaks" of heterogeneity and to difference between days with low or high heterogeneity.

Figs. 8 and 9 represent the percentage of heterogeneous and homogeneous days per each month. Fig. 8 shows horizontal heterogeneity, where the heterogeneity (in some of the two categories of heterogeneity) is greater than 60% in all the months. In all the year, more than 80% of days are heterogeneous.

Similarly, Fig. 9 shows the vertical heterogeneity per months. It must be highlighted that the greenhouse is much more heterogeneous horizontally than vertically as it can be seen from the figures. In addition, when the environment is heterogeneous vertically, it is for less time than horizontally. Around 49% of the days are heterogeneous vertically in the complete year.

Figs. 10 and 11 shows the percentage of heterogeneous and homogeneous days, but in this case per season. In Fig. 10 the percentage of horizontal heterogeneous and homogeneous days per season is plotted. In winter and summer there is a higher percentage of homogeneous days than in autumn and spring.

In the same way, the percentage of vertical heterogeneous and homogeneous days is shown in Fig. 11. In this case, it seems that heterogeneity is concentrated in cold seasons (winter and autumn)

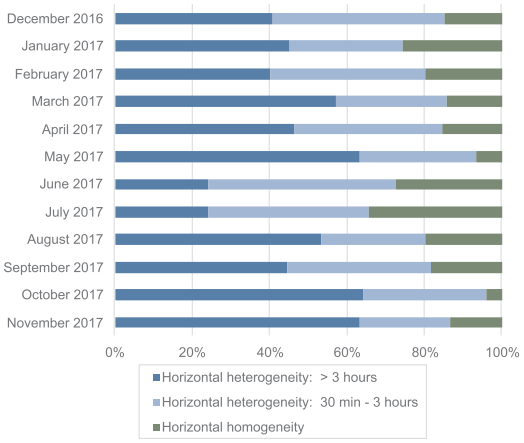

Fig. 8. Percentage of horizontal heterogeneous days per months.

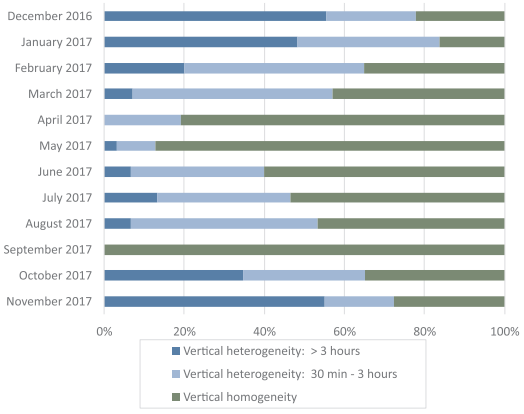

Fig. 9. Percentage of vertical heterogeneous days per months.

whereas in spring and summer there is a big quantity of homogeneous days.

Regarding the climatic conditions that favour the presence of heterogeneity, it has been observed a great influence of the clouds in the air temperature distribution inside the greenhouse. Thus, respect to the total horizontal homogeneous days (which were around 55), 75% of them correspond to cloudy days. On the other hand, only 33% of the heterogeneous days are cloudy. In the case of vertical homogeneity, 64% of the total homogeneous days (around 153) were cloudy. The percentage of cloudy days in the total heterogeneous days is only 16%. An example of this behaviour can be observed in Fig. 12, where horizontal heterogeneity, vertical heterogeneity and UVI are represented for two consecutive days (January, 27th and 28th 2017). In the graph of horizontal heterogeneity, the weighted mean air temperature of each measurement station is plotted in colour lines. The mean value of the 12 measurement stations is plotted in continuous black line, while discontinuous lines are the heterogeneity limits. It can be observed that the cloudy day is totally homogeneous whereas in the sunny day some of the measurements station surpass the heterogeneity limits at midday when UVI is high. In the graph that shows the vertical heterogeneity, the mean value for each height are represented in colour lines, while the weighted mean value and the heterogeneity limits are plotted in continuous and discontinuous black lines respectively. As for the

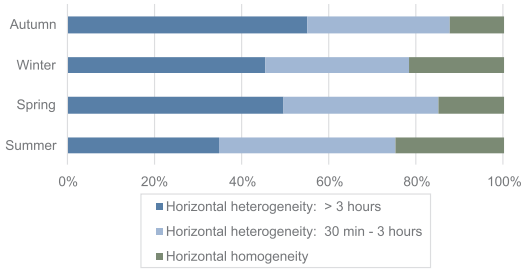

Fig. 10. Percentage of horizontal heterogeneous days per seasons.

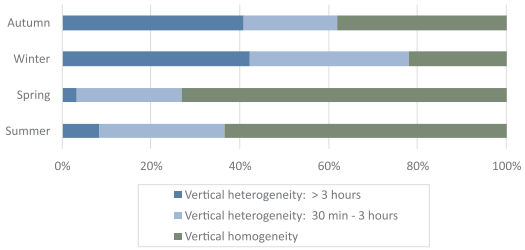

Fig. 11. Percentage of vertical heterogeneous days per seasons.

horizontal case, cloudy day remains homogeneous along the day, while the sunny day shows heterogeneity conditions.

Next, it has studied the periods of the day when heterogeneity is produced. In order to do it, it has been obtained the percentage of heterogeneous days (with respect to the total days of each season) but evaluated at every moment of time throughout the day. Heterogeneity, both vertical and horizontal, is produced in the central hours of the day and never at night. Fig. 13 shows the results for horizontal heterogeneity. Between 9 and 15 h are concentrated the greater percentages of heterogeneous days and it can also be observed that from 19 to 7 h the environment in the greenhouse is homogeneous. As in Fig. 10, spring and autumn are more heterogeneous horizontally than winter and summer.

In like manner, Fig. 14 shows the periods of the day when vertical heterogeneity occurs. In this case, the greenhouse is homogeneous approximately from 17 to 7 h. The period of heterogeneity is concentrated in less time and with lower percentages than horizontal heterogeneity. Winter and autumn (the coldest seasons) are more heterogeneous vertically than spring and summer as it can also be seen in Fig. 11. It must be highlighted that winter is the less horizontal heterogeneous season, but results to be the most heterogeneous vertically. Inversely occurs with spring, that is the most horizontal heterogeneous season and the less heterogeneous vertically.

For all the seasons except spring the shape of the curves are more or less similar both for horizontal heterogeneity and for vertical heterogeneity, increasing the percentage of heterogeneity until the maximum value was reached and from this point they decreased gradually until homogeneity is reached. However, in spring it can be observed that when the maximum value is reached, the percentage decreases but later increases again until finally decreases, producing a kind of valley in the shape of the curve around 13 h. In Figs. 13 and 14 also can be observed that heterogeneity lasts more time in seasons in which the day is longer as spring and summer. Therefore, it can be affirmed that heterogeneity depends on the sun hours during a day.

Finally, to evaluate quantitatively the heterogeneity, maximum air temperature differences respect to the mean value (in absolute value) and overall maximum air temperature differences inside the

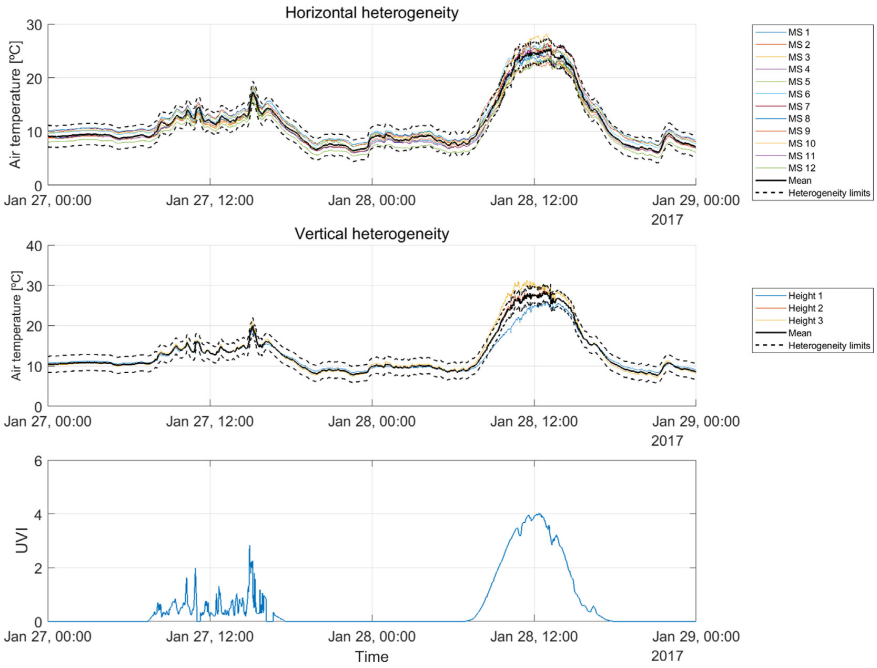

Fig. 12. Horizontal heterogeneity, vertical heterogeneity and UVI for two consecutive days (January, 27th and 28th 2017), the first one cloudy and the second one sunny.

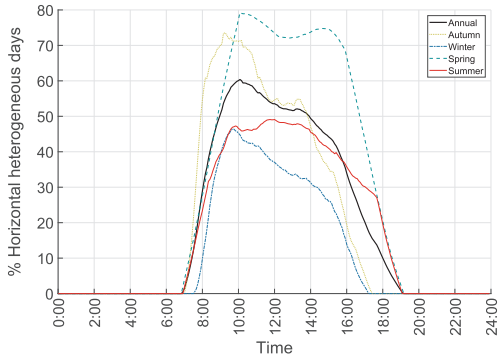

Fig. 13. Percentage of horizontal heterogeneous days at every moment of time throughout the day.

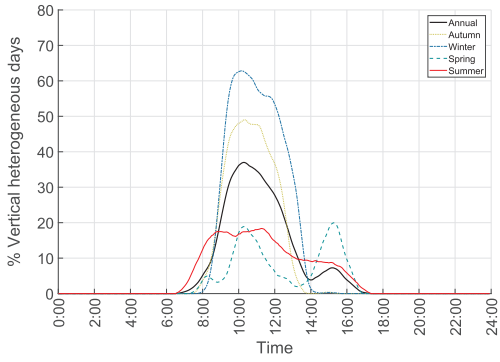

Fig. 14. Percentage of vertical heterogeneous days at every moment of time throughout the day.

greenhouse have been obtained for all the days in the complete year. For each instant of time, it have been calculated the mean, maximum and minimum values of these maximum air temperature differences for all the days of each season. This values have been plotted and compared in Figures from Figs. 15–19. Fig. 15 shows the maximum horizontal air temperature differences respect to mean value, in absolute value. The mean of these values exceed the heterogeneity limit for all the seasons, and the maximum value occurs in summer with a difference of 6.3 °C.

In Fig. 16 the maximum vertical air temperature differences respect to mean value are shown, in absolute value. In this case, the mean of these values is lower than for horizontal heterogeneity and only exceed the heterogeneity limit for autumn and winter, justly in the seasons when there is more percentage of vertical heterogeneity. The maximum value takes place in winter (5.8 °C). It also can be observed that minimum values for vertical heterogeneity are close to 0 °C of difference and lower than for horizontal heterogeneity. It was seen before in Figs. 13 and 14 that heterogeneity occurs during the day and never at night, confirming in Figs. 15 and 16 that the maximum air temperature difference never exceeds the heterogeneity limit.

Figs. 17 and 18 represent the maximum horizontal and vertical air temperature differences, respectively. For horizontal differences, the mean values reach around 4 °C in all the seasons and the maximum value occurs in spring with a value of 8.4 °C. For vertical differences, it can be observed that the mean value is higher in autumn and winter, reaching values close to 4 °C while in spring and summer the mean value reaches around 2 °C. Something similar occurs for the maximum values, which are higher in autumn and spring, reaching up to 10.6 °C in winter. The minimum values for vertical dimension are lower than for horizontal one, in like manner that for the maximum air temperature differences respect to mean value (Figs. 15 and 16).

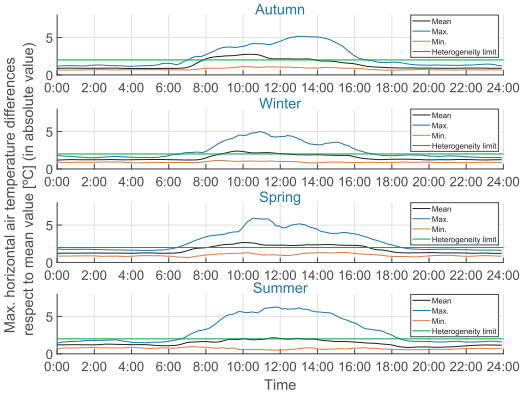

Fig. 15. Maximum horizontal air temperature differences respect to mean value, in absolute value.

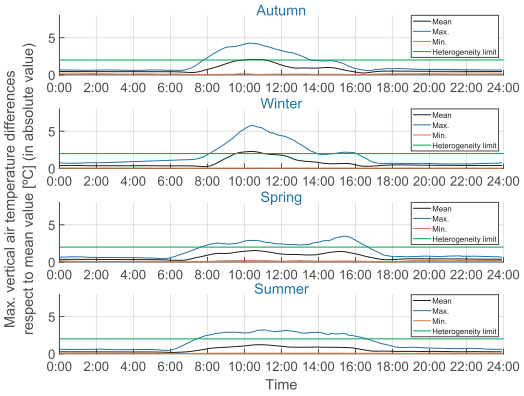

Fig. 16. Maximum vertical air temperature differences respect to mean value, in absolute value.

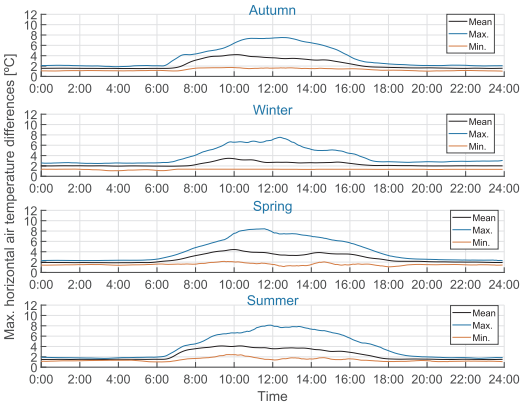

Fig. 17. Maximum horizontal air temperature differences.

Finally, Fig. 19 shows global maximum air temperature differences in the greenhouse. The maximum global air temperature difference is reached in spring and is 15.8 °C. It is observed that the mean value

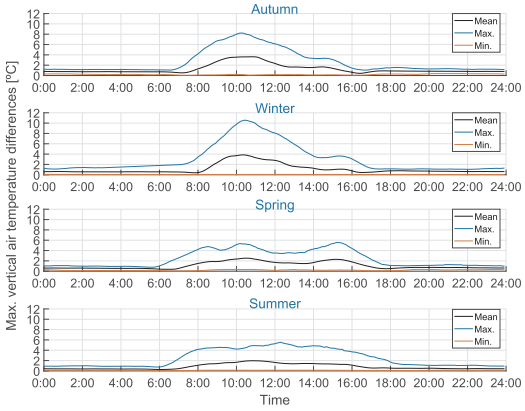

Fig. 18. Maximum vertical air temperature differences.

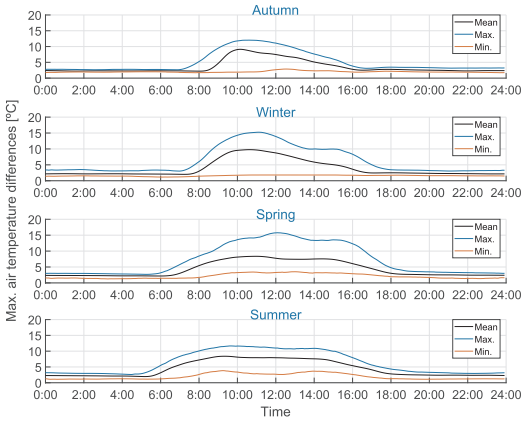

Fig. 19. Global maximum air temperature differences.

reaches more than 8 °C in all the seasons.

3.3. Relationship between air temperature and globe temperature inside the greenhouse

Greenhouse workers are exposed to diffuse solar radiation that goes through the plastic cover. This radiation is a factor to consider in the evaluation of the thermal conditions of the workers. Globe temperature is a qualitative measure of the incident radiation when compared with respect to the air temperature. Although to lesser extend tan direct solar radiation, diffuse solar radiation also causes an increment in globe temperature. Fig. 20 shows mean monthly air temperatures vs. mean monthly globe temperatures. Since including the 24 h of the day will do not give relevant information, especially at night, when air temperature and globe temperatures equals, the daily time interval included has been only from 10 to 15 h, when solar radiation is high (see Fig. 12). In Fig. 20, globe temperature vary from around 25 °C in December to more than 50 °C in July. The largest differences between globe temperature and air temperature occur in March and April (around 7–8 °C), while the shortest differences take place in November and December (around 4 °C). It can be observed that the consecutive monthly values draw a closed curve without loops. This representative curve shows that the diffuse solar radiation produces larger variations between globe temperature and air temperature in winter and spring than in autumn and

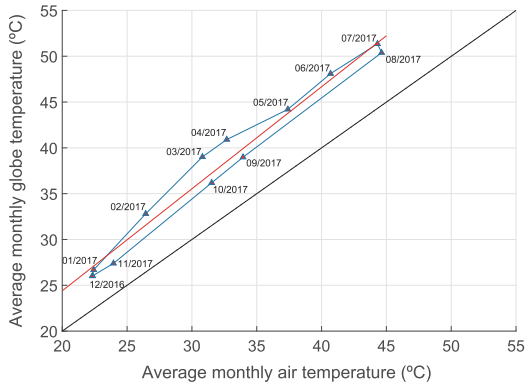

Fig. 20. Relationship between mean monthly air temperature and mean monthly globe temperature inside the greenhouse from 10:00 to 15:00 h.

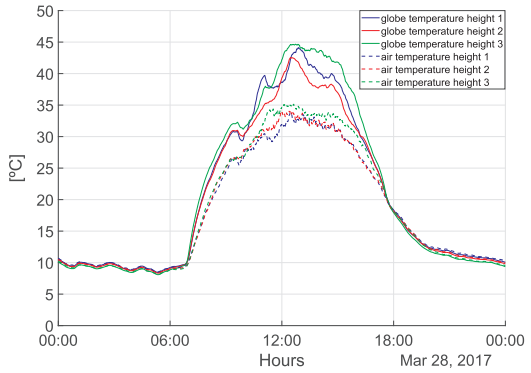

Fig. 21. Globe temperature and air temperature for the 3 heights measured during March, 28th 2017.

summer, respectively. In view of these results, although there is a trend to increase this difference when sun altitude is higher (summer solstice), this is not only related with the solar radiation, where in the months of June and July would achieve the maximum values.

In Fig. 21, globe temperature and air temperature for a day (March, 28th 2017) are plotted for the three heights measured. This day has been selected because is a day with high differences between globe temperature and air temperature, obtaining a maximum difference of 11.6 °C.

3.4. Recommendations for assessing the thermal environment inside greenhouses

Based on the results discussed above, the authors of this work propose the following recommendations for assessing the thermal environment inside a greenhouse:

- Any greenhouse will probably be a heterogeneous environment with respect to the air temperature according to the ISO 7726 Standard. Therefore, measurements must be taken at different locations, both horizontally and vertically, to asses the horizontal and vertical heterogeneity, respectively.
- Whether the environment must be considered heterogeneous or not is a condition that changes along the day. Larger air temperature differences usually take place at the central hours of the day, which also correspond with the highest values of air temperature. Therefore, it is recommended to include this period of time in the measuring schedule. Besides this, the work schedule of workers must be, obviously, also considered when designing the measurement schedule.
- The presence of clouds is a critical factor for the air temperature distribution inside the greenhouse. Cloudy days favour homogeneity, while also softening temperature values. Therefore, measurements should be scheduled preferably during sunny days.
- According to the ISO 7726, measurements must be taken at three heights (ankle, abdomen, and head) to evaluate the vertical heterogeneity. Regarding the horizontal heterogeneity, the Standard does not provide recommendations about the number of points or the places where measuring stations must be placed. The results obtained in the present work shows that the horizontal air distribution is conditioned by the azimuth and elevation of the sun. North–South and East–West air temperature differences have been observed along the greenhouse. Accordingly, at least four measurement points distributed with respect the Cardinal points are recommended.
- Greenhouse thermal conditions inside greenhouses are not controlled and show large variations along the year. For a complete evaluation of the heat stress or cold risk, the study should be extended along a complete year. Results provided in this work may be useful to select the most appropriate periods to evaluate the heat stress risk.
- Regarding the WSN used to gather the measurements, it is strongly recommended to place radio antennas at a height high enough to avoid the loss of line of sight between antenna pairs for each transmission link, taking into account the over-the-year growth of the crop. This becomes particularly important for radio bands in the GHz range, due to the strong absorption (attenuation) of radio waves by living (wet) plants.

4. Conclusions

This work has been focused on studying the air temperature distribution and its heterogeneity conditions in a “raspa y amagado” greenhouse through a complete year. The results provide experimental measurements for a typical greenhouse during a complete year, in an area where agriculture under plastic have a great influence in the economy and is an important source of employment. Until now, there is no deep study on the thermal conditions and risk of heat stress of the greenhouse workers that meets with ISO 7726 requirements. The measurements together with the measuring instruments used in the present work meet with the requirements and methods gathered in ISO 7726 to study the thermal environments. Therefore, the results obtained of air temperature distribution and heterogeneity conditions can be useful for further studies of the heat stress risk of workers.

Heterogeneity has been confirmed for large periods of time, in both vertical and horizontal directions. The study reveals that the environment is more heterogeneous horizontally than vertically. Besides, winter and summer are more homogeneous horizontally than autumn and spring whereas vertical heterogeneity is concentrated in cold seasons. Globally, Periods of time during the day of horizontal heterogeneity are greater than of vertical heterogeneity. It has been also observed a big influence of clouds in horizontal and vertical homogeneous days, with most cloudy days correlating with homogeneous days. Air temperature heterogeneity fundamentally depends on the sun, with heterogeneity happening in the central hours of the day and never at night. Also, the differences of temperature along the greenhouse has been observed in West-East and North–South direction according with the sun movement.

Plastic cover of greenhouses allows the incidence of diffuse solar radiation towards its interior. This is a factor to take into account for the evaluation of the thermal conditions of the workers, since it causes variations of up to around 12 °C between globe temperature and air temperature.

Finally, based on the results obtained some recommendations are presented for assessing the thermal environment of greenhouses.

Acknowledgment

The authors would like to thank to Research Contract Number 401250 of University of Almeriía for financing this study. Also to Laboratory-Observatory Andalusian Working Conditions in the Agricultural Sector (LASA), and to D. José Atienza Piedra and D. José Antonio López Martínez.

References

Balendonck, J., Sapounas, A.A., Kempkes, F., Van Os, E.A., Van Der Schoor, R., Van Tuijl, B.A.J., Keizer, L.C.P., 2014. Using a wireless sensor network to determine climate heterogeneity of a greenhouse environment. Acta Horticult. 1037, 539–546. http://dx.doi.org/10.17660/ActaHortic.2014.1037.67.

Bojacá, C.R., Gil, R., Cooman, A., 2009. Use of geostatistical and crop growth modelling to assess the variability of greenhouse tomato yield caused by spatial temperature variations. Comput. Electron. Agric. 65, 219–227. http://dx.doi.org/10.1016/j.compag.2008.10.001.

Boulard, T., Roy, J.-C., Pouillard, J.-B., Fatnassi, H., Grisey, A., 2017. Modelling of micrometeorology, canopy transpiration and photosynthesis in a closed greenhouse using computational fluid dynamics. Biosyst. Eng. 158, 110–133. http://dx.doi.org/10.1016/j.biosystemseng.2017.04.001.

Cabrera, A., Uclés, D., Agüera, T., 2016. Informes y Monografías/ Análisis de la campaña hortofrutícola de Almería 2015/2016 [Reports and monographs/ Analysis of the fruit and vegetable sector of Almería 2015/2016]. Almería, España. Fundación Cajamar (in Spanish). In: http://www.publicacionescajamar.es/pdf/series-tematicas/informes-coyuntura-analisis-de-campana/analisis-de-la-campana-hortofruticola-17.pdf (accessed 2018-02-26).

Callejón-Ferre, A.J., Manzano-Agugliaro, F., Díaz-Pérez, M., Carreño-Sánchez, J., 2011a. Improving the climate safety of workers in Almería-type greenhouses in Spain by predicting the periods when they are most likely to suffer thermal stress. Appl. Ergonom. 42, 391–396. http://dx.doi.org/10.1016/j.apergo.2010.08.014.

Callejón-Ferre, A.J., Pérez-Alonso, J., Carreño-Ortega, A., Velázquez-Martí, B., 2011b. Indices of ergonomic-psycholsociological workplace quality in the greenhouses of Almería (Spain): crops of cucumbers, peppers, aubergines and melons. Saf. Sci. 49, 746–750. http://dx.doi.org/10.1016/j.ssci.2010.12.009.

Callejón-Ferre, A.J., Pérez-Alonso, J., Sánchez-Hermosilla, J., Carreño-Ortega, A., 2009. Ergonomics and psycho-sociological quality indexes in greenhouses, Almería (Spain). Span. J. Agricult. Res. 7, 50–58. http://dx.doi.org/10.5424/sjar/2009071-397.

Carmona-Benjumea, A., 2001. Datos antropométricos de la población laboral española. Prevención, trabajo y salud: Revista del Instituto Nacional de Seguridad e Higiene en el Trabajo 14, 22–35. (accessed 2018-02-26), (in Spanish). http://www.insht.es/InshtWeb/Contenidos/Documentacion/TextosOnline/Rev_INSHT/2001/14/artFondoTextCompl.pdf .

Cecchini, M., Colantoni, A., Massantini, R., Monarca, D., 2010. Estimation of the risks of thermal stress due to the microclimate for manual fruit and vegetable harvesters in central Italy. J. Agricult. Saf. Health 16, 141–159. http://dx.doi.org/10.13031/2013.32040.

Chad, K.E., Brown, J.M.M., 1995. Climatic stress in the workplace: its effect on thermoregulatory responses and muscle fatigue in female workers. Appl. Ergonom. 26, 29–34. http://dx.doi.org/10.1016/0003-6870(95)95749-P.

Diano, M., Valentini, M., Samele, P., Di Gesu, I., 2016. Exposure to hot environments of horticultural greenhouses workers of the center of Calabria: evaluative comparison methods. Ital. J. Occupat. Environ. Hygiene 7, 56–114. (accessed 2018-02-26). http://refhub.elsevier.com/S0168-1699(17)30818-9/h0075 .

Ferentinos, K.P., Katsoulas, N., Tzounis, A., Bartzanas, T., Kittas, C., 2017. Wireless sensor networks for greenhouse climate and plant condition assessment. Biosyst. Eng. 153, 70–81. http://dx.doi.org/10.1016/j.biosystemseng.2016.11.005.

Granados, M.R., López, J.C., Bonachela, S., Hernández, J., Magán, J.J., 2016. Perfiles de temperatura en invernadero con acolchado negro y cultivo de pepino en periodos fríos. II Simposio Nacional de Ingeniería Hortícola. Almería, Spain (in Spanish).

Hernández, J., Bonachela, S., Granados, M.R., López, J.C., Magán, J.J., Montero, J.I., 2017. Microclimate and agronomical effects of internal impermeable screens in an unheated mediterranean greenhouse. Biosyst. Eng. 163, 66–77. http://dx.doi.org/10.1016/j.biosystemseng.2017.08.012.

ISO 7243:2017, 2017. Ergonomics of the thermal environment? Assessment of heat stress using the WBGT (wet bulb globe temperature) index. Standard International Organization for Standardization, Geneva, Switzerland.

ISO 7726:1998, 1998. Ergonomics of the thermal environment e instruments for measuring physical quantities. Standard International Organization for Standardization, Geneva, Switzerland.

ISO 7730:2005, 2005. Ergonomics of the thermal environment: analytical determination and interpretation of thermal comfort using calculation of the PMV and PPD indices and local thermal comfort. Standard International Organization for Standardization, Geneva, Switzerland.

ISO 8996:2004, 2004. Ergonomics of the thermal environment: Determination of metabolic rate. Standard International Organization for Standardization, Geneva, Switzerland.

ISO 9920:2007, 2007. Ergonomics of the thermal environment: Estimation of thermal insulation and water vapour resistance of a clothing ensemble. Standard International Organization for Standardization, Geneva, Switzerland.

Kittas, C., Bartzanas, T., Jaffrin, A., 2003. Temperature gradients in a partially shaded large greenhouse equipped with evaporative cooling pads. Biosyst. Eng. 85, 87–94. http://dx.doi.org/10.1016/S1537-5110(03)00018-7.

Kittas, C., Katsoulas, N., Bartzanas, T., Mermier, M., Boulard, T., 2008. The impact of insect screens and ventilation openings on the greenhouse microclimate. Trans. ASABE 51, 2151–2165. (accessed 2018-02-26). https://elibrary.asabe.org/abstract.asp?aid=25396 .

López, A., Valera, D.L., Molina-Aiz, F., Peña, A., 2012a. Sonic anemometry measurements to determine airflow patterns in multi-tunnel greenhouses. Span. J. Agricult. Res. 10, 631–642. http://dx.doi.org/10.5424/sjar/2012103-660-11.

López, A., Valera, D.L., Molina-Aiz, F.D., Peña, A., 2012b. Sonic anemometry to evaluate airflow characteristics and temperature distribution in empty mediterranean greenhouses equipped with pad–fan and fog systems. Biosyst. Eng. 113, 334–350. http://dx.doi.org/10.1016/j.biosystemseng.2012.09.006.

López, A., Valera, D.L., Molina-Aiz, F.D., Peña, A., 2013. Effectiveness of horizontal air flow fans supporting natural ventilation in a mediterranean multi-span greenhouse. Scient. Agricola 70, 219–228. http://dx.doi.org/10.1590/S0103-90162013000400001.

López-Martínez, J., Blanco-Claraco, J.L., Pérez-Alonso, J., Callejón-Ferre, A.J., 2018. Distributed network for measuring climatic parameters in heterogeneous environments: application in a greenhouse. Comput. Electron. Agric. 145, 105–121. http://dx.doi.org/10.1016/j.compag.2017.12.028.

Marucci, A., Pagniello, B., Monarca, D., Cecchini, M., Colantoni, A., Biondi, P., 2012. Heat stress suffered by workers employed in vegetable grafting in greenhouses. J. Food, Agric. Environ 10, 1117–1121. (accessed 2018-02-26). http://refhub.elsevier.com/S0168-1699(17)30818-9/h0205 .

Molina-Aiz, F.D., Valera, D.L., Álvarez, A.J., 2004. Measurement and simulation of climate inside Almería-type greenhouses using computational fluid dynamics. Agric. For. Meteorol. 125, 33–51. http://dx.doi.org/10.1016/j.agrformet.2004.03.009.

Okushima, L., Sase, S., Lee, I.-B., Bailey, B., 2001. Thermal environment and stress of workers in naturally ventilated greenhouses under mild climate. Acta Horticult. 559, 793–798. http://dx.doi.org/10.17660/ActaHortic.2001.559.118.

Parsons, K., 2013. Occupational health impacts of climate change: Current and future ISO Standards for the assessment of heat stress. Indus. Health 51, 86–100. http://dx.doi.org/10.2486/indhealth.2012-0165.

Pérez-Alonso, J., Callejón-Ferre, A.J., Carreño-Ortega, A., Sánchez-Hermosilla, J., 2011. Approach to the evaluation of the thermal work environment in the greenhouse-construction industry of SE Spain. Build. Environ. 46, 1725–1734. http://dx.doi.org/10.1016/j.buildenv.2011.02.014.

Riemer, R., Bechar, A., 2016. Investigation of productivity enhancement and biomechanical risks in greenhouse crops. Biosyst. Eng. 147, 39–50. http://dx.doi.org/10.1016/j.biosystemseng.2016.03.009.

Soni, P., Salokhe, V.M., Tantau, H.J., 2005. Effect of screen mesh size on vertical temperature distribution in naturally ventilated tropical greenhouses. Biosyst. Eng. 92, 469–482. http://dx.doi.org/10.1016/j.biosystemseng.2005.08.005.

Srbinovska, M., Gavrovski, C., Dimcev, V., Krkoleva, A., Borozan, V., 2015. Environmental parameters monitoring in precision agriculture using wireless sensor networks. J. Clean. Prod. 88, 297–307. http://dx.doi.org/10.1016/j.jclepro.2014.04.036.

Tong, G., Christopher, D., Li, B., 2009. Numerical modelling of temperature variations in a chinese solar greenhouse. Comput. Electron. Agricult. 68, 129–139. http://dx.doi.org/10.1016/j.compag.2009.05.004.

Vox, G., Losito, P., Valente, F., Consoletti, R., Scarascia-Mugnozza, G., Schettini, E., Marzocca, C., Corsi, F., 2014. A wireless telecommunications network for real-time monitoring of greenhouse microclimate. J. Agricult. Eng. 45, 70–79. http://dx.doi.org/10.4081/jae.2014.237.

Vox, G., Teitel, M., Pardossi, A., Minuto, A., Tinivella, F., Schettini, E., 2010. Sustainable Greenhouse Systems. Sustainable Agriculture: Technology, Planning and Management. Nova Science Publishers, Inc., New York, NY, USA Chapter 1, pp. 1–79.

Zhao, J., Zhu, N., Lu, S., 2009. Productivity model in hot and humid environment based on heat tolerance time analysis. Build. Environ. 44, 2202–2207. http://dx.doi.org/10.1016/j.buildenv.2009.01.003.

Zhao, Y., Teitel, M., Barak, M., 2001. SE–structures and environment: vertical temperature and humidity gradients in a naturally ventilated greenhouse. J. Agric. Eng. Res. 78, 431–436. http://dx.doi.org/10.1006/jaer.2000.0649.

Zorzeto, T.Q., Leal, P.A.M., 2017. Wireless sensor network to map the meteorological variability in a greenhouse with evaporative cooling. Acta Horticult. 1154, 213–220. http://dx.doi.org/10.17660/ActaHortic.2017.1154.28.

2.2. Publicación científica 2

Título: Uncertainty-aware Calibration of a Hot-Wire Anemometer With Gaussian Process Regression.

Autores: Rubén A. García-Ruiz, José L. Blanco-Claraco, Javier López-Martínez, y Ángel J. Callejón-Ferre.

Revista científica: IEEE Sensors Journal.

Volumen: 19.

Número: 17.

Páginas: 7515-7524.

Año: 2019.

doi: 10.1109/JSEN.2019.2915093

Datos JCR (Journal Citation Reports):

Factor de impacto (2018): 3.076.

Categoría: INSTRUMENTS & INSTRUMENTATION.

Ranking categoría: 13/61.

Cuartil: Q1.

Editor: IEEE-INST ELECTRICAL ELECTRONICS ENGINEERS INC.

País: Estados Unidos.

IEEE SENSORS JOURNAL, VOL. 19, NO. 17, SEPTEMBER 1, 2019 7515

Uncertainty-Aware Calibration of a Hot-Wire Anemometer With Gaussian Process Regression

Rubén A. García-Ruiz, José L. Blanco-Claraco, Javier López-Martínez, and Ángel J. Callejón-Ferre

***Abstract*— Expensive ultrasonic anemometers are usually required to measure wind speed accurately. The aim of this work is to overcome the loss of accuracy of a low cost hot-wire anemometer caused by the changes of air temperature, by means of a probabilistic calibration using Gaussian Process Regression. Gaussian Process Regression is a non-parametric, Bayesian, and supervised learning method designed to make predictions of an unknown target variable as a function of one or more known input variables. Our approach is validated against real datasets, obtaining a good performance in inferring the actual wind speed values. By performing, before its real use in the field, a calibration of the hot-wire anemometer taking into account air temperature, permits that the wind speed can be estimated for the typical range of ambient temperatures, including a grounded uncertainty estimation for each speed measure.**

***Index Terms*— Sensor calibration, Gaussian processes, hot-wire anemometer.**

I. Introduction

HOT-WIRE sensors are low-cost devices usually employed to measure wind speed, and sometimes the speed of other fluids. They comprise a thin metallic wire with a typical diameter in the range 0.5-5 μm, and a length of 1 mm. They are usually made of platinum, tungsten, or platinum-iridium.

Their operating principle consists in heating the wire with an electric current (Joule effect) up to some temperature above the ambient and then exposing it to the incident fluid flow such that it is cooled by, mainly, convective heat transfer. The fluid velocity can then be inferred as a function of the heat transfer from the heated wire and the fluid. Hot-wire anemometers can be classified, depending on their control architecture, into: constant-temperature anemometer (CTA), constant-current anemometer (CCA), and constant-voltage anemometer (CVA). The difference between them depends on the variable whose set-point is the input of the control circuitry, namely, resistance temperature, electric current, or applied voltage, respectively.

Hot-wire anemometers have been used for decades in a wide range of applications that require measuring the speed of a fluid [1]–[4]. In particular, they are well suited for low-flow rate measurements, and manufacturers often recommend its use for low to medium wind speeds. As will be seen in section III.C, a good performance has been observed for speeds up to 20 m/s, and we would not recommend using this kind of sensors for higher speeds. The reason is twofold: (a) the error and the uncertainty of the prediction would increase, and (b) due to the mechanical fragility of the sensor. Although a minimum detectable velocity is not provided by the manufacturer of the sensor at test in this work, this research found that small changes in the range 0.1-0.2 m/sare resolvable.

Hot-wire anemometers are nowadays widely-used for their high measuring bandwidth, which allows detecting fast velocity fluctuations. Their small size and low weight also make them suitable for applications with limited space. They are easy to handle, low cost and additionally, they require very little power to operate, enabling their use in battery-powered devices [5].

Calibration of hot-wire anemometers is typically carried out for some predefined *constant temperature*. This becomes one of the main disadvantages of this type of sensors [6]: if they operate inside a fluid flow at a different temperature than the one used during the calibration, measurements will not be accurate. Some authors have developed different methods for correcting wind speed measurements in hot-wire anemometers [7]–[10]. These methods typically require other application-specific parameters such that the kinematic viscosity and thermal conductivity of the fluid. However, air temperature has a significant influence in wind speed corrections [11], [12].

Most practical applications of wind speed sensing imply operating at temperatures that vary through the day and the different seasons in the year. Even if the sensor works isolated or covered, the temperature might still present significant variations. It is well-known that readings from hot-wire anemometers depend on both, the ambient and the wire

Manuscript received April 30, 2019; accepted May 2, 2019. Date of publication May 7, 2019; date of current version August 6, 2019. This work was partly supported by the University of Almería under Research Contract no. 401250, the Andalusian Laboratory-Observatory of Working Conditions in the Agricultural Sector (LASA), and the National R+D+i Plan Project DPI2017-84259-C2-1-R of the Spanish Ministry of Economy, Industry and Competitiveness. The associate editor coordinating the review of this paper and approving it for publication was Dr. Cheng-Ta Chiang. *(Corresponding author: Rubén A. García-Ruiz.)*

R. A. García-Ruiz, J. L. Blanco-Claraco, and J. López-Martínez are with the Agrifood Campus of International Excellence, Department of Engineering, University of Almería, Research Center CIMEDES (CeiA3) (e-mail: rgr051@ual.es; jlblanco@ual.es; javier.lopez@ual.es).

Á. J. Callejón-Ferre is with the Agrifood Campus of International Excellence, Department of Engineering, University of Almería, Research Center CIMEDES (CeiA3), and also with the Laboratory-Observatory Andalusian Working Conditions in the Agricultural Sector (LASA), 41092 Seville, Spain (e-mail: acallejo@ual.es).

Digital Object Identifier 10.1109/JSEN.2019.2915093

temperature [7]–[10]. For this reason, we need to consider ambient temperature as an extra variable to obtain wind speed from their non-linear relationship (generally, wire temperature is always considered).

The present work proposes using machine learning (ML) techniques to approach this calibration problem. In particular, we show how *Gaussian Process Regression* (GPR) [13] has the best performance from all the methods included in our comparison. A *Gaussian Process* (GP) is a distribution over functions, and GPR is a non-parametric, Bayesian, supervised learning method, with wide applications in the industry and academic research [14]–[16]. In a nutshell, GPR takes a set of samples and builds a model from them by estimating the posterior joint probability of the GP, hence building a model able to make predictions about values not observed in the samples. A key characteristic of GP is its capability of providing a *measure of uncertainty* for each prediction. Also, a GPR can express any prior knowledge, e.g. from a human expert, by means of *a priori* probability density functions. It has a good adaptability in dealing with complex non-linear problems with small samples.

In comparison to other non-linear, widely-used machine learning methods such as Support Vector Machines (SVM) [17]–[20] or Artificial Neural Networks (ANN) [21]–[23], GPR has the advantages of being easier to implement, self-adaptive to enable superior parameter estimation, flexible enough to make non-parametric inferences [24], and providing a grounded estimation for the output uncertainty. We claim that the latter is of paramount importance for any engineering process, since any physical measurement, direct or indirect, should be accompanied by its expected accuracy.

The main contribution of the present work is two-fold: (i) we discuss and justify what metrics should be observed to decide among different competing regression techniques in order to select the one with the best predictive performance, and (ii) we apply such methodology to the study of how a low-cost hot-wire anemometer can be calibrated by means of machine learning techniques to overcome its most important drawback, namely its loss of accuracy when air temperature changes. The result is the identification of a method that enables the use of low-cost anemometers with reasonable accuracy within a typical range of ambient temperatures, therefore enabling its use in a wide range of applications where the low cost of these devices might be a significant advantage, for example, in large networks of sensors.

This paper is organized as follows. First, the theoretical bases of GPR are introduced in Section II. The experimental setup and the metrics used for the evaluation of the model are detailed in Section III, together with the experimental results and its discussion. Finally, some conclusions are drawn in Section IV.

II. Background

This section first provides a brief summary of common regression techniques, including Gaussian Process Regression (GPR), and then introduces the basis of GPR for the particular setup employed in this work with a greater detail, given the importance of this method in subsequent experimental results.

A. Regression Methods

Regression is the problem of finding a suitable model to predict the values of one or more dependent variables (outputs) given the known values of the independent variables (inputs). Each one of the existing regression models typically has a small number of *parameters* which must be *learned* or *fitted* from training data: pairings of input and output variables.

Next, we enumerate the different regression methods included in our comparison (refer to Table II), as named in their reference implementation from MATLAB's *Statistics and Machine Learning Toolbox* (SMLT). In-depth reviews on each technique can be found elsewhere in the vast related bibliography [25]–[29].

Linear regression models [27] are easy to interpret and fast to evaluate, but often lack a precise predictive accuracy.

Regression trees are non-parametric models which naturally define subgroups, scale well with the complexity of the data, and are not limited by the number of predictor variables [30]. They are easy to interpret, fast for fitting and predicting, and have a reduced memory cost.

Support Vector Machine (SVM) regression is a nonparametric technique, relying on kernel functions, where data are mapped into a high dimensional feature space via nonlinear mapping, after which a linear regression is performed in this feature space [25]. Linear SVMs are easy to interpret, but may have low predictive accuracy, while nonlinear SVMs are more difficult to interpret, but can be more accurate. The SVM regressions compared in this work are:

- Linear: the kernel function is linear. The model flexibility is low.
- Quadratic: the kernel function is quadratic. The model flexibility is medium.
- Cubic: the kernel function is cubic. The flexibility of the model is medium.
- Fine, medium, and coarse: These models are the same except for different Kernel scale values of $\sqrt{P}/4$, $\sqrt{P}$, and $4\sqrt{P}$, respectively, with P the number of predictors. The response function of "fine" is well-suited for rapid variations, while "coarse" better fits very slowly-varying signals.

Ensembles of Trees combine several regression trees to achieve better predictive performance than the corresponding single regression trees [31]. The following versions are compared:

- Boosted Trees: it consists in least-squares boosting with regression tree learners. The model flexibility is medium-high.
- Bagged Trees: it consists in bootstrap aggregating or bagging, with regression tree learners. The flexibility of this model is high.

Gaussian Process Regression provides a probabilistic model on the space of functions, as discussed in Section II-B. MATLAB's toolbox implementation automatically fits the method flexibility to offer a small error while simultaneously

protecting against overfitting. Kernel functions that are frequently used in the literature are: Rational Quadratic, Squared Exponential, Matern 5/2, and Exponential.

B. Background on Gaussian Process Regression

Consider a training data set $\mathbf{D}$ of n observations, $\mathbf{D} = \{(\mathbf{x}_i, y_i)|i = 1, \ldots, n\}$, where $\mathbf{x}$ is an input vector of dimension N, and y is a scalar output or target. Given a new input $\mathbf{x}^*$ (test input), the goal of the regression is to obtain the predictive distributions that have not been seen in the training set. On the basis of training data, the aim is to obtain a function that makes predictions for all possible input values. To carry out this, assumptions about the characteristics of the underlying function must be made, as otherwise any function which is consistent with the training data would be equally valid.

GPs can be seen as a generalization of the Gaussian probability distribution to a distribution over *functions*. A GP performs inference directly in the space of functions, giving a prior probability to each possible function (where higher probabilities are given to functions that are considered to be more likely) and learning the target function from the training data.

The specification of the prior is important, because it fixes the properties of the functions considered for inference. These properties are entirely dictated by the covariance function, which is symmetric and positive semi-definite for any input point $\mathbf{x}$. The covariance function specifies the covariance between two or more random variables and, typically, the covariance functions have a number of free parameters called hyperparameters. Finding suitable hyperparameters for the covariance function is the biggest problem of learning in GP. The hyperparameters give us a model of the data and characteristics (such as smoothness, length-scale and stationary) which we can interpret. Thus, the covariance function is the most important factor in order to control the properties of a GP, thus it must be carefully selected [11], [32]. In our study, we will use different covariance functions and we will compare them in order to choose the one achieving the best predictive performance for our training data set.

A GP over a function (to be estimated) $f : \mathbb{R}^N \to \mathbb{R}$ is entirely specified by its mean function, $m(\mathbf{x})$, and a covariance function, $\mathbf{k}(\mathbf{x}, \mathbf{x}')$, for any two points of the state space $\mathbf{x}, \mathbf{x}' \in \mathbb{R}^N$, such that:

$$m(\mathbf{x}) = \mathbb{E}[f(\mathbf{x})] \tag{1}$$

$$\begin{aligned}\mathbf{k}(\mathbf{x}, \mathbf{x}') &= cov(f(\mathbf{x}), f(\mathbf{x}')) \\ &= \mathbb{E}[(f(\mathbf{x}) - m(\mathbf{x}))(f(\mathbf{x}') - m(x'))]\end{aligned} \tag{2}$$

and the GP itself is denoted as:

$$f(\mathbf{x}) \sim GP(m(\mathbf{x}), \mathbf{k}(\mathbf{x}, \mathbf{x}')) \tag{3}$$

where we used $a \sim b$ to denote "a follows the probability distribution b". In practice, we should also take into account the *noise*, which is customarily assumed to be an additive, independent identically distributed (i.i.d.) Gaussian noise ε with zero mean and variance σ_n^2, that is:

$$y = f(\mathbf{x}) + \varepsilon, \quad \varepsilon \sim \mathcal{N}(0, \sigma_n^2) \tag{4}$$

and where $\mathcal{N}(\cdot, \cdot)$ denotes the multivariate Gaussian or normal distribution with the given mean and covariance matrix. For the sake of simplicity in notation, the mean function is usually taken to be zero and we will consider it in this way (note that the mean of the posterior process is not confined to be zero). Then, the prior distribution of the observation target y is:

$$y \sim \mathcal{N}(0, \mathbf{K}(\mathbf{X}, \mathbf{X}) + \sigma_n^2 \mathbf{I}_n), \quad \text{with } \mathbf{K}(\mathbf{X}, \mathbf{X}) = (K_{ij})_{n \times n} \tag{5}$$

where $\mathbf{X}$ denotes the $n \times N$ matrix of the n training samples of dimensionality N, $K(\cdot, \cdot)$ refers to the matrix with the entries given by the covariance function $k(\cdot, \cdot)$ being the matrix elements $K_{ij} = k(x_i, x_j)$ and $\mathbf{I}_n$ is the n-dimensional identity matrix.

The joint probability distribution of the training and test sets according to the definition of GP follow a Gaussian distribution. Then, the joint distribution of the observed target values ($\mathbf{y}$) and the test function at new inputs values (f_*) is:

$$\begin{bmatrix} \mathbf{y} \\ f_* \end{bmatrix} \sim \mathcal{N}\left(\mathbf{0}_{n \times 1}, \begin{bmatrix} \mathbf{K}(\mathbf{X}, \mathbf{X}) + \sigma_n^2 \mathbf{I}_n & \mathbf{K}(\mathbf{X}, \mathbf{X}_*) \\ \mathbf{K}(\mathbf{X}_*, \mathbf{X}) & \mathbf{K}(\mathbf{X}_*, \mathbf{X}_*) \end{bmatrix}\right) \tag{6}$$

where, in a similar way to X, X_* is defined as the $n \times N$ matrix of the n testing N-length input vectors.

Conditioning the prior to the observed training outputs and taking into account that the posterior distribution over functions is also a Gaussian, we obtain the key predictive equations for GPR:

$$\begin{aligned}\overline{f_*} &\triangleq \mathbb{E}[f_*|\mathbf{X}, \mathbf{y}, \mathbf{X}_*] \\ &= \mathbf{K}(\mathbf{X}_*, \mathbf{X})[\mathbf{K}(\mathbf{X}, \mathbf{X}) + \sigma_n^2 \mathbf{I}_n]^{-1}\mathbf{y}\end{aligned} \tag{7}$$

$$\begin{aligned}\mathbf{cov}(f_*) = &\mathbf{K}(\mathbf{X}_*, \mathbf{X}_*) - \mathbf{K} \cdot \\ &\cdot(\mathbf{X}_*, \mathbf{X})[\mathbf{K}(\mathbf{X}, \mathbf{X}) + \sigma_n^2 \mathbf{I}_n]^{-1}\mathbf{K}(\mathbf{X}, \mathbf{X}_*)\end{aligned} \tag{8}$$

where $\overline{f_*}$ and $\mathbf{cov}(f_*)$ are the estimated mean of the predictive distribution and its covariance matrix, respectively. Therefore, given a test sample, and on the basis of the training set and covariance function, a GPR model can predict a mean value $\overline{f_*}$ (our best estimation for $\mathbf{y}_*$) and a variance which represents the uncertainty of the estimated output.

C. Hyperparameters Selection

The selection of hyperparameters, together with the choice for the covariance function, are the key design factors of GPR. Selection of optimal hyperparameters, stacked in the vector $\boldsymbol{\theta}$, is done by maximizing the marginal likelihood function $p(\mathbf{y}|\mathbf{X}, \boldsymbol{\theta})$. However, following the common practice, due to its superior numerical stability and efficiency, the corresponding negative log likelihood is minimized instead:

$$\log p(\mathbf{y}|\mathbf{X}, \boldsymbol{\theta}) = -\frac{1}{2}\mathbf{y}^T \mathbf{K}_y^{-1}\mathbf{y} - \frac{1}{2}\log|\mathbf{K}_y| - \frac{n}{2}\log 2\pi \tag{9}$$

where $\mathbf{K}_y = \mathbf{K}(\mathbf{X}, \mathbf{X}) + \sigma_n^2 \mathbf{I}_n$ is the covariance matrix for the output vector $\mathbf{y}$. The negative log marginal likelihood is a statistical technique used for estimating the optimal parameters of a model. The first term ($-\frac{1}{2}\mathbf{y}^T \mathbf{K}_y^{-1}\mathbf{y}$) measures how well the model fits the data, the second term ($-\frac{1}{2}\log|\mathbf{K}_y|$) is a complexity penalization term and the third term ($-\frac{n}{2}\log 2\pi$) is a normalization constant.

(a)

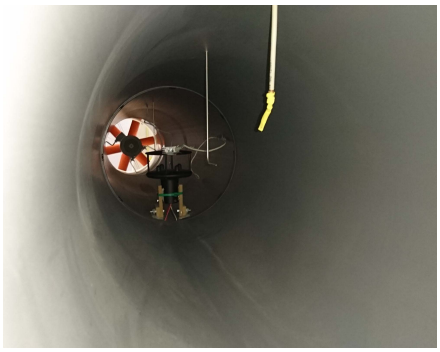

(b)

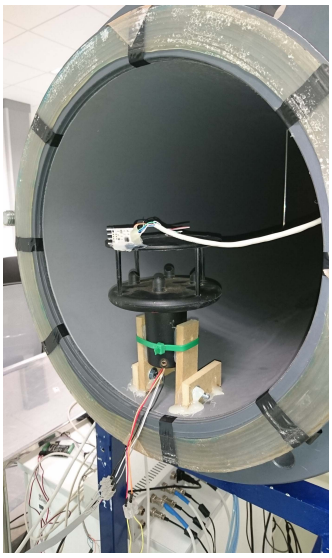

(c)

Fig. 1. Wind tunnel used in this work. (a) Overview of the entire system. (b) View of inside of the tunnel, where the temperature and wind sensors are installed. (c) Detail view of the placing of sensors, with the tunnel split in two during the experiment preparation.

To find out the minimum of Eq. (9) and, consequently to find the optimal hyperparameters, the conjugate gradient method is usually used. The conjugate gradient is an iterative method of optimizing functions based on gradient-ascent. The calculation of the partial derivatives of the log marginal likelihood with respect to the hyperparameters is required [13]:

$$\frac{\partial}{\partial \boldsymbol{\theta}_i} \log p(\mathbf{y}|\mathbf{X}, \boldsymbol{\theta}) = \frac{1}{2}\mathbf{y}^T \mathbf{K}_y^{-1} \frac{\partial \mathbf{K}_y}{\partial \boldsymbol{\theta}_i} \mathbf{K}_y^{-1}\mathbf{y} \tag{10}$$

$$-\frac{1}{2} tr(\mathbf{K}_y^{-1} \frac{\partial \mathbf{K}_y}{\partial \boldsymbol{\theta}_i})$$

$$= \frac{1}{2} tr((\boldsymbol{\alpha}\boldsymbol{\alpha}^T - \mathbf{K}_y^{-1}) \frac{\partial \mathbf{K}_y}{\partial \boldsymbol{\theta}_i}) \tag{11}$$

where $tr(\cdot)$ is the trace of its matrix argument, and $\boldsymbol{\alpha} = \mathbf{K}_y^{-1}\mathbf{y}$.

One of the main drawbacks of GPR is the complexity of computing the marginal likelihood because of the matrix inverse operation. In theory, it has a complexity of $\mathcal{O}(n^3)$ with n the dimension of training inputs. Although efficient factorizations can be applied (e.g. Cholesky) instead of naive matrix inversion, this operation still remains as a bottleneck of the training procedure.

III. Case Study

A. Experimental Setup

Experiments were carried out inside a wind tunnel at the University of Almería (Spain). The tunnel has a length of 4.74 m, a circular cross-section of 38.8 cm diameter, contraction ratio of 1:5:32 and the coefficient between the entrance diameter and the length of the contraction section is 0.92 [33], [34]. An axial fan (Model HCT-45-2T-3/AL, Sodeca S.A., Sant Quirze of Besora, Spain) induces the air flow in the wind tunnel, and a Micromaster 420 Inverter (Siemens Energy & Automation Inc., Alpharetta, GA, USA) is used to control the fan speed, by modulating the current frequency between 0 and 50 Hz.

The anemometer under calibration is a hot-wire anemometer of the popular model "revision C" by "Modern Device". To perform the calibration we rely on a more reliable anemometer, model "Windsonic" by Gill Instruments Ltd, as ground truth. The latter is an ultrasonic anemometer, with a measurement range of 0 to 60 m/s and a precision of $\pm$ 2%. In addition, air temperature is measured by means of a PT100 in order to improve the accuracy of the hot-wire anemometer own temperature measurements.

In order to achieve the calibration of the wind sensor, it is necessary to find the relationship (if it exists) between the inputs and outputs, such that the calibrated model predicts outputs as close as possible to the real values. The inputs of our system are considered to be the raw voltage readings from the hot-wire anemometer and the air temperature from the PT100 sensor, while the output of the system is the wind speed measured from the ultrasonic anemometer. Data of these three sensors (voltage of hot-wire anemometer in volts, air temperature in Celsius degrees and wind of ultrasonic anemometer in meters per second) were measured every 2 seconds while wind speed was varied between 0 and 21 m/s. The controller allows changing the speed continuously (e.g. a velocity ramp) but speed was increased step by step instead, in order to allow the flow inside the tunnel to stabilize. We waited 20 seconds

after each speed change to ensure that both the sensor and the flow were stable before picking a measure for the dataset. Several campaigns of measurements were performed at different temperatures from 19 to 30 °C.

The measurement cycle was similar for all temperatures at test: starting at 0 m/s, the wind speed was increased in small steps, while attempting to provide a good sampling of low to medium wind speeds, where hot-wire anemometers are more reliable and find their most common working conditions. Therefore, our experiments mainly focus on wind speed values up to 10-15 m/s, approximately. On the other hand, wind speed was increased modulating the current frequency manually and waiting for a determined time to stabilization and then for another time period to allow enough data records to be grabbed. These periods were measured manually, hence the existence of more data in some measure cycles. Overall, more than 4000 input-output data points were obtained.

B. Evaluation of the Model

To assess the performance of the model, different metrics have been used:

- *Mean Absolute Error (MAE):* it measures the average of all absolute errors between predictions and ground truth values. It reveals how similar the predicted values are to the ground truth values. $MAE = \frac{1}{n}\sum_{i=1}^{n} |y_i - \hat{y}_i|$, where y_i is the ground truth value of the i-th sample, and $\hat{y}_i$ is the corresponding predicted value.
- *Root Mean Square Error (RMSE):* it measures the square root of the average of all squared absolute errors between predictions and ground truth values. It reveals the overall deviation of both values. $RMSE = \sqrt{\frac{1}{n}\sum_{i=1}^{n} |y_i - \hat{y}_i|^2}$, where y_i is the ground truth value of the i-th sample, and $\hat{y}_i$ is the corresponding predicted value.

Models having low MAE and RMSE are preferred. Both metrics evaluate the model prediction error and are indifferent to the sign of error. The main differences between them is that RMSE gives a relatively high weight to large errors, since the errors are squared before they are averaged. For that reason, RMSE is preferred when large errors are particularly undesirable.

- *Coefficient of determination or R^2:* it provides a measure of how well future samples are likely to be predicted by the model. The value of R^2 always lies between -1 and $+1$. Values close to zero represent no association between the variables, whereas values close to -1 or 1 indicate strong relationship between predictions and ground truth values.

$$R^2 = 1 - \frac{\sum_{i=1}^{n} (y_i - \hat{y}_i)^2}{\sum_{i=1}^{n} (y_i - \overline{y})^2}, \text{ where: } \overline{y} = \frac{1}{n}\sum_{i=1}^{n} y_i \quad (12)$$

where $\overline{y}$ is the average of the ground truth values, y_i is the ground truth value of the i-th sample and $\hat{y}_i$ is the corresponding predicted value.

C. Experimental Results and Discussion

Next, we expose the experimental validation of the proposed GPR-based wind speed estimator. The flow chart of the calibration process can be seen in figure 2. As it can be observed in figure 2, the entire training set has been used to train the GPR model: both the matrix X, corresponding to hot-wire anemometer voltage and air temperature, and the vector Y corresponding to the real wind speed measured with the ultrasonic anemometer. Once the model has been trained, the matrix X_* of the test set (hot-wire anemometer voltage and air temperature) is used to predict wind speed and obtain the corresponding confidence interval. Finally, the vector Y_* (real wind speed) of the test set is used to analyze the error committed and evaluate the GPR model.

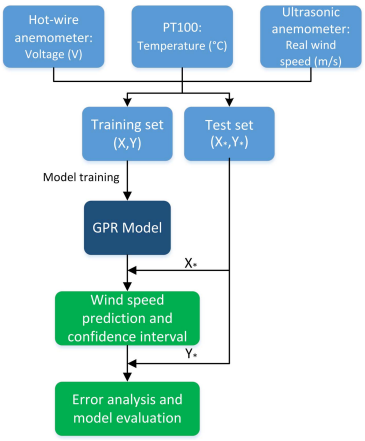

Fig. 2. Flow chart describing the proposed calibration and validation process.

TABLE I
TRAINING AND TEST SETS SELECTED IN SECTION III.C.3

	Traning set	**Test set**
Section III.C.1	Cross Validation with 6 folds (4112 points)	
Section III.C.2	4112 points	
Section III.C.3	70% (2878 points)	30% (1234 points)
Section III.C.4a	3583 points	529 points
Section III.C.4b	2691 points	1421 points
Section III.C.4c	3319 points	793 points
Section III.C.4d	3554 points	558 points
Section III.C.5	70% (2878 points)	30% (1234 points)

Different sizes of data are included in the training and test sets. In Table I are summarized the number of points selected for the training and test sets in the GPR model for each subsection of Section III.C.

To ensure a correct estimation of credible intervals,[1] the GPR model needs to account for the additive Gaussian noise employed in the model [16]. MATLAB's toolbox for Gaussian process models optimizes the standard deviation of that noise, denoted as "Sigma", while training from a given input data set. Finally, when the GPR model makes a prediction, it also generates a prediction interval by considering the uncertainty of both, the additive noise (the "Sigma" value),

[1]Although in most Engineering literature the term used is "confidence interval", according to [35], [36] in the Bayesian Statistics "credible interval" is a more accurate term.

TABLE II

EVALUATION OF DIFFERENT REGRESSION MODELS FOR OUR WIND SPEED DATASET. (LR: LINEAR REGRESSION; RT: REGRESSION TREE; SVM: SUPPORT VECTOR MACHINE; ET: ENSEMBLES OF TREES; GPR: GAUSSIAN PROCESS REGRESSION

Model	**MAE (m/s)**	**RMSE (m/s)**	**R^2**
LR: Linear	1.4243	1.8351	0.82
LR: Interactions Linear	1.4238	1.8354	0.82
LR: Robust Linear	1.3403	1.9453	0.80
LR: Stepwise Linear	1.4243	1.8351	0.82
RT: Fine Tree	0.1843	0.3304	0.99
RT: Medium Tree	0.2384	0.4086	0.99
RT: Coarse Tree	0.4091	0.6579	0.98
SVM: Linear	1.3240	1.9231	0.80
SVM: Quadratic	0.6526	0.8154	0.96
SVM: Cubic	3.7074	5.4092	-0.55
SVM: Fine Gaussian	0.3327	0.4224	0.99
SVM: Medium Gaussian	0.3899	0.5156	0.99
SVM: Coarse Gaussian	0.5761	0.7449	0.97
ET: Boosted Trees	0.4181	0.5974	0.98
ET: Bagged Trees	0.2349	0.3682	0.99
GPR: Rational Quadratic	0.1699	0.2820	**1.00**
GPR: Squared Exponential	0.1964	0.3122	0.99
GPR: Matern 5/2	0.1808	0.2918	**1.00**
GPR: Exponential	**0.1582**	**0.2776**	**1.00**

and the uncertainty value of the parameters learned from the data.

1) Comparison of Regression Methods: First, it is convenient to assess whether GPR is the best technique for the data under study, in terms of being able to make accurate predictions. To verify this fact, we trained multiple regression models and evaluated their "validation" errors. These process was carried out with MATLAB's regression Learner App, included in the Statistics and Machine Learning Toolbox. The entire data set was used to training the models, and Cross Validation was used with 6 folds. Folds can be understood as subsets of data. Cross Validation partitions the data in folds, trains the model using the out-of-fold observations, assesses the model performance using in-fold data and finally calculates the average test error over all folds. This method makes an efficient use of all the data and permits to obtain a good estimation of the predictive accuracy of the final model. The resulting errors of the regression models are shown in Table II.

The results confirm that Gaussian Process Regression is the regression model that best fits the data. In particular, Gaussian Process Regression with exponential as covariance function produce the lowest MAE and RMSE, and a good value of R^2.

2) Information-Based Comparison of GPR Models: In order to compare the GPR models, the Bayesian Information Criterion (BIC) [37], [38] has been used. BIC is a metric based on the on the highest posterior probability to finding the best model for make predictions. BIC model is defined as:

$$BIC = -2\ L + m \log n \tag{13}$$

where L denotes the log marginal likelihood, p the number of Kernel parameters and n the number of data points employed in the model. The model fits better the data when lower value of BIC is obtained. The likelihood takes into account both, how close the predicted values are to ground-truth, and how large is the predicted uncertainty.

TABLE III

COMPARISON BETWEEN THE DIFFERENT GPR MODELS AT TEST, USING AN INFORMATION-BASED CRITERION (BIC)

Kernel function	Log marginal likelihood (L)	Kernel parameters (m)	Number of data points (n)	**BIC**
Rational Quadratic	-868,5	3	4112	1748.9
Squared Exponential	-1115,1	2	4112	2237.5
Matern 5/2	-964,7	2	4112	1936.7
Exponential	**-755,4**	2	4112	**1518.1**

TABLE IV

RESULTS OF MAE, RMSE AND R^2 FOR TRAINING AND TEST POINTS, OF THE GPR MODEL WITH EXPONENTIAL AS COVARIANCE FUNCTION, USING RANDOMLY-SELECTED 70% OF ALL DATA POINTS FOR TRAINING AND THE OTHER 30% FOR TESTING

	MAE (m/s)	**RMSE (m/s)**	**R^2**
Training	0.0958	0.1718	0.99846
Test	0.1620	0.2833	0.99563

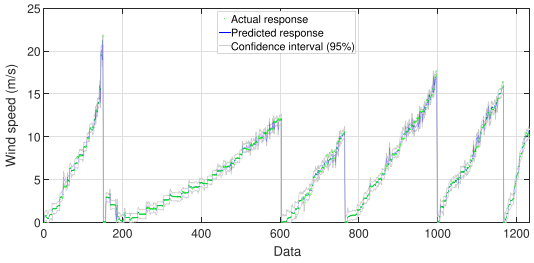

Fig. 3. Predictions, 95% credible interval of the GPR model and real wind values for the test points. Each individual ramp represents data from a run at a different ambient temperature.

Table III shows the BIC obtained for each GPR model, where it is clear that GPR model with exponential as covariance function is the best one, in accordance with the metrics MAE, RMSE, and R^2 discussed above.

3) Cross Validation of GPR: Method 1: Gaussian Process Regression with exponential covariance function is applied to the data. Training points are selected randomly and constitute the 70% of the full data, whereas test points are the remaining 30%. The training and test sets are normalized in [0,1] and the optimal hyperparameters are obtained through the conjugate gradient method. The predictions and the variance are calculated with the training and test sets using Matlab2017b. The results of the GPR model are summarized in Table IV, where it can be seen the MAE, RMSE and R^2 values for both training and test points. MAE and RMSE for test points are 0.1620 m/s and 0.2833 m/s, respectively, while R^2 for these test points is also high (0.99563); ultimately, errors in the prediction are therefore small.

In Figure 3 are presented the predictions of the GPR model for the test points, along with the estimation 95% credible interval and the ground truth values corresponding to the ultrasonic anemometer. As it can be observed, the predicted values are close to the real ones and the real values in almost

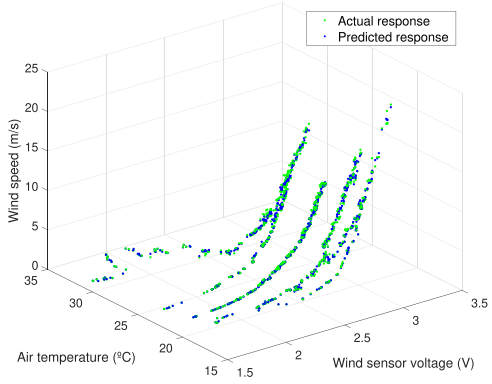

Fig. 4. Predictions and real wind values for the test points, plotted as raw voltage output from the hot-wire anemometer vs. air temperature. Each filament-like cluster of data points represents a run at a different room temperature.

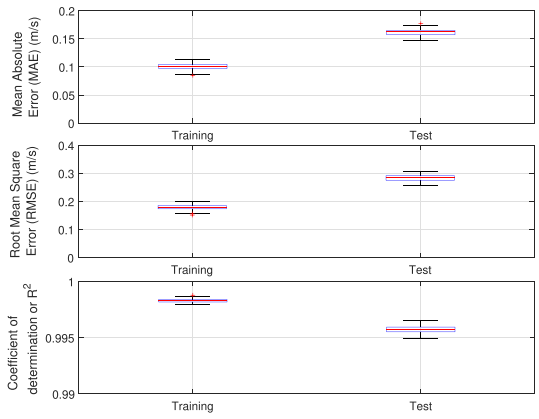

Fig. 5. Boxplot of MAE, RMSE, and R^2 of the GPR model for 100 iterations with different training (70% of all data set points) and test sets (the remaining 30%). As expected, in any cross-validation test the performance obtained for the training set is better than that for the test subset of the data.

all the cases fall within the credible interval, which indicates a high accuracy in the GPR model.

In Figure 4, the same predictions and ground truth values are shown in 3D along with the voltage of the hot-wire anemometer and the air temperature. It can be observed the strong relationship between both variables and also the accuracy of the predictions.

The results are obviously influenced by the training data, which are selected randomly. It could be thought that with other training data, worse results would be obtained. To evaluate it, 100 iterations have been done selecting randomly different training sets and consequently test sets, always complying that 70% of the data is used for training and the remaining 30% for test. The results of the evaluation of the model are shown in a boxplot in Figure 5. On each box, the red line is the median, the box edges are the 25th and 75th percentiles, the whiskers include until the most extreme data points not considering outliers, which are represented individually as red crosses. Similar MAE, RMSE and R^2 are obtained, which indicates that the model gives a good approximation of the real wind as function of the hot-wire anemometer voltage and air temperature.

4) Cross Validation of GPR: Method 2: As an alternative cross validation of GPR to predict wind speed, we now propose to select training and testing sets, not as a given fraction of the overall data set, as done in the previous section, but selecting entire dataset runs for some given temperature values. In this case the GPR is trained *without* any single observation of the sensor response for some specific temperature, and we will evaluate its performance in *inferring* ("interpolating") its behavior from the response at other temperatures.

Part of the results are shown in Figure 6. In this case, the average RMSE of all cases is 0.024 m/s for the training datasets and 1.734 m/s for the testing datasets. The average MAE is 0.012 m/s and 1.373 m/s for the training and testing datasets, respectively. As expected, these values are similar to the results in Table IV for the training parts, but much higher for the test datasets. This could be explained by the lack of information the GPR has to make predictions about the sensor behavior in conditions it has not been able to learn from. However, it is remarkable that the probabilistic nature of GPR allows to have a predicted uncertainty for each prediction, and in most cases where the error is large, uncertainty is high as well –refer to Figure 6. In particular, notice how disallowing the GPR to learn the sensor behavior for one of the extreme temperatures included in our study (the dataset for 30°C), leads to the largest errors, since the estimator in this case is extrapolating, not interpolating, the sensor behavior for those conditions. To quantify and demonstrate this fact, we evaluated the average RMSE (1.51 m/s) and MAE (1.13 m/s) when predictions are "interpolated". On the other hand, the average RMSE and MAE values of the two datasets in which predictions are "extrapolated" are 2.305 m/s and 1.968 m/s, respectively, validating the insight that predictions are less accurate when they need to be extrapolated.

5) Sensibility to Ground-Truth Errors: Since our model proposes using the *actual* air temperature as an input to the wind speed sensor model, it is in order wondering how much does the air temperature measurement of the sensor affects the results. Our experimental set up employs a PT100 for air temperature measurement, with an accuracy of $\pm$ 0.06 $^\circ C$ at 0 $^\circ C$. To assess its influence in the performance of the GPR model, different errors in the ambient temperature measurement have been introduced. First, GPR model have been trained with the real values of air temperature measured with the PT100. Next, we have introduced two different errors in the test datasets and have evaluated the predictions:

- *Random error:* four levels of random noise have been evaluated in order to simulate different degrees of sensor accuracy. We considered the scenarios of air temperature accuracies of: $\pm$ 0.1 $^\circ C$, $\pm$ 0.2 $^\circ C$, $\pm$ 0.5 $^\circ C$, and $\pm$1 $^\circ C$, respectively.
- *Systematic error:* an example of a typical systematic error might be not protecting the temperature sensor from direct solar radiation, which strongly affects its measurements. Four levels of systematic error have been

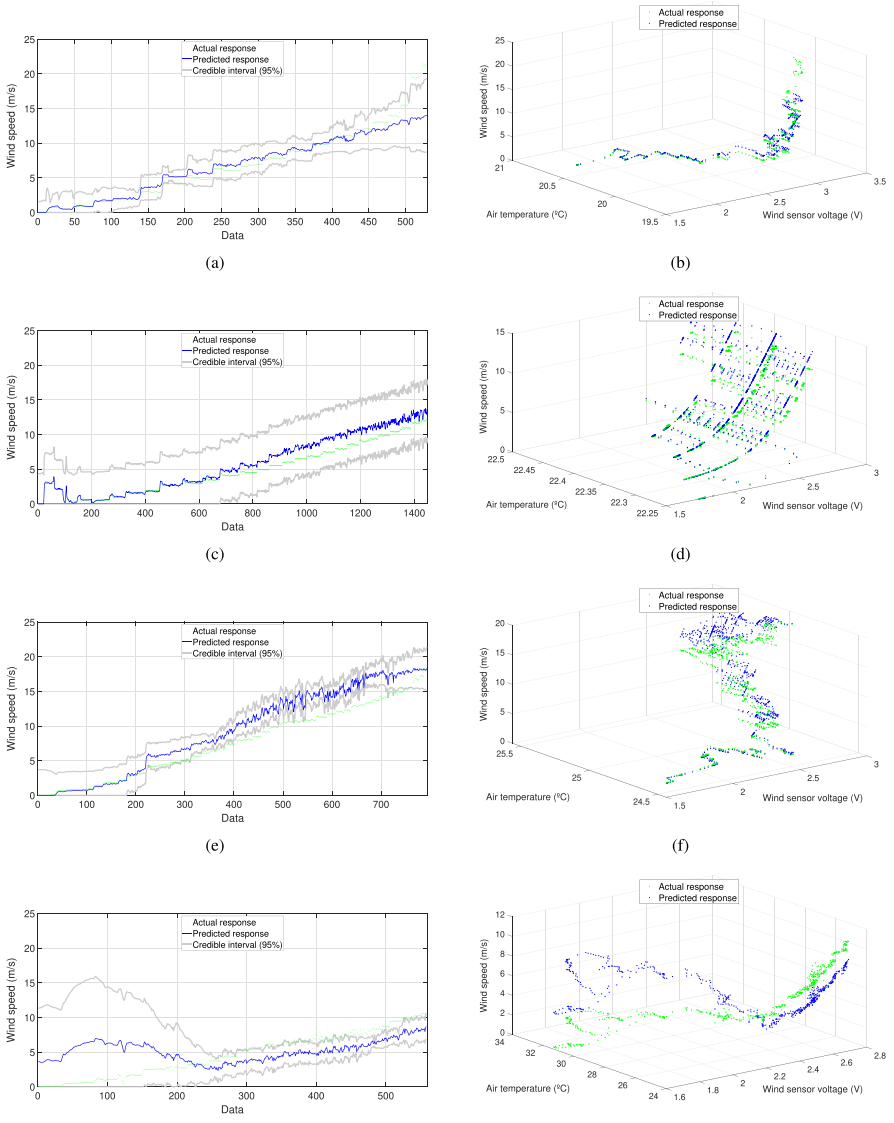

Fig. 6. Results for the GPR cross validation ("method 2"): the GPR is trained with all data set runs, except that for one particular temperature, and the resulting model is evaluated against the missing ("testing") data set. Left column shows the real wind speed and the model prediction for each point, together with its 95% credible interval. Right column shows the same data but including the raw sensor voltage and air temperature as second and third axis. Each row of images illustrates the results for a cross validation run using a different data set as "testing" data set. We show four representative such runs out of a total of seven. Notice that large errors are typically associated with large predicted uncertainty. Refer to the text for further discussion. (a) Prediction vs. ground truth (Test dataset: 20°C). (b) Prediction vs. ground truth (Test dataset: 20°). (c) Prediction vs. ground truth (Test dataset: 22°C). (d) Prediction vs. ground truth (Test dataset: 22°C). (e) Prediction vs. ground truth (Test dataset: 24°C) (f) Prediction vs. ground truth (Test dataset: 24°C). (g) Prediction vs. ground truth (Test dataset: 30°C). (h) Prediction vs. ground truth (Test dataset: 30°C).

evaluated: $+\ 0.25\ ^{\circ}C$, $+\ 0.5\ ^{\circ}C$, $+\ 1\ ^{\circ}C$, and $+\ 1.5\ ^{\circ}C$, with respect to the real value.

Table V summarizes the results for MAE, RMSE, and R^2, for test points of the GPR model for both types of error above. These values should be contrasted to Table IV, which shows MAE, RMSE, and R^2 without adding any additional noise to measurements. As can be seen, for air temperature random errors of $\pm\ 0.1\ ^{\circ}C$ and $\pm\ 0.2\ ^{\circ}C$, the results of MAE, RMSE, and R^2 for test points are similar. For an accuracy of air temperature of $\pm\ 0.5\ ^{\circ}C$ the variation is more remarkable

TABLE V

RESULTS OF MAE, RMSE AND R^2 FOR THE SENSITIVITY ANALYSIS WITH DIFFERENT AIR TEMPERATURE GROUND-TRUTH RANDOM AND SYSTEMATIC ERRORS IN TEST POINTS, FOR THE GPR MODEL WITH EXPONENTIAL AS COVARIANCE FUNCTION

Random error	**MAE (m/s)**	**RMSE (m/s)**	**R^2**
$\pm$ 0.1 $^\circ C$	0.1802	0.3057	0.99491
$\pm$ 0.2 $^\circ C$	0.2069	0.3411	0.99366
$\pm$ 0.5 $^\circ C$	0.3030	0.4855	0.98717
$\pm$ 1 $^\circ C$	0.4596	0.6885	0.97419
Systematic error	**MAE (m/s)**	**RMSE (m/s)**	**R^2**
+ 0.1 $^\circ C$	0.2483	0.4443	0.98950
+ 0.2 $^\circ C$	0.3620	0.5658	0.98257
+ 0.5 $^\circ C$	0.6622	0.9849	0.94719
+ 1 $^\circ C$	0.9992	1.4516	0.88529

although it might still be acceptable, whereas for $\pm$ 1 $^\circ C$ the error is, as expected, much greater. According to the results for systematic errors, the GPR model is more sensitive to them and consequently producing worse predictions. Systematic errors of up to $+$ 0.2 $^\circ C$ are acceptable.

Summarizing, attending to the results obtained, we can conclude that GPR model works with a reasonable accurate with random errors of up to $\pm$ 0.5 $^\circ C$ or with systematic errors of up to $+$ 0.2 $^\circ C$.

IV. CONCLUSION

Wind speed is a parameter hard to measure with accuracy and with low-cost devices. In this paper, the calibration of a low-cost hot-wire anemometer is proposed via machine learning techniques, attempting to solve its main drawback, namely, the loss of accuracy when air temperature changes. After comparing the performance of different regressions models, Gaussian Process Regression is the model that best fits the data and offers more precise predictions. Therefore, the problem has been addressed using Gaussian Process Regression to estimate a posterior distribution over the wind speed, given the response of a hot-wire anemometer and air temperature measurements, while also using an ultrasonic anemometer as ground truth value to rigorously evaluate the prediction error. According to the results, a low-cost hot-wire anemometer can be used, after the proposed calibration process, in different applications with reasonable accurate and over a typical range of ambient temperature.

REFERENCES

[1] H. H. Bruun, *Hot-Wire Anemometry: Principles and Signal Analysis*. London, U.K.: Oxford Univ. Press, 1995.

[2] P. Bradshaw, *An Introduction to Turbulence and Its Measurement*. New York, NY, USA: Pergamon, 1971.

[3] J. O. Hinze, *Turbulence*, vol. 218. New York, NY, USA: McGraw-Hill, 1975.

[4] N. P. Cheremisinoff and P. N. Cheremisinoff, *Flow Measurement for Engineers and Scientists*, vol. 2. New York, NY, USA: Marcel Dekker, 1988.

[5] A. Al-Salaymeh, "Flow velocity and volume flow rate sensors with a wide band width," Ph.D. dissertation, Technischen Fakultät Univ. Erlangen-Nürnberg, Erlangen, Germany, 2001.

[6] A. E. Perry, *Hot-Wire Anemometry*. New York, NY, USA: Oxford Univ. Press, 1982.

[7] C. G. Lomas, *Fundamentals of Hot Wire Anemometry*. Cambridge, U.K.: Cambridge Univ. Press, 1986.

[8] M. Hultmark and A. J. Smits, "Temperature corrections for constant temperature and constant current hot-wire anemometers," *Meas. Sci. Technol.*, vol. 21, no. 10, Aug. 2010, Art. no. 105404.

[9] P. W. Bearman, "Corrections for the effect of ambient temperature drift on hot-wire measurements in incompressible flow," *DISA Inf.*, vol. 11, no. 11, pp. 25–30, May 1971.

[10] N. Khamshah, A. N. Abdalla, S. P. Koh, and H. Rashag, "Issues and temperature compensation techniques for hot wire thermal flow sensor: A review," *Int. J. Phys. Sci.*, vol. 6, no. 14, pp. 3270–3278, Jul. 2011.

[11] R. K. Pandit and D. Infield, "Comparative analysis of Gaussian process power curve models based on different stationary covariance functions for the purpose of improving model accuracy," *Renew. Energy*, vol. 140, pp. 190–202, Sep. 2019.

[12] R. K. Pandit, D. Infield, and J. Carroll, "Incorporating air density into a Gaussian process wind turbine power curve model for improving fitting accuracy," *Wind Energy*, vol. 22, no. 2, pp. 302–315, Feb. 2019.

[13] C. E. Rasmussen and C. K. I. Williams, *Gaussian Processes for Machine Learning*, vol. 1. Cambridge, MA, USA: MIT Press, 2006.

[14] F. di Sciascio and A. N. Amicarelli, "Biomass estimation in batch biotechnological processes by Bayesian Gaussian process regression," *Comput. Chem. Eng.*, vol. 32, no. 12, pp. 3264–3273, Dec. 2008.

[15] L. JingDong, H. Li, and Z. HongBo, "Forming defects prediction for sheet metal forming using Gaussian process regression," in *Proc. 29th Chin. Control Decis. Conf.*, May 2017, pp. 472–476.

[16] R. K. Pandit and D. Infield, "Using Gaussian process theory for wind turbine power curve analysis with emphasis on the confidence intervals," in *Proc. 6th Int. Conf. Clean Electr. Power (ICCEP)*, Aug. 2017, pp. 744–749.

[17] W.-Z. Lu and W.-J. Wang, "Potential assessment of the 'support vector machine' method in forecasting ambient air pollutant trends," *Chemosphere*, vol. 59, no. 5, pp. 693–701, Apr. 2005.

[18] Y. Chuan and L. Chen, "The application of support vector machine in the hysteresis modeling of silicon pressure sensor," *IEEE Sensors J.*, vol. 11, no. 9, pp. 2022–2026, Sep. 2011.

[19] J. Alonso, A. R. Castañon, and A. Bahamonde, "Support vector regression to predict carcass weight in beef cattle in advance of the slaughter," *Comput. Electron. Agricult.*, vol. 91, pp. 116–120, Feb. 2013.

[20] R. Pandit and D. Infield, "Comparative analysis of binning and support vector regression for wind turbine rotor speed based power curve use in condition monitoring," in *Proc. 53rd Int. Univ. Power Eng. Conf. (UPEC)*, Sep. 2018, pp. 1–6.

[21] L. Hadjiiski, P. Geladi, and P. Hopke, "A comparison of modeling nonlinear systems with artificial neural networks and partial least squares," *Chemometrics Intell. Lab. Syst.*, vol. 49, no. 1, pp. 91–103, Sep. 1999.

[22] F. Gebben, S. Bader, and B. Oelmann, "Configuring artificial neural networks for the prediction of available energy in solar-powered sensor nodesc," in *Proc. IEEE SENSORS*, Nov. 2015, pp. 1–4.

[23] M. S. Ashhab and A. Al-Salaymeh, "Optimization of hot-wire thermal flow sensor based on a neural net model," *Appl. Therm. Eng.*, vol. 26, nos. 8–9, pp. 948–955, Jun. 2006.

[24] J. Hu and J. Wang, "Short-term wind speed prediction using empirical wavelet transform and Gaussian process regression," *Energy*, vol. 93, pp. 1456–1466, Dec. 2015.

[25] B. Schlkopf and A. J. Smola, *Learning With Kernels: Support Vector Machines, Regularization, Optimization, and Beyond* . Cambridge, MA, USA: MIT Press, 2001.

[26] K. J. Preacher, P. J. Curran, and D. J. Bauer, "Computational tools for probing interactions in multiple linear regression, multilevel modeling, and latent curve analysis," *J. Educ. Behav. Statist.*, vol. 31, no. 4, pp. 437–448, Dec. 2006.

[27] D. C. Montgomery, E. A. Peck, and G. G. Vining, *Introduction to Linear Regression Analysis*, vol. 821. Hoboken, NJ, USA: Wiley, 2012.

[28] N. R. Draper and H. Smith, *Applied Regression Analysis*, vol. 326. Hoboken, NJ, USA: Wiley, 2014.

[29] J. J. Hox, M. Moerbeek, and R. van de Schoot, *Multilevel Analysis: Techniques and Applications*. Evanston, IL, USA: Routledge, 2017.

[30] W.-Y. Loh, X. He, and M. Man, "A regression tree approach to identifying subgroups with differential treatment effects," *Statist. Med.*, vol. 34, no. 11, pp. 1818–1833, May 2015.

[31] D. Kocev, C. Vens, J. Struyf, and S. Džeroski, "Tree ensembles for predicting structured outputs," *Pattern Recognit.*, vol. 46, no. 3, pp. 817–833, Mar. 2013.

[32] F. Kang, B. Xu, J. Li, and S. Zhao, "Slope stability evaluation using Gaussian processes with various covariance functions," *Appl. Soft Comput.*, vol. 60, pp. 387–396, Nov. 2017.
[33] D. L. Valera, A. J. Álvarez, and F. D. Molina, "Aerodynamic analysis of several insect-proof screens used in greenhouses," *Spanish J. Agricult. Res.*, vol. 4, no. 4, pp. 273–279, Dec. 2006.
[34] A. Lopez-Martinez, D. L. Valera-Martínez, F. Molina-Aiz, A. Peña-Fernandez, and P. Marín-Membrive, "Microclimate evaluation of a new design of insect-proof screens in a Mediterranean greenhouse," *Spanish J. Agricult. Res.*, vol. 12, no. 2, pp. 338–352, 2014.
[35] P. M. Lee, *Bayesian Statistics: An Introduction*. London, U.K.: Arnold, 1997.
[36] J. VanderPlas, "Frequentism and Bayesianism: A Python-driven primer," in *Proc. 13th Python Sci. Conf.*, 2014, pp. 85–93.
[37] G. Schwarz, "Estimating the dimension of a model," *Ann. Statist.*, vol. 6, no. 2, pp. 461–464, 1978.
[38] J. R. Lloyd, D. Duvenaud, R. Grosse, J. Tenenbaum, and Z. Ghahramani, "Automatic construction and natural-language description of nonparametric regression models," in *Proc. 28th AAAI Conf. Artif. Intell.*, Jan. 2014, pp. 1242–1250.

Rubén A. García-Ruiz received the M.S. degree in industrial engineering from the University of Jaén in 2015. He is currently pursuing the Ph.D. degree in technology of greenhouses and industrial engineering with the University of Almería.

He is the author of two journal papers.

José L. Blanco-Claraco received the M.S. degree in electrical engineering and the Ph.D. degree in robotics from the University of Málaga in 2005 and 2009, respectively.

During six years, he worked with the Department of System Engineering and Automation, University of Málaga in the context of a number of Spanish and European projects on mobile robotics and computer vision. In 2012, he joined the Engineering Department, University of Almeria. His research interests include mobile robotics, estimation theory, SLAM, and multibody dynamics. He is the author of one book and more than 30 journal and 45 conference papers in these fields.

Javier López-Martínez received the M.S. degree in industrial engineering from the School of Industrial Engineering, University of Málaga, in 2005, and the Ph.D. degree from the University of Almería, in 2014.

After some years of professional work as a Project Engineer, he began teaching at the University of Almería and obtained a Ph.D. scholarship. He is currently a Professor with the Department of Engineering, University of Almería. His research is mainly involved in mechanical design, contributing with more than ten journals papers and seven patents.

Ángel J. Callejón-Ferre received the M.S. degree in agronomy engineering and the Ph.D. degree in agronomy from the University of Almería in 1997 and 2003, respectively.

During 18 years, he worked with the Department of Engineering, University of Almería, in the context of a number of Spanish Projects on "Renewable Energy in Greenhouses" and "Occupational Health and Safety in Agriculture." He is the author/co-author of more than 35 journal and 40 conference papers in these fields. Moreover, he is the Manager of the Laboratory-Observatory Andalusian Working Conditions in the Agricultural Sector.

2.3. Publicación científica 3

Título: Ultraviolet Index (UVI) inside an Almería-Type Greenhouse (Southeastern Spain).

Autores: Rubén A. García-Ruiz, Javier López-Martínez, José L. Blanco-Claraco, José Pérez-Alonso y Ángel J. Callejón-Ferre.

Revista científica: Agronomy.
Volumen: 10.
Páginas: 145.
Año: 2020.
doi: 10.3390/agronomy10010145

Datos JCR (Journal Citation Reports):

Factor de impacto (2018): 2.259.
Categoría: AGRONOMY.
Ranking categoría: 19/89.
Cuartil: Q1.
Editor: MDPI AG.
País: Suiza.

agronomy

MDPI

Article

Ultraviolet Index (UVI) inside an Almería-Type Greenhouse (Southeastern Spain)

Rubén A. García-Ruiz [1,*,†], Javier López-Martínez [2,†], José L. Blanco-Claraco [3,†], José Pérez-Alonso [1,†] and Ángel J. Callejón-Ferre [1,4,†]

1 Department of Engineering, University of Almería, Research Center CIMEDES, Agrifood Campus of International Excellence (ceiA3), Ctra. de Sacramento s/n, 04120 Almería, Spain; jpalonso@ual.es (J.P.-A.); acallejo@ual.es (Á.J.C.-F.)
2 CIAIMBITAL Research Centre, University of Almería, Ctra. de Sacramento s/n, 04120 Almería, Spain; javier.lopez@ual.es
3 Department of Engineering, University of Almería, Centro Mixto CIESOL, Agrifood Campus of International Excellence (ceiA3), Ctra. de Sacramento s/n, 04120 Almería, Spain; jlblanco@ual.es
4 Laboratory-Observatory Andalusian Working Conditions in the Agricultural Sector (LASA). C/ Albert Einstein s/n. 2ªplanta. Isla de la Cartuja, 41092 Sevilla, Spain
* Correspondence: rgr051@ual.es; Tel.: +34-950-214-233
† These authors contributed equally to this work.

Received: 30 December 2019; Accepted: 13 January 2020; Published: 19 January 2020

Abstract: Greenhouse workers, despite being in a space beneath a plastic cover, may be susceptible to risks associated to ultraviolet (UV) radiation in skin and eyes. The present work focuses on experimentally analysing this risk throughout a complete year. For this purpose, a network of sensors has been designed, comprising 12 UV radiation measuring stations inside the greenhouse and one outside. It is shown that the UVI risk limit established by World Health Organization (WHO) is exceeded for some particular dates and times, thus there exist risk of damage caused by UV radiation for greenhouse workers. The results allow to identify the UV risk periods for the location studied. A diagram called "UVIgram" has been created which offers weather and UV radiation information for a particular location, for each month, and also in general for the whole year. Finally, a series of recommendations and protection measures are given, highlighting the whitening of the plastic cover of the greenhouse and an alarm system which has been designed to alert workers when UV risk exists.

Keywords: greenhouse; Occupational Safety and Health (OSH); UV risk; workers; UVI

1. Introduction

Ultraviolet (UV) radiation is a part of the optical radiation that covers the wavelengths between 100 and 400 nm. At the same time, UV radiation is divided into three different bands: UVA (315–400 nm), UVB (280–315 nm), and UVC (100–280 nm). The intensity of the UV radiation increases with the sun elevation, lower latitude, higher altitude and ground reflection, and it decreases with the presence of clouds and certain gases in the atmosphere as ozone, oxygen, and carbon dioxide. Precisely these gases absorb all the UVC radiation and 90% of UVB radiation [1]. Thus, only UVA radiation and a small amount of UVB radiation coming from the sun reaches the surface of the Earth.

The UV Index (UVI henceforth) was introduced in Canada in 1992 by Kerr et al. [2] to inform about the increasing of UV levels because of the ozone depletion. Latter, it was adopted and recommended as a global standard by the World Health Organisation et al. [3], as in addition to quantify the UV

irradiance, it indicates its potential effect over humans. UVI is based on the reference action spectrum for UV-induced erythema on the human skin [4], and is mathematically defined as:

$$UVI = K_{er} \int_{250\ \text{nm}}^{400\ \text{nm}} E_\lambda S_{er}(\lambda) d\lambda \quad (1)$$

where E_λ is the solar irradiance at wavelength λ (expressed in $W/m^{-2}nm$), $S_{er}(\lambda)$ is the erythema reference action spectrum and K_{er} is a constant equal to 40 m^2W^{-1}. The term $S_{er}(\lambda)$ quantifies the spectral dependence of UV radiation to produce erythema in human skin and is defined as:

$$\begin{cases} S_{er}(\lambda) = 1, & for\ 250 \leq \lambda \leq 298\ \text{nm} \\ S_{er}(\lambda) = 10^{0.094(298-\lambda)}, & for\ 298 < \lambda \leq 328\ \text{nm} \\ S_{er}(\lambda) = 10^{0.015(140-\lambda)}, & for\ 328 < \lambda \leq 400\ \text{nm} \end{cases} \quad (2)$$

UVI is a non-dimensional index with values from zero upward and indicates the potential damage of UV over humans so that while UVI is higher, higher potential damage and less time to produce it. To a better understanding and public awareness, World Health Organisation et al. [3] recommend using colour codes depending on the exposure category (Figure 1) and establishes a UVI equal to 3 as the threshold from which there exists risk of damage caused by UV radiation and, therefore, sun protection is necessary. Each colour is standardised by the Pantone Matching System (PMS). However, according [5], there is also risk for people with clear skin (skin type I and II, according to Fitzpatrick [6,7] and defined later in Table 1) when they are exposed to a UVI between 2 and 3 during more than 1.5 h.

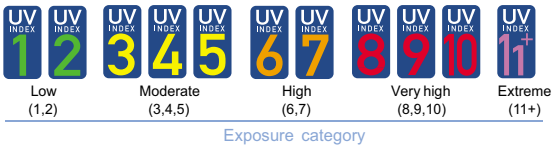

Figure 1. UV radiation exposure categories and International colour codes. Figure extracted from [3].

Although UV radiation represents only around 5% of the overall solar radiation [8,9], it has considerable harmful effects on humans, depending on the intensity of their UV exposure. In the short term, UV produces erythema (or sunburn) that could worsen resulting in oedema, pain, blistering, and finally peeling [8]. In the long term, UV produces skin ageing (as consequence of degenerative changes in cells, fibrous tissue and blood vessels) [3], skin cancer (cutaneous malignant melanoma and non-melanoma skin cancer) [10], eye injuries (cataracts, pterigyum, photokeratitis, retinal damage and deterioration) [11], and damage to the immune system [3]. Skin ageing produces skin dryness, sagging, loss of elasticity, wrinkles, skin furrows, mottled pigmentation, and telangiectasia [8]. Incidence and mortality of skin cancer have both increased in the last years [12–14]. Specially, cutaneous malignant melanoma (CMM), which represents 5–10% of all skin cancers [15,16] but has a much higher mortality rate than non-melanoma skin cancer (NMSC), since the latter progresses slower and is located in sun-exposed body parts facilitating early detection [16]. It must be highlighted that UV also has benefits for health. 90% of vitamin D needed by humans comes from UV radiation [17], although a daily exposure of 10–15 min in the face, arms and hands at low intensity radiation could be enough to obtain it [18]. However, depending on the recommended daily dose of vitamin D and other factors as clouds, air pollution, intensive skin pigmentation, advanced age or excessive usage of sun protection cosmetics [19], it may be necessary to increase the time or intensity of exposure, always taking preventive measures and precautions to avoid taking a risk. However, in some countries at medium or high latitudes there is not enough UV radiation during winter [20], causing deficiency of vitamin D and consequently skin pigmentation problems [21]. Besides, several diseases as rickets, psoriasis

and eczema, are treated with UV radiation, always under medical supervision and considering the potential risk [3].

The effects of UV is greater in people with lighter colours of skin, hair and eyes, and also with the presence of freckles [8]. Respect to skin colour, Fitzpatrick defined different skin types [6,7]. The characteristics of each skin type are summarised in Table 1. Although most skin cancers are produced in people with skin type I or II, dark-skinned people are also sensible to UV effects, specially those that affect to the eyes and the immune system. In addition, when skin cancers affect them, they are usually detected in more advanced and dangerous stages. On the other hand, the dose of UV radiation [22,23] and sunburn susceptibility [8] is equal between sexes. However, incidence and mortality of skin cancer is greater in males [13,14]. This could be due to the fact that females might be more careful regarding sun protection [24,25] and they are more aware of UV risk [26] in comparison with males.

Table 1. Skin types defined by Fitzpatrick and its characteristics [6,7].

Skin Type	Skin Colour	Skin Photoype	Sunburn after Sun Exposure	Tan after Sun Exposure
I	Very white, with light eyes and hair	Deficient in melanin	Always	Never
II	White, with light eyes and hair	Deficient in melanin	Usually	Sometimes
III	White, with intermediate eyes and hair	With enough melanin	Sometimes	Usually
IV	Tanned, with dark eyes and hair	With enough melanin	Occasionally	Always
V	Dark, with dark eyes and hair	With melanic protection	Seldom	Intense tanning
VI	Black, with black eyes and hair	With melanic protection	Never	Maximum tanning

Outdoor workers receive between 2 and 8 times the UV exposure of indoor workers according different authors [27,28]. This fact makes to outdoor workers more vulnerable to the negative effects of UV over health. Several works have reported health risk for prolonged UV exposure in outdoor workers all around the world: Serrano et al. in Spain [29], Milon et al. in Switzerland [16], Gies et al. in Australia [30], Thieden et al. in Denmark [22], Stepanski et al. in the United States [23] and Hammond et al. in New Zealand [31], among others. These health risk also exists in cloudy days because, although clouds reduce the intensity of the UV radiation, intensity of infrared radiation is reduced even more. This reduces the heat sensation (which usually helps to warn about the UV risk) and increases the risk of sun overexposure [8]. In addition, the greatest eye damage occurs when UVI is higher and light clouds cover the sky, as UV radiation is scattered and strikes the eyes at different angles where natural defenses of the eye as eyebrows, eyelids and eye sockets do not offer protection [32].

In recent times, the depletion of the ozone layer [15,33] has been causing an increase of UVI levels. In addition, UVI in rural areas is higher than in cities because of the clearness of the atmosphere and less air pollution (which blocks a part of UV radiation) [15,34]. In Almería, around 55,000 people work in greenhouses [35], which are agricultural buildings destined to maintain adequate climate conditions for crops. Greenhouses are composed of transparent plastic covers supported by light metal structures, with ventilation through windows in the ceiling and walls, and diffuse solar radiation [36]. Greenhouse workers can be considered as outdoor workers, since are exposed to wind and UV radiation. The main working period in greenhouses lasts since the end of July until the middle of June; however, it extends to almost the complete year as maintenance tasks are also carried out in non-crop periods [37–40]. Although only diffuse solar radiation reaches the interior of a greenhouse, UV radiation also can be high [17]. In addition, the soil of greenhouses is covered of sand, which reflect until 15% of UV radiation and increases UVI. However, in spite of all this factors, UV radiation usually is not measured in greenhouses and workers are not aware of the very possibility of UV risk existing inside of the greenhouses.

In the present work, a UV sensor network has been designed and deployed to measure UVI at different points inside a greenhouse and also outdoors during an annual period. The data recorded

in this period allows us to learn about the conditions of greenhouse workers regarding UV radiation and to determinate whether UVI exceeds the WHO risk threshold. To the best of our knowledge, this work is the first one to study UV radiation on workers inside a greenhouse. This study is particularly interesting for greenhouses located in areas with low latitude, such as the south of Spain. Besides, some recommendations and prevention measures are proposed to reduce at maximum the negative effects of UV radiation in greenhouse workers.

This paper is organized as follows. First, the material and methods are detailed in Section 2. The experimental results and their discussion are presented in Section 3. Finally, some conclusions are outlined in Section 4.

2. Materials and Methods

2.1. Experimental Setup

The study was performed in a greenhouse located at 15 km east of Almería (36°51′54″ N–2°17′02″ W and 98 m above sea level), in Spain. The type of greenhouse is the most common in the province of Almería: "raspa y amagado", as it can be observed in Figure 2. The greenhouse has an area of 1024 m^2 (32×32 m), with a height of 3.4 m and 4.1 m in the gutter and ridge, respectively. It has three polyethylene layers with a 200 µm thickness, with visible light transmittance of 81% and diffuse light transmittance of 29% at the beginning of its useful life, supported by a structure made of steel and with automatic lateral and roof windows that allow natural ventilation. The soil of the greenhouse is covered of gravel and sand and the air temperature inside the greenhouse ranges from around 0 °C in winter to 55 °C in summer [41]. It is worth noting that the greenhouse plastic cover was installed in July 2016 and will have a useful life of 3 campaigns (2016-17, 2017-18 and 2018-19) due to its wear and loss of transmittance. Therefore, the data obtained in this study start from the end of the second campaign of the plastic cover and extend until almost the end of the third campaign.

Figure 2. Interior of the greenhouse studied and detail of one of the sensors installed for the measurement of UV radiation.

The sensors used to measure UV radiation (Figure 2) have a spectral response curve and a field of view that meet the requirements defined in ISO/CIE 17166 [4]. The rest of the characteristics of the sensors are detailed in Table 2. Each sensor has been calibrated to measure the UV index in accordance with ISO/CIE 17166, and subsequently it has been checked by comparing it with the data offered by the State Meteorological Agency (AEMet, "Agencia Estatal de Meteorología" in Spanish), specifically with the station located at the Almeria airport. In addition, these sensors can measure air temperature, and in this work these data are also used in Section 3.4.

Table 2. Characteristics of the sensors for the measurement of UV radiation.

Manufacturer	Model	Measurement Range	Accuracy	Operating Temperature	Degree of Protection Against Dust and Water
Sglux GmbH	UV-Cosine-UVI	0–30 UVI	± 1.3%	−25 a 80 °C	IP 68

Figure 3 shows a plan of the greenhouse and the distribution of the measurement stations. Twelve measuring stations are evenly distributed inside the greenhouse and another one is located outside. The infrastructure of existing stations has been reused, as reported in past works [42], adding new sensors and software. This infrastructure consists of a vertical pole and three horizontal bars at different heights, using the uppermost one for the installation of the UVI sensors. This upper height is 1.56 m above the ground which correspond to the head (equivalent to eye height) according to the 50th percentile of the Spanish population [43]. In this way, the UV radiation that affects the parts of the body where there may be greater risk to health is analysed, such as the eyes, and the face and neck (which are normally uncovered and exposed to radiation).

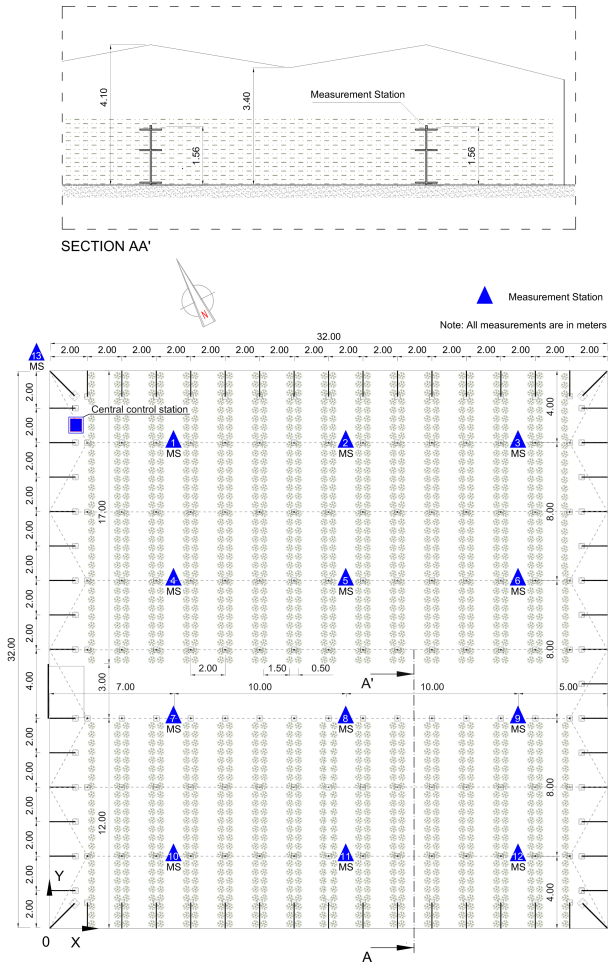

Figure 3. Drawing of the greenhouse, where are indicated the locations of the measurement stations.

The experimental campaign was carried out in the greenhouse described above during a complete year, since 1 July 2018 to 31 June 2019. The crop from the beginning of this study is melon, until its harvest between 21 and 23 June 2018. Then, on 14 July 2018, the crop was removed and on 16 August 2018, the plastic cover of the greenhouse was whitewashed. Whitewashing is usually performed at the beginning of each crop (transplant) and its main objective is to reduce the amount of solar radiation entering the greenhouse and thus lower the inside air temperature, avoiding stress on the seedling. The product used was "Blanco España" (a compound product based on calcium carbonate), with doses of 50 kg of Blanco España per 1000 m^2 of plastic cover. Subsequently, on 21 August 2018, pear tomato was cultivated for a long cycle. On 6 March 2019, a new bleaching of the plastic cover was carried out with similar doses of the previous. The tomato crop was removed on 25 April 2019 and since then, maintenance tasks and preparation of the next crop cycle were carried out until the end of the study.

During the time that this study was carried out, the farmers have conducted its labours in the greenhouse, especially for the tomato crop, as the melon crop only coincided for a short period at the beginning of the study. These labours are: transplanting, formative pruning, ridging up (cover the lower part of the plant with sand), hoeing (stir the earth with a hoe), weeding, trellising (tying the stem of the plant by means of a thread, in such way that one end of the thread is located in the basal part of the plant and the other end is attached to a horizontal fabric of wires located inside the greenhouse at a certain heigh above the ground), fertigation, application of phytosanitary products, bee pollination, shoot thinning (remove the axillary buds to improve the development of the main stem), leaf thinning (remove senescent and infected leaves), inflorescences and fruit thinning (remove deformed, damaged, small sized and bad positioned fruits), harvesting and plant removal. Therefore, farmers have worked inside the greenhouse performing these tasks during the study, being susceptible to damage by the effects of UV radiation.

2.2. Network Architecture

The diagram of the designed data network architecture is shown in Figure 4. As it can be observed, there are four types of entities:

- Measurement stations: there are 13 of them, 12 evenly distributed inside the greenhouse and another one outside. Each measurement station consists of an single board computer (SBC), a UV sensor and an audible and luminous warning device to alert workers when the measured UVI is close to the threshold from which there is risk of damage by UV radiation.
- Central control station: it is installed in a register box inside the greenhouse and is responsible for sending the data to the server.
- Server: it is installed in the Data Processing Centre of the University of Almería (CPD-UAL).
- Remote operators: this type of entity is optional, since the system works regardless of whether remote operators are connected or not.

The core of the system has fully autonomous operational capacity without external intervention and is composed of the central control station and the measurement stations. The external elements (server and remote operators) are added with the aim of improving the usability of the system, since they allow access to data and system status in real time from anywhere via Internet. In addition, the server is also used to store backups of data collected during the day, as long as good mobile connectivity exists in the greenhouse area.

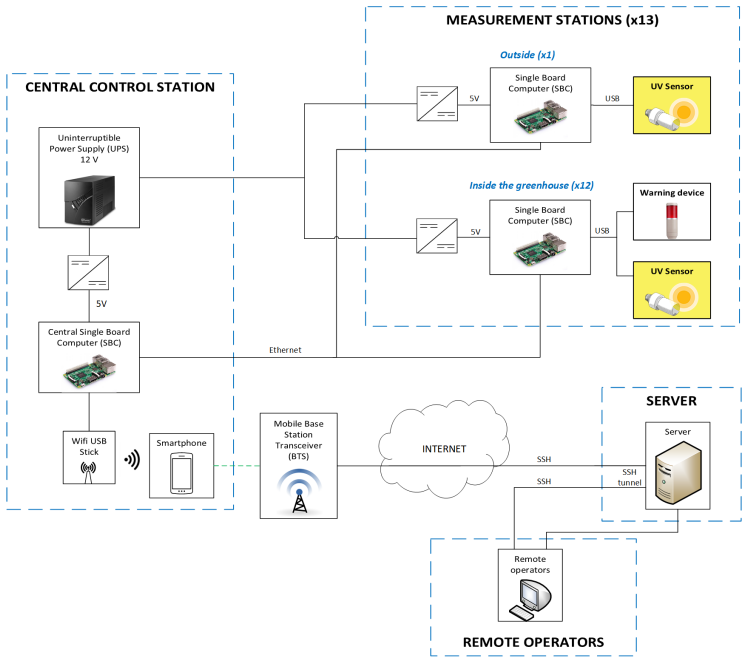

Figure 4. Diagram of the designed data network architecture.

The core of the system is powered by a 12V uninterruptible power supply (UPS). DC to DC converters are used to obtain 5V to power the SBCs. The SBCs located in the measurement stations are responsible for powering the UV sensors and warning devices, while the SBC located in the central station provides power to both, a smartphone, and a USB WiFi adapter.

To receive and store the data from the UV sensor and activate the warning device, a script has been programmed in Python. This script receives the data and saves it with a periodicity of 30 s and activates the warning device when UVI is close to 3. The data is stored in a memory card in the SBC of each measurement station, distributed in daily files. At the end of the day, these daily files from each measurement station are sent via Ethernet cable to the SBC of the central control station. In turn, the SBC of the central control station stores the data received from all the sensors in a memory card. Then, also once a day, at the end of the day, it proceeds to send it to the server located in the CPD-UAL. This requires Internet connectivity, achieved through a 4G Smartphone and shared by wifi to the SBC.

The operators (the researchers in this project) can access the data on the server by means of two protocols: a simple web interface (HTTP), or via Secure Shell (SSH). Likewise, the system has been configured in such a way that connections can be made from any place provided with Internet access, to the central computer of the greenhouse. This is not trivial, as the latter is behind a NAT (Network Address Translation) of the mobile operator that prevents direct connection from the outside. To solve this problem, a reverse SSH connection was created from the central control station of the greenhouse to the server in the CPD-UAL, opened 24 h a day waiting to be requested by an external operator.

2.3. Data Analysis

First, the results of the UVI measurement campaign inside and outside the greenhouse and its spatial distribution are presented, together with a 3D representation of the UVI data in video for every instant of time. It is also included a figure that shows the UVI ratio between inside and outside. Next, a seasonal analysis of UVI is performed.

Then, a new term is then established to study the average monthly temperature and maximum monthly UVI within a greenhouse, denominated "UVIgram". This has been created based on the Péguy climogram [44], which relates average monthly air temperatures on the "x" axis and precipitation on the "y" axis. To draw it, first, a triangle with vertices (A, B, C) and coordinates (0 °C, 0mm), (23 °C, 45 mm) and (16 °C, 200 mm), respectively, is projected. This triangle divides the Cartesian space into four climatological regions: temperate (points within the ABC triangle), arid (points under the AB segment), tropical or warm-dry (points to the right of the BC segment) and cold (points to the left of the CA segment). Next, the data of all the months are introduced during a year (or the average of the data of several years), so that each month is framed in a category, and therefore climatological information is obtained for each month for a given location, as well as a global overview of the entire year.

Finally, from the results obtained, some recommendations and prevention measures are exposed to reduce the risk of UV radiation damage in greenhouse workers.

2.4. Considerations and Study Limitations

It is worth to point that UTC (Coordinated Universal Time) have been used to analyse the data and must be taken into account for the interpretation of the results. Local time in Almería is CET (Central European Time) with daylight saving time in summer.

On the other hand, measurement stations have been exposed to a peculiar environment such as that of a greenhouse, with diffuse solar radiation, low wind speed and high humidity. In addition, plastic covers are not fully waterproof and are whitewashed. Therefore, the measurement stations have also been exposed to small droplets of water, dust and calcium carbonate.

3. Results and Discussion

3.1. Annual UVI Variation

First, the UVI data of a random day for the 13 measurement stations is shown by way of example in Figure 5. In this case, the day shown is a sunny day due to the perfect bell shape of the graphic and it is observed that the risk limit (UVI = 3) is not exceeded at any of the measurement stations inside the greenhouse, although it is exceeded outside.

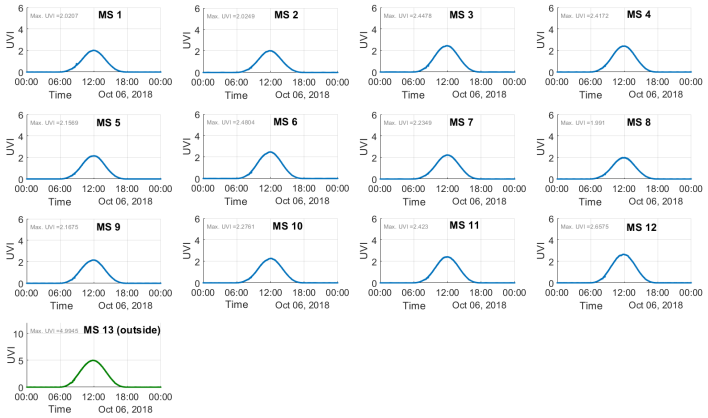

Figure 5. UVI measured by all measurement stations during 6 October 2018.

This work also includes a video produced with a 3D representation of the UVI data obtained during the period in which the study has been carried out (See: https://www.youtube.com/watch?v=W6B5GWTYLtA). It shows the variation of UVI for each measurement station at every moment and throughout the year. The four images show different perspectives of the greenhouse and represent

Agronomy **2020**, *10*, 145

the UVI values of the 12 measurement stations inside the greenhouse. For the two images on the left, a fixed UVI colour scale is set (between 0 and 6), while for the two images on the right, the UVI colour scale is variable to show greater sensitivity to changes. A blue marker represents the measure of each station, along with its numerical value at the top. The UVI colour scale is displayed at the bottom of the z-axis, using Markov Random Fields (MRF) to interpolate the rest of the points on the greenhouse colour scale. In the lower right part the date and time represented at each moment are shown. In the lower right part, it can be observed the minimum UVI, the maximum and the maximum difference between the measurement stations. Figure 6 shows an instant capture of this video.

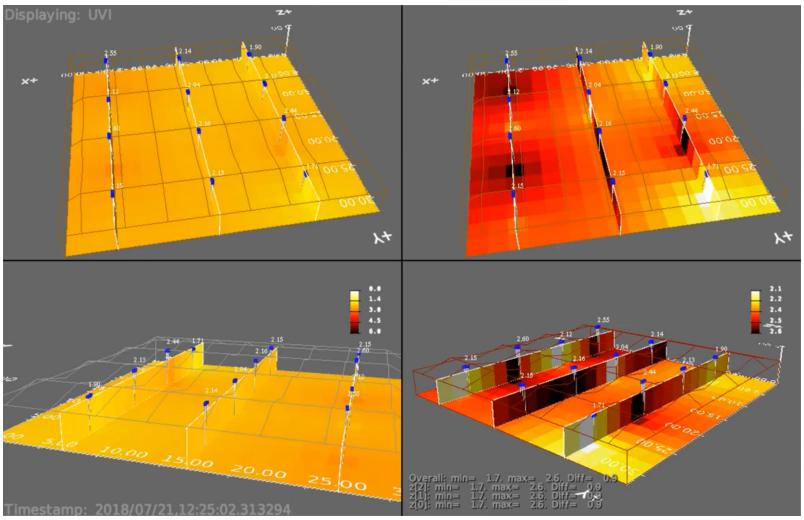

Figure 6. Image capture of the 3D video of the UVI measurements inside the greenhouse at 12:25 a.m., 21st July 2018.

In Figure 7 the daily maximum values for UVI both inside and outside the greenhouse during the experimental campaign are gathered. In the case of the interior of the greenhouse, the maximum UVI value shown corresponds to the maximum daily value measured between the 12 measurement stations located inside the greenhouse. The dashed red line represents the limit defined by the World Health Organization from which exists risk of damage to people for UV radiation, as it was explained in Section 1. The maximum UVI value was 4.69 and was measured on 5 July 2019 at 12:44 a.m. by the measurement station 5, while outside the maximum UVI of that same day was 9.48 and was measured at 12:16 a.m.. It can be observed that UVI surpass the risk limit up to in five months: July, August, September, May and June. It has been observed that most of the UVI maximums are recorded by the measure stations 7, 10, 11 and 12, i.e., most of the UVI maximums are recorded in the southwest corner of the greenhouse. It is noticeable a significant drop in UVI between 16 August and 8 September, which results in the risk limit not being exceeded in this period. This is because the plastic cover of the greenhouse was whitewashed on 16 August, which caused part of the UV radiation to be blocked while the effect lasted. This effect usually lasts until the arrival of the first rains.

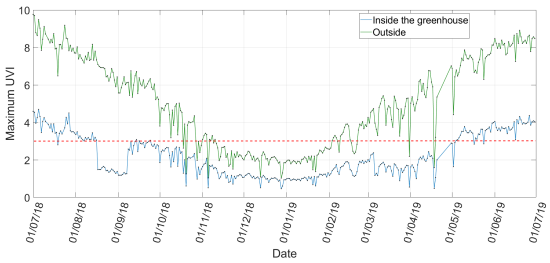

Figure 7. Maximum daily UVI outside and inside the greenhouse.

It is worth mentioning that from November 2018 and until its removal on 25 April 2019, the tomato crop reached around 2.20 m high, as it can be observed in Figure 8. This has been able to produce shade, reducing UV radiation and the potential risk of damage to workers by UV radiation. However, this only occurs in high crops (long cycle tomato, cucumber and aubergine, among others).

Figure 8. Image of the greenhouse on November 2018, when the tomato crop reached around 2.20 m high.

Figure 9 shows the ratio between the maximum UVI value inside the greenhouse (UVI_{inside}) and the maximum UVI outside ($UVI_{outside}$) in dB, expressed as:

$$UVIRatio(dB) = 10\log_{10}(UVI_{inside}/UVI_{outside}) \quad (3)$$

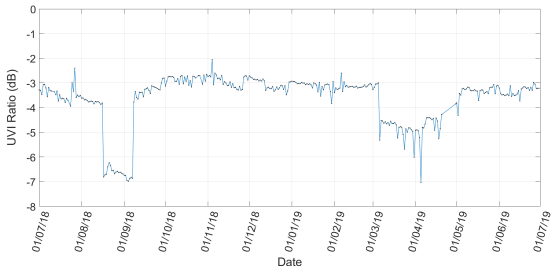

Figure 9. UVI ratio (UVI inside the greenhouse / UVI outside) in dB.

This ratio is equivalent to the capacity of the plastic cover of the greenhouse to block UV radiation. It can be clearly seen when the cover of the greenhouse was whitewashed (16 August 2018 and 6 March 2019), since from those days there is a great decrease in the ratio until the effect lasts. Greenhouse whitewashing is usually performed in periods of high radiation or temperature to avoid stress in

the crop, mainly in its initial stage. However, it has been shown that the UV radiation reaching the interior of the greenhouse is considerably reduced, so it can be used not only for the crop, but also as an effective method to protect workers against UV radiation. It could be applied both in the summer months, where maintenance work is carried out, and in some spring periods (from February or March). In certain spring crops it would not be possible, since it would be harmful for them (especially for melon and watermelon, although it is not disposable). On the other hand, it also can be observed small drops in UVI mainly in November 2018 and February 2019, that could be caused by crop shadows, as mentioned in the previous paragraph.

3.2. UVI Variation inside the Greenhouse

The UVI measured among the 12 measurement stations of the interior of the greenhouse has been compared for the year studied. The maximum monthly differences of UVI inside the greenhouse are gathered in Table 3. The maximum differences take place in periods where the UVI is greater, as summer and spring, being 2.54 the maximum UVI difference measured, obtained in July 2018.

Table 3. Maximum monthly differences of UVI inside the greenhouse.

Month	Maximum UVI Differences
July 2018	2.54
August 2018	1.11
September 2018	1.23
October 2018	1.51
November 2018	0.70
December 2018	0.38
January 2019	0.51
February 2019	1.42
March 2019	1.15
April 2019	1.26
May 2019	2.34
June 2019	2.37

These UVI differences may be due to the heterogeneity of the whitewashing, the wear of the plastic cover and the accumulation of dirt in said plastic cover.

In Figure 10 two consecutive days of summer are plotted. The particularity of these days is the application of whitewash on the plastic cover. The whitewashing occurred early in the second day, so we can observe one day without whitewashing and then another day with the effect of it. It can be observed what has been commented in the previous paragraph, that the heterogeneity of whitewashing is one of the causes of the greatest differences in UVI inside the greenhouse. In addition, it is demonstrated that the whitewashing of the plastic cover of the greenhouse is an effective method of reducing UV radiation and thus avoiding the risk of damage to workers.

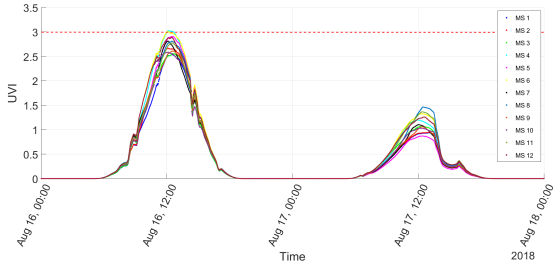

Figure 10. UVI measured by the 12 measurement stations of inside the greenhouse for two consecutive days (without and with whitewashing, respectively).

3.3. Seasonal UVI Analysis

The average daily UVI values for each season of the year in each instant has been calculated for the inside and outside of the greenhouse, obtaining an average day per season. In the case of the interior of the greenhouse, this average day corresponds to the average between the 12 measurement stations during the considered seasonal period. This is shown in Figure 11, together with its standard deviation, which is high due to the cloudiness.

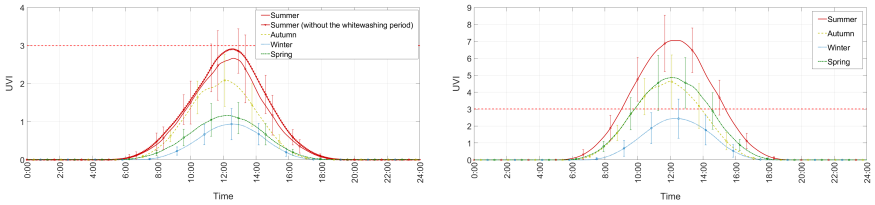

(**a**) Inside the greenhouse. (**b**) Outside.

Figure 11. Average day and standard deviation ($\pm 1\sigma$) of UVI per season:

For the interior of the greenhouse, the risk limit is not exceeded by the average day of any season, although it does exceed the standard deviation in summer. However, as can be seen in Figure 7, on many days of spring and summer the risk limit is exceeded, and it must also be borne in mind that whitewashing of the greenhouse cover has contributed to the reduction of the average UVI. For that reason, in Figure 11 summer also has been added without taking into account the whitewashing period. In this case, it can be observed how the mean is very close to the risk limit and also the typical deviation is reduced. In addition, it is observed that most of the UV radiation is logically concentrated between 10 and 14 h, obtaining the maximum UVI around 12 h. Standard deviation logically is higher in the middle of the day than at night where is null. In addition, standard deviation also seems to increase with UVI. These behaviors also occurs for the UVI measured outside the greenhouse.

For outside the greenhouse, the average day of all the seasons except winter surpass the risk limit. Certain tasks such as whitewashing of the cover or construction of greenhouses are carried out outdoors. Therefore, and based on the data obtained, it is clear the need to take extreme precautions against UV radiation.

3.4. "UVIgram"

Similarly to the Péguy climogram, we think that it is possible to relate monthly average temperatures and maximum value of the UV index, being able to establish different categories in the Cartesian space that allow to explain the behaviour of the UV radiation and temperature of each month and of the whole year for a determined location. For this, 3 limits have been defined to divide the Cartesian space,: a horizontal line for UVI equal to 3 that defines the risk limit for UV radiation, a vertical line for 20 °C of average temperature that is the limit from cold to temperate and another vertical line for 35 °C of average temperature that is the limit from temperate to hot. The temperature limits has been defined taking into account the climate study carried out by Callejon-Ferre et al. [45]. In this way, 6 categories are established: cold without UV risk, cold with UV risk, temperate without UV risk , temperate with UV risk, hot without UV risk and hot with UV risk, allowing to frame each month in a category and obtaining information of temperature and UV relevant for the interior of a greenhouse, especially useful for the prevention of risks in workers. This has been called "UVIgram" and Figure 12 shows the UVIgram of this study.

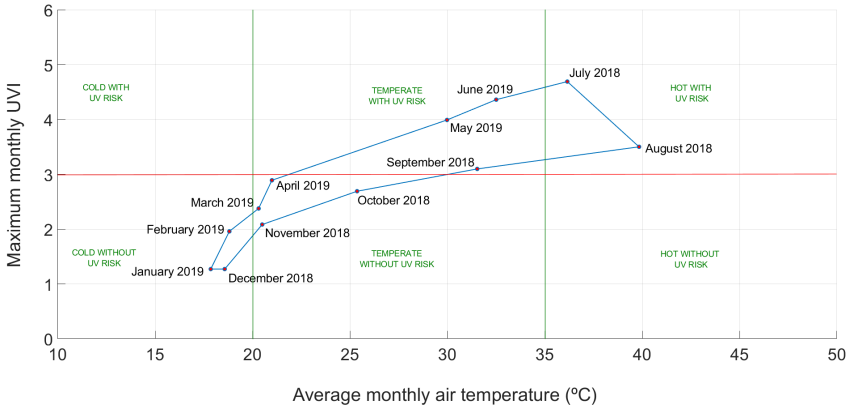

Figure 12. UVIgram that relates the average monthly temperature and the maximum monthly UVI inside the greenhouse; the maximum monthly UVI were measured on 5 July 2018 at 12:44 a.m. by MS (Measure Station) 5, 2 August 2018 at 12:27 a.m. by MS 4, 14 September 2018 at 12:21 a.m. by MS 12, 13 October 2018 at 11:59 a.m. by MS 12, 4 November 2018 at 11:59 a.m. by MS 12, 4 December 2018 at 11:58 a.m. by MS 12, 31 January 2019 at 12:40 a.m. by MS 10, 25 February 2019 at 12:14 a.m. by MS 11, 5 March 2019 at 12:42 a.m. by MS 11, 30 April 2019 at 12:47 a.m. by MS 11, 31 May 2019 at 12:16 a.m. by MS 12 and 26 June 2019 at 12:12 a.m. by MS 12.

In Figure 12 can be observed that cold months do not always produce lower UVI, since the factors explained in Section 1 also influence, such as the rise of the sun (depending on the season) and the presence of clouds, among others. On the other hand, logically the highest UVI are registered in summer (June and July), while the lowest UVI are registered in winter (December and January). Figure 12 also shows that autumn has lower UVI than those registered in spring.

3.5. UVI Risk Periods. Recommendations and Prevention Measures to Reduce the Risk of UV Radiation Damage in Greenhouse Workers

According to the results obtained in Sections 3.1 and 3.3, the UVI risk periods for this location are distributed in spring and summer (from May to September) and concentrated between 10 and 14 h, obtaining the maximum UVI value very close to 12:00 a.m..

In view of these results obtained, it is observed that there is a risk of damage to people due to UV radiation since an UVI greater than the risk threshold defined in 3 is exceeded, and therefore the following recommendations for protective measures are proposed:

- Analogous to the sun protection factor of sunscreens (SPF), it was developed a protection factor for clothing (UPF) according to its protection against radiation UV [46]. Factors of 15–24 offer good protection, 25–39 very good and greater than 40 excellent protection. Garments with a UPF factor of 30 or higher must be used. Garments must completely cover the legs and use long sleeves as much as possible, always adapted to the working environment and to the acceptance of the workers so that they are respected and allow the accomplishment of the tasks with comfort.
- Wide-brimmed hats are recommended, as they provide shade to a large part of the head and neck, protecting them from UV radiation. If wide-brimmed hats are not available or are uncomfortable for any of the tasks to be carried out, it would be advisable to use sunglasses with high protection against UV radiation and wrap-around design or with side panels [9].
- For areas of difficult protection against the sun, it is recommended to use sunscreen with SPF factor of 30 or higher, similar to UPF. The sunscreen should be applied 15 min before sun exposure and renewed every two hours. The sunscreen may be useless if perspiration is high, and the application should be renewed more frequently. The amount of cream used should be around

2 mg/cm^2, as it is under these conditions that the sunscreen protects according to its specified SPF protection factor [47].

- Work times must be managed to avoid the central hours of the day. Shadows should also be used when possible, especially during breaks. Although the presence of shadows is not usual in greenhouses, small awnings or tents with UV protection could be installed.
- It is recommended that the worker examine his/her skin regularly. If a new spot, freckle, or a change in the shape, size, or colour of any of his/her moles are observed, he/she should see a dermatologist for a skin examination as soon as possible.
- Alternatively to the previous individual protection measures, it is recommended as a collective protection measure, to perform greenhouse whitewashing in periods of higher UV radiation. This will be done whenever possible and does not harm the crop.
- Finally, as it was explained in Section 2.2, an alarm system has been designed to alert workers to the risk of damage by UV radiation inside the greenhouse. This system consists of a device connected to the SBC of the measurement station and which alerts workers by means of a audible and luminous signal when values close to the risk threshold are reached.

4. Conclusions

This work has been focused on analysing the greenhouse workers risk of being exposed to UV radiation through a complete year , in a "raspa and amagado" greenhouse located in Almería. Although it can be thought that there is no risk due to being under the plastic cover of the greenhouse, it is shown that the limit established by [3] is exceeded existing risk of damage for UV radiation. This has been evaluated by means of a network of ultraviolet radiation sensors located inside and outside the greenhouse.

UVI surpass the risk limit up to in five months in the greenhouse studied, being the UVI risk periods distributed in spring and summer and concentrated between 10 a 14 h, obtaining the maximum UVI values very close to 12:00 a.m.. Outside, logically, the risk is even greater, the risk limit is exceeded practically the whole year except the winter months. Greenhouse workers also perform certain tasks outside, so it is necessary to take even more precautions.

Inside the greenhouse it has been shown that there are UVI differences due to various factors as the heterogeneity of the whitewashing, the wear of the plastic cover and the accumulation of dirt in said plastic cover. These UVI differences are greater in periods where the UVI is greater, as summer and spring. In addition, it is observed that the highest UVI values are usually located in the south-west corner of the greenhouse.

On the other hand, a diagram called "UVIgram" has been created which offers climatological and UV radiation information about of a location for each month and global of the whole year. It relates monthly average temperatures and maximum value of the UV index.

Finally, some recommendations and prevention measures to reduce the risk of UV radiation damage in greenhouse workers are given. One of them is especially interesting and its effectiveness has been observed in this study. It is about the whitening of the plastic cover of the greenhouse, being recommended whenever possible and has no negative effects on the harvest. In addition, an alarm system has been designed to alert workers by means of a audible and luminous signal when UVI values close to the risk limit are reached.

Author Contributions: Conceptualization, R.A.G.-R., J.L.-M., J.L.B.-C., J.P.-A. and Á.J.C.-F.; methodology, R.A.G.-R., J.L.-M., J.L.B.-C., J.P.-A. and Á.J.C.-F.; software, R.A.G.-R., and J.L.B.-C.; validation, R.A.G.-R., J.L.-M., J.L.B.-C., J.P.-A. and Á.J.C.-F.; formal analysis, R.A.G.-R., J.L.-M., J.L.B.-C., J.P.-A. and Á.J.C.-F.; investigation, R.A.G.-R., J.L.-M., J.L.B.-C., J.P.-A. and Á.J.C.-F.; resources, J.L.-M., J.L.B.-C., J.P.-A. and Á.J.C.-F.; data curation, R.A.G.-R., and J.L.B.-C.; writing—original draft preparation, R.A.G.-R.; writing–review and editing, R.A.G.-R., J.L.-M., J.L.B.-C., J.P.-A. and Á.J.C.-F.; visualization, R.A.G.-R., J.L.-M., J.L.B.-C., J.P.-A. and Á.J.C.-F.; supervision, J.L.-M., J.L.B.-C., J.P.-A. and Á.J.C.-F.; project administration, J.L.-M., J.L.B.-C., J.P.-A. and Á.J.C.-F.; funding acquisition, Á.J.C.-F. All authors have read and agreed to the published version of the manuscript.

Funding: This research was funded by Research Contract CG 401370 of University of Almería and by Laboratory-Observatory Andalusian Working Conditions in the Agricultural Sector (LASA).

Conflicts of Interest: The authors declare no conflict of interest. The funders had no role in the design of the study; in the collection, analyses, or interpretation of data; in the writing of the manuscript, or in the decision to publish the results.

Abbreviations

The following abbreviations are used in this manuscript:

CET	Central European Time
CMM	Cutaneous Malignant Melanoma
CPD-UAL	Data Processing Centre of the University of Almería
HTTP	Hypertext Transfer Protocol
NMSC	Non-Melanoma Skin Cancer
MRF	Markov Random Fields
NAT	Network Address Translation
OSH	Occupational Safety and Health
PMS	Pantone Matching System
SBC	Single Board Computer
SPF	Sun Protection Factor of sunscreens
SSH	Secure SHell
UPF	Ultraviolet Protection Factor for clothing
UPS	Uninterruptible Power Supply
UTC	Coordinated Universal Time
UV	Ultraviolet
UVI	Ultraviolet Index
WHO	World Health Organization

References

1. Amar, S.K.; Goyal, S.; Srivastav, A.K.; Chopra, D.; Ray, R.S. Combined effect of Benzophenone-2 and ultraviolet radiation promote photogenotoxicity and photocytotoxicity in human keratinocytes. *Regul. Toxicol. Pharmacol.* **2018**, *95*, 298–306. [CrossRef]
2. Kerr, J.; McElroy, C.; Tarasick, D.; Wardle, D. The Canadian ozone watch and UV-B advisory programs. *Ozone Troposphere Stratos. NASA Conf. Publ.* **1994**, *3266*, 794–797.
3. World Health Organization(WHO); World Meteorological Organization (WMO); United Nations Environment Programme (UNEP). International Commission on Non-Ionizing Radiation Protection (ICNIRP). *Global Solar UV Index: A Practical Guide;* WHO: Geneva, Switzerland, 2002.
4. ISO/CIE 17166:2019. *Erythema Reference Action Spectrum and Standard Erythema Dose*; Standard, International Organization for Standardization: Geneva, Switzerland, 2019.
5. Lehmann, M.; Pfahlberg, A.B.; Sandmann, H.; Uter, W.; Gefeller, O. Public Health Messages Associated with Low UV Index Values Need Reconsideration. *Int. J. Environ. Res. Public Health* **2019**, *16*, 2067. [CrossRef] [PubMed]
6. Fitzpatrick, T.B. The validity and practicality of sun-reactive skin types I through VI. *Arch. Dermatol.* **1988**, *124*, 869–871. [CrossRef] [PubMed]
7. Fitzpatrick, T.B. Soleil et peau. *J. Med. Aesthet.* **1992**, *2*, 33–34.
8. Diffey, B.L. Ultraviolet radiation and human health. *Clin. Dermatol.* **1998**, *16*, 83–89. [CrossRef]
9. Vecchia, P.; Hietanen, M.; Stuck, B.E.; van Deventer, E.; Niu, S. *Protecting Workers from Ultraviolet Radiation*; International Commission on Non-Ionizing Radiation Protection: Oberschleißheim, Germany, 2007; Volume 14.
10. International Agency for Research on Cancer. Solar and ultraviolet radiation. In *Monographs on the Evaluation of Carcinogenic Risks to Humans*; International Agency for Research on Cancer: Lyon, France, 1992; Volume 55.
11. Young, R.W. The family of sunlight-related eye diseases. *Optom. Vis. Sci. Off. Publ. Am. Acad. Optom.* **1994**, *71*, 125–144. [CrossRef]

12. Jemal, A.; Bray, F.; Center, M.M.; Ferlay, J.; Ward, E.; Forman, D. Global Cancer Statistics. *CA Cancer J. Clin.* **2011**, *61*, 69–90. [CrossRef]
13. Torre, L.A.; Bray, F.; Siegel, R.L.; Ferlay, J.; Lortet-Tieulent, J.; Jemal, A. Global Cancer Statistics, 2012. *CA Cancer J. Clin.* **2015**, *65*, 87–108. [CrossRef]
14. Radespiel-Tröger, M.; Meyer, M.; Pfahlberg, A.; Lausen, B.; Uter, W.; Gefeller, O. Outdoor work and skin cancer incidence: A registry-based study in Bavaria. *Int. Arch. Occup. Environ. Health* **2009**, *82*, 357. [CrossRef]
15. Coldiron, B.M. The UV index: A weather report for skin. *Clin. Dermatol.* **1998**, *16*, 441–446. [CrossRef]
16. Milon, A.; Sottas, P.E.; Bulliard, J.L.; Vernez, D. Effective exposure to solar UV in building workers: Influence of local and individual factors. *J. Expo. Sci. Environ. Epidemiol.* **2007**, *17*, 58. [CrossRef] [PubMed]
17. Silva, A.A. The diffuse component of erythemal ultraviolet radiation. *Photochem. Photobiol. Sci.* **2015**, *14*, 1941–1951. [CrossRef] [PubMed]
18. Cañada, J.; Esteve, A.; Marin, M.; Utrillas, M.; Tena, F.; Martínez-Lozano, J. Study of erythemal, UV (A+B) and global solar radiation in Valencia (Spain). *Int. J. Climatol.* **2008**, *28*, 693–702. [CrossRef]
19. Rusińska, A.; Pludowski, P.; Walczak, M.; Borszewska-Kornacka, M.K.; Bossowski, A.; Chlebna-Sokół, D.; Czech-Kowalska, J.; Dobrzańska, A.; Franek, E.; Helwich, E.; et al. Vitamin D supplementation guidelines for general population and groups at risk of vitamin D deficiency in Poland–recommendations of the Polish Society of Pediatric Endocrinology and Diabetes and the Expert Panel with participation of National Specialist Consultants and Representatives of Scientific Societies—2018 update. *Front. Endocrinol.* **2018**, *9*, 246. [CrossRef]
20. Krzyścin, J.W.; Lesiak, A.; Narbutt, J.; Sobolewski, P.; Guzikowski, J. Perspectives of UV nowcasting to monitor personal pro-health outdoor activities. *J. Photochem. Photobiol. B Biol.* **2018**, *184*, 27–33. [CrossRef]
21. Webb, A.R.; Holick, M.F. The role of sunlight in the cutaneous production of vitamin D3. *Annu. Rev. Nutr.* **1988**, *8*, 375–399. [CrossRef]
22. Thieden, E.; Philipsen, P.A.; Heydenreich, J.; Wulf, H.C. UV radiation exposure related to age, sex, occupation, and sun behavior based on time-stamped personal dosimeter readings. *Arch. Dermatol.* **2004**, *140*, 197–203. [CrossRef]
23. Stepanski, B.M.; Mayer, J.A. Solar protection behaviors among outdoor workers. *J. Occup. Environ. Med.* **1998**, *40*, 43–48. [CrossRef]
24. Kasparian, N.A.; McLoone, J.K.; Meiser, B. Skin cancer-related prevention and screening behaviors: A review of the literature. *J. Behav. Med.* **2009**, *32*, 406–428. [CrossRef]
25. Buller, D.B.; Cokkinides, V.; Hall, H.I.; Hartman, A.M.; Saraiya, M.; Miller, E.; Paddock, L.; Glanz, K. Prevalence of sunburn, sun protection, and indoor tanning behaviors among Americans: Review from national surveys and case studies of 3 states. *J. Am. Acad. Dermatol.* **2011**, *65*, S114.e1–S114.e11. [CrossRef]
26. Hault, K.; Rönsch, H.; Beissert, S.; Knuschke, P.; Bauer, A. Knowledge of outdoor workers on the effects of natural UV radiation and methods of protection against exposure. *J. Eur. Acad. Dermatol. Venereol.* **2016**, *30*, 34–37. [CrossRef] [PubMed]
27. Larkö, O.; Diffey, B.L. Natural UV-B radiation received by people with outdoor, indoor, and mixed occupations and UV-B treatment of psoriasis. *Clin. Exp. Dermatol.* **1983**, *8*, 279–285. [CrossRef] [PubMed]
28. Holman, C.D.J.; Gibson, I.M.; Stephenson, M.; Armstrong, B.K. Ultraviolet irradiation of human body sites in relation to occupation and outdoor activity: Field studies using personal UVR dosimeters. *Clin. Exp. Dermatol.* **1983**, *8*, 269–277. [CrossRef] [PubMed]
29. Serrano, M.A.; Cañada, J.; Moreno, J.C. Erythemal Ultraviolet exposure in two groups of outdoor workers in Valencia, Spain. *Photochem. Photobiol.* **2009**, *85*, 1468–1473. [CrossRef]
30. Gies, P.; Wright, J. Measured solar ultraviolet radiation exposures of outdoor workers in Queensland in the building and construction industry. *Photochem. Photobiol.* **2003**, *78*, 342–348. [CrossRef]
31. Hammond, V.; Reeder, A.; Gray, A. Patterns of real-time occupational ultraviolet radiation exposure among a sample of outdoor workers in New Zealand. *Public Health* **2009**, *123*, 182–187. [CrossRef]
32. Sliney, D.H. UV radiation ocular exposure dosimetry. *J. Photochem. Photobiol. B Biol.* **1995**, *31*, 69–77. [CrossRef]
33. World Meteorological Organization (WMO). *Scientific Assessment of Ozone Depletion: 2014, Global Ozone Research and Monitoring Project—Report*; WMO: Geneva, Switzerland, 2014; Volume 55, p. 416.

34. Robaa, S. A study of ultraviolet solar radiation at Cairo urban area, Egypt. *Sol. Energy* **2004**, *77*, 251–259. [CrossRef]
35. Cabrera, A.; Uclés, D.; Agüera, T. *Informes y Monografías / Análisis de la Campaña Hortofrutícola de Almería 2015/2016 [Reports and Monographs/ Analysis of the Fruit and Vegetable Sector of Almería 2015/2016]*; Fundación Cajamar: Almería, España, 2016.
36. Statuto, D.; Picuno, P.; Abdel-Ghany, A.M. Shading methods for crop protection under greenhouse in Mediterranean areas. In Proceedings of the 47th International Symposium, Actual Tasks on Agricultural Engineering, Opatija, Croatia, 5–7 March 2019; University of Zagreb, Faculty of Agriculture: Zagreb, Croatia, 2019; pp. 297–306.
37. Callejón-Ferre, A.J.; Pérez-Alonso, J.; Sánchez-Hermosilla, J.; Carreño-Ortega, A. Ergonomics and psycho-sociological quality indexes in greenhouses, Almería (Spain). *Span. J. Agric. Res.* **2009**, *7*, 50–58. [CrossRef]
38. Pérez-Alonso, J.; Callejón-Ferre, A.J.; Carreño-Ortega, A.; Sánchez-Hermosilla, J. Approach to the evaluation of the thermal work environment in the greenhouse-construction industry of SE Spain. *Build. Environ.* **2011**, *46*, 1725–1734. [CrossRef]
39. Gómez-Galán, M.; Pérez-Alonso, J.; Callejón-Ferre, Á.J.; Sánchez-Hermosilla-López, J. Assessment of postural load during melon cultivation in Mediterranean greenhouses. *Sustainability* **2018**, *10*, 2729. [CrossRef]
40. Gómez-Galán, M.; González-Parra, J.M.; Pérez-Alonso, J.; Golasi, I.; Callejón-Ferre, Á.J. Forced Postures in Courgette Greenhouse Workers. *Agronomy* **2019**, *9*, 253. [CrossRef]
41. García-Ruiz, R.A.; López-Martínez, J.; Blanco-Claraco, J.L.; Pérez-Alonso, J.; Callejón-Ferre, Á.J. On air temperature distribution and ISO 7726-defined heterogeneity inside a typical greenhouse in Almería. *Comput. Electron. Agric.* **2018**, *151*, 264–275. [CrossRef]
42. López-Martínez, J.; Blanco-Claraco, J.L.; Pérez-Alonso, J.; Callejón-Ferre, A.J. Distributed network for measuring climatic parameters in heterogeneous environments: Application in a greenhouse. *Comput. Electron. Agric.* **2018**, *145*, 105–121. [CrossRef]
43. Carmona-Benjumea, A. Datos antropométricos de la población laboral española. In *Prevención, Trabajo y Salud*; Revista del Instituto Nacional de Seguridad e Higiene en el Trabajo: Madrid, Spain, 2001; Volume 14, pp. 22–35.
44. Scordo, A.; Maltese, A.; Ciraolo, G.; La Loggia, G. Estimation of the time lag occurring between vegetation indices and aridity indices in a Sicilian semi-arid catchment. *Ital. J. Remote Sens.* **2009**, *41*, 33–46. [CrossRef]
45. Callejon-Ferre, A.J.; Manzano-Agugliaro, F.; Diaz-Perez, M.; Carreno-Sanchez, J. Improving the climate safety of workers in Almería-type greenhouses in Spain by predicting the periods when they are most likely to suffer thermal stress. *Appl. Ergon.* **2011**, *42*, 391–396. [CrossRef]
46. Gambichler, T.; Laperre, J.; Hoffmann, K. The European standard for sun-protective clothing: EN 13758. *J. Eur. Acad. Dermatol. Venereol.* **2006**, *20*, 125–130. [CrossRef]
47. CIE. *Sunscreen Testing (UVB)*; Report cie 90; CIE: Vienna, Austria, 1991; ISBN 3900734275.

Capítulo 3

Resumen de las publicaciones científicas

Como se ha explicado en el Capítulo 2, esta Tesis Doctoral está compuesta de 3 publicaciones científicas. A continuación, se hará un resumen de cada una de ellas:

3.1. Publicación científica 1

“ **On air temperature distribution and ISO 7726-defined heterogeneity inside a typical greenhouse in Almería**”

A pesar de que los invernaderos suavizan el ambiente climático con respecto al exterior, se producen grandes variaciones de temperatura del aire y humedad a lo largo del día. Humedad y especialmente temperatura del aire son los principales parámetros que afectan tanto a trabajadores como a cultivo en el interior de los invernaderos [12, 13]. En Almería, la temperatura de aire dentro de un invernadero varia desde cerca de 0°C por la noche en invierno a alrededor de 50°C a mediodía en verano [9].

Varios autores [14, 15, 16, 17, 18, 19] han informado de la existencia de riesgo por estrés térmico por calor fundamentalmente durante los meses más cálidos (primavera y verano). Ambientes con alta temperatura y humedad pueden afectar a la seguridad de los trabajadores, causando problemas severos a su sistema cardiovascular y termorregulador [20, 21]. Además, ese tipo de ambiente también tiene influencia en la productividad de los trabajadores. También se ha informado de la existencia de riesgo por estrés térmico por frío en invierno [14].

Para evaluar el ambiente térmico y su influencia sobre los trabajadores, es

necesario seguir ciertas normas [22]. De acuerdo al Organización Internacional de Normalización (ISO), el ambiente es clasificado en moderado o extremo. Dependiendo de la categoría, se utilizan determinados índices y normas ISO. Para calcular esos índices, en cualquier caso, se requiere la medida de varios parámetros climáticos y en algunos casos también la tasa metabólica relacionada con la actividad física llevada a cabo por los trabajadores, basada en la ISO 8996 [23], y el aislamiento de ropa y la tasa de sudor según la ISO 9920 [24]. Además, la ISO 7726 [25] define las especificaciones y métodos que deben cumplirse para evaluar el ambiente térmico. Las especificaciones son relativas a las características de medida de los instrumentos como el rango de medida, la precisión y el tiempo de respuesta. Con respecto a los métodos, las magnitudes físicas pueden variar con el espacio tanto horizontal como verticalmente y el ambiente puede ser considerado homogéneo o heterogéneo. Un ambiente será homogéneo si la magnitud física considerada es prácticamente uniforme en el área analizado. Contrariamente, para considerar ambientes heterogéneos, las magnitudes físicas deben ser medidas en diferentes puntos tanto en horizontal como en vertical. En vertical, la ISO 7726 [25] específicamente establece tres alturas donde las medidas deben ser realizadas: tobillo, abdomen y cabeza.

Hay escasez de datos experimentales en invernaderos sobre temperatura de aire relativos al estudio del estrés térmico de trabajadores, ya que normalmente los datos experimentales existentes están centrados en el cultivo y analizan cortos periodos de tiempo. Algunos trabajos han detectado diferencias de temperatura de aire considerables en dirección horizontal y vertical dentro de un invernadero. López et al. (2013) y Kittas et al. [26, 27] obtuvieron diferencias horizontales de temperatura de aire de alrededor de 6°C y 8°C, respectivamente. Zhao et al., Soni et al. y Zorzeto et al. [13, 28, 29] obtuvieron diferencias verticales de temperatura de aire de alrededor de 7°C, 10°C y 14°C, respectivamente. En simulaciones tales como CFD (Computational Fluids Dynamics) también se han observado grandes variaciones de temperatura de aire en invernaderos: Molina-Aiz et al. [30] obtuvieron variaciones de temperatura de alrededor de 9°C en un invernadero similar y en una localización cercana a este trabajo, y Tong et al. [31] obtuvieron variaciones de temperatura de hasta 12°C. Además, López-Martínez et al. [32] previamente analizaron las condiciones de heterogeneidad según la ISO 7726 dentro de un invernadero, siendo confirmadas durante un corto periodo de tiempo en invierno.

En los últimos años, las redes de sensores inalámbricas (WSNs o Wireless Sensor Networks) han sido usadas para realizar medidas en diferentes puntos en lugares como invernaderos. Este tipo de redes consisten en nodos alimentados por baterías y compuestos por sensores que proporcionan la información

correspondiente en tiempo real y la transmiten a una estación central donde serán procesados para ser monitoreados y controlados [33]. Las principales ventajas de las WSN son la capacidad de medir múltiples puntos evitando el uso de cables, los cuales normalmente son dañados y se desgastan al ser expuestos a un ambiente agresivo (grandes variaciones de temperatura de aire o humedad) y pueden entorpecer las labores de cultivo. Además, gracias a los avances en electrónica y comunicación inalámbrica, es posible desarrollar WSNs con bajo coste y bajo consumo de energía.

El experimento se llevó a cabo en un invernadero "raspa y amagado"de 1024 m^2 de área y localizado a 15 km al este de Almería (36°51'54"N – 2°17'02"W y 98 m sobre el nivel del mar), en el sureste de España. La campaña experimental se llevó a cabo durante un año completo, desde diciembre de 2016 a noviembre de 2017, con una frecuencia de medidas de 30 segundos. La estructura del invernadero es de acero y esta cubierta por tres capas de polietileno de 200 μ m, con 81 % de transmitancia de luz visible y 29 % de transmitancia de luz difusa. El suelo del invernadero esta cubierto de arena y gravilla, y el cultivo durante el estudio es tomate. La ventilación es natural a través de ventanas laterales y cenitales. Cada ventana es abierta y cerrada mediante motores eléctricos, y están programadas para lograr las condiciones fisiológicas y de producción optimas para el cultivo.

Se implementó una WSN con 12 estaciones de medida distribuidas en el interior del invernadero y una en el exterior. Cada estación consiste en una estructura con 3 alturas (0.23 m, 0.93 m and 1.56 m,equivalentes a tobillo, abdomen y cabeza de acuerdo al percentil 50 de la población española [34]) donde los sensores fueron instalados. En cada altura se midió temperatura de aire (ta), temperatura de globo (tg), humedad de aire relativa (RH) y velocidad de aire(v_a). Además, se midió el índice de ultravioleta (UVI) en la altura superior. Las características de los instrumentos de medida cumplen con las especificaciones definidas en la ISO 7726 (excepto por la medida de UVI, que no esta considerada en esta norma). La WSN empleó IEEE 802.15.4 y ZigBee como protocolo de comunicación, y un smartphone para transmitir los datos por 4G a un servidor instalado en el Centro de Proceso de Datos de la Universidad de Almería (CPD-UAL).

A pesar de los diferentes parámetros medidos, el estudió finalmente se centró en la temperatura de aire. La norma ISO 7726 define diferentes escenarios dependiendo del tipo de ambiente considerado, siendo en este caso un ambiente de clase S o de estrés por calor, y especifica que para evaluar si el ambiente es heterogéneo las medidas deben realizarse a tres alturas, correspondientes a tobillo, abdomen y cabeza. En el caso estudiado, la norma ISO 7726 define el limite de ambiente heterogéneo en ±2°C respecto de la media ponderada. Para calcular la media ponderada, se deben aplicar los siguien-

tes factores de ponderación a las medidas: 1 para tobillo y cabeza, y 2 para abdomen. La heterogeneidad se evalúa en dirección horizontal (calculando la media de la estación de medida completa, es decir, de las tres alturas, resultando 12 valores para cada medida y comparándolos con los límites de heterogeneidad) y en dirección vertical (calculando la media de cada altura para todas las estaciones de medida, resultando 3 valores para cada medida, y comparándolos con los límites de heterogeneidad). Si alguno de los valores excede la media ponderada, existirá heterogeneidad, ya sea horizontal o vertical.

En primer lugar se evalúa la variación de temperatura de aire, obteniendo temperaturas entre 1°C y 55°C en el interior del invernadero. Se observa que la temperatura de la altura 3 es mayor que el resto de alturas durante el día, pero la menor durante la noche. Esto puede ser debido a que el gradiente térmico se invierte, actuando el suelo como acumulador de calor y por la noche transfiriendo calor al ambiente. La temperatura en primavera se observa que durante el día es mayor que en otoño. Además, se muestran vídeos en 3D que representan las medidas de la temperatura de aire en cada instante durante el año completo, donde se puede observar como se calienta el sureste del invernadero sobre el resto en la primera parte del día, y progresivamente estas temperaturas van disminuyendo a medida que la posición del sol va cambiando, hasta que al final del día la zona oeste del invernadero tiene una mayor temperatura de aire que el resto.

A continuación, se evalúa la heterogeneidad de temperatura de aire, demostrándose dicha heterogeneidad tanto en horizontal como en vertical. Se obtiene que más del 80 % de los días se produce heterogeneidad horizontal y alrededor del 49 % se produce heterogeneidad vertical durante el año completo, concentrándose en una mayor cantidad en estaciones frías (invierno y otoño), durante las horas centrales del día y con ausencia de nubosidad. Se observan variaciones horizontales y verticales de temperatura de aire respecto al valor medio de 6.3°C y 5.8°C, respectivamente. Respecto a variaciones horizontales y verticales globales de temperatura de aire, se registran 8.4°C y 10.6°C, respectivamente.

Por otro lado, se estudia la relación entre temperatura de aire y temperatura de globo en el interior del invernadero. La temperatura de globo es una medida cualitativa de la radiación incidente cuando se compara con la temperatura de aire. Se comparan ambas temperaturas en las horas centrales del día, que es cuando se producen diferencias significativas, graficándose los valores medidos de cada mes y obteniéndose una curva cerrada sin bucles. Esta curva representativa muestra que la radiación solar difusa produce mayores variaciones entre la temperatura de globo y temperatura de aire en invierno y primavera que en otoño y verano, respectivamente. En vista de estos re-

sultados, aunque existe una tendencia a aumentar esta diferencia cuando la altitud del sol es más alta (solsticio de verano), esto no solo está relacionado con la radiación solar, donde en los meses de junio y julio alcanzaría los valores máximos.

Finalmente, se ofrecen recomendaciones para evaluar el ambiente térmico dentro de invernaderos, destacando las siguientes:

- Las medidas deben tomarse a diferentes localizaciones, tanto horizontal como verticalmente de acuerdo a la norma ISO 7726. Verticalmente las medidas deben realizarse a 3 alturas (tobillo, abdomen y cabeza), pero horizontalmente la norma no especifica el número de puntos donde realizar las medidas. Debido a que se observa que la distribución horizontal de temperatura de aire esta condicionada por el acimut y la elevación del sol, se recomienda realizar medidas en al menos 4 puntos distribuidos con respecto a los puntos cardinales en el interior del invernadero.

- Es indispensable incluir la parte central del día en las medidas, ya que es donde se podrá producir mayor heterogeneidad, así como considerar el periodo de trabajo en el análisis.

- Las medidas deben incluir periodos sin nubosidad, que es donde se producen las mayores diferencias de temperatura de aire.

- Debido a las variaciones durante el año, para una completa evaluación del estrés térmico el estudio se debe extender durante un año completo.

- Con respecto a la WSN usada para realizar las mediciones, se recomienda situar las radio antenas en zonas altas para evitar las interferencias y perdidas de señal, teniendo en cuenta el crecimiento del cultivo durante la cosecha. Esto se vuelve particularmente importante para las bandas de radio en el rango de GHz, debido a la fuerte absorción (atenuación) de las ondas de radio por las plantas (por su humedad).

3.2. Publicación científica 2

“ **Uncertainty-Aware Calibration of a Hot-Wire Anemometer With Gaussian Process Regression**”

Los anemómetros de hilo térmico son dispositivos de bajo coste que son normalmente empleados para medir velocidad de viento, aunque también se

utilizan para medir otros fluidos. Están compuestos de un alambre delgado con un diámetro de entre 0.5-5 μm, y una longitud de 1 mm. Por lo general, están hechos de platino, tungsteno o platino-iridio. Su principio de funcionamiento consiste en calentar el alambre con una corriente eléctrica (efecto Joule) hasta cierta temperatura por encima del ambiente y luego exponerlo al flujo de fluido incidente de modo que se enfríe, principalmente, por transferencia de calor por convección. La velocidad del fluido se puede inferir en función de la transferencia de calor desde el cable calentado a el fluido. Los anemómetros de hilo caliente se pueden clasificar, según su arquitectura de control, en: anemómetro de temperatura constante (CTA), anemómetro de corriente constante (CCA) y anemómetro de voltaje constante (CVA). La diferencia entre ellos depende de la variable cuyo punto de ajuste es la entrada de los circuitos de control, ya sea, temperatura de resistencia, corriente eléctrica o voltaje aplicado, respectivamente.

Los anemómetros de hilo caliente se han utilizado anteriormente en una amplia gama de aplicaciones que requieren medir la velocidad de un fluido [35, 36, 37, 38]. En particular, son muy adecuados para mediciones de bajo caudal, y los fabricantes a menudo recomiendan su uso para velocidades de viento bajas a medias. Como se demuestra en la publicación, se ha observado un buen rendimiento para velocidades de hasta 20 m/s, no recomendándose utilizar este tipo de sensores para velocidades más altas debido a que el error e incertidumbre de la predicción aumentaría, y debido a la fragilidad mecánica del sensor. Aunque el fabricante del anemómetro de hilo caliente utilizado no proporciona una velocidad mínima detectable, en esta investigación se permitió detectar cambios en un rango de 0.1-0.2 m/s. Los anemómetros de hilo caliente son hoy en día ampliamente utilizados por su alto ancho de banda de medición, que permite detectar fluctuaciones de velocidad rápidas. Su pequeño tamaño y bajo peso también los hacen adecuados para aplicaciones con espacio limitado. Son fáciles de manejar, de bajo costo y, además, requieren muy poca energía para funcionar, lo que permite su uso en dispositivos que funcionan con baterías [39].

La calibración de anemómetros de hilo caliente se lleva a cabo típicamente para una temperatura constante predefinida. Esta se convierte en una de las principales desventajas de este tipo de sensores [40]: si operan en un flujo de fluido a una temperatura diferente que la utilizada durante la calibración, las mediciones no serán precisas.

Algunos autores han desarrollado diferentes métodos para corregir las mediciones de la velocidad del viento en anemómetros de hilo caliente [41, 42, 43, 44]. Estos métodos generalmente requieren otros parámetros específicos de la aplicación, como la viscosidad cinemática y la conductividad térmica del fluido, pero siempre con una influencia significativa de la temperatura de

aire en las correcciones [45, 46].

La mayoría de las aplicaciones prácticas de detección de la velocidad del viento implican operar a temperaturas que varían durante el día y las diferentes estaciones del año. Incluso si el sensor funciona aislado o cubierto, la temperatura aún puede presentar variaciones significativas. Es conocido el hecho de que las lecturas de los anemómetros de hilo caliente dependen tanto de la temperatura ambiente como de la temperatura del alambre [41, 42, 43, 44]. Por esta razón, la temperatura ambiente se debe considerar como una variable adicional para obtener la velocidad del viento a partir de su relación no lineal (generalmente la temperatura del alambre siempre es considerada).

En esta publicación se utilizan técnicas de aprendizaje automático (o ML, por sus siglas en inglés, Machine Learning) para realizar la calibración de un anemómetro de hilo caliente. En particular, se utilizan Regresión de Procesos Gaussianos (GPR, por Gaussian Process Regression) [47], por ser el método que arroja los mejores resultados entre los métodos comparados en este estudio. Un Proceso Gaussiano (GP) es una distribución sobre funciones, y GPR es un método de aprendizaje supervisado, no paramétrico, bayesiano, con amplias aplicaciones en la industria y la investigación académica [48, 49, 50]. En resumen, el GPR toma un conjunto de muestras y construye un modelo a partir de ellas estimando la probabilidad probabilidad a posteriori del GP, construyendo un modelo capaz de hacer predicciones sobre valores no observados en las muestras. Una característica clave del GP es su capacidad de proporcionar una medida de incertidumbre para cada predicción. Además, un GPR puede expresar cualquier conocimiento previo, por ejemplo, de un experto, mediante funciones de densidad de probabilidad a priori y tiene una buena adaptabilidad al tratar problemas complejos no lineales con muestras pequeñas.

En comparación con otros métodos de aprendizaje automático no lineales y ampliamente utilizados, como Máquinas de Soporte Vectorial (SVM o Support Vector Machines) [51, 52, 53, 54] o Redes Neuronales Artificiales (ANN o Artificial Neural Networks) [55, 56, 57], GPR tiene las ventajas de ser más fácil de implementar, auto-adaptativo para permitir una estimación de parámetros superior, lo suficientemente flexible como para hacer inferencias no paramétricas [58] y proporcionar una estimación basada en la incertidumbre de salida. Este último aspecto es de suma importancia para cualquier proceso de ingeniería, ya que cualquier medición física, directa o indirecta, debe ir acompañada de su precisión esperada.

Los experimentos se llevaron a cabo en un túnel de viento en la Universidad de Almería (España). El túnel tiene una longitud de 4.74 m, una sección transversal circular de 38.8 cm de diámetro, una relación de contracción de 1:5:32 y el coeficiente entre el diámetro de entrada y la longitud de

la sección de contracción es 0.92 [59, 60]. Un ventilador axial (Modelo HCT-45-2T-3/AL, Sodeca S.A., Sant Quirze de Besora, España) induce el flujo de aire en el túnel de viento, y un Inversor Micromaster 420 (Siemens Energy & Automation Inc., Alpharetta, GA , EE. UU.) se utiliza para controlar la velocidad del ventilador, modulando la frecuencia actual entre 0 y 50 Hz.

El anemómetro bajo calibración es un anemómetro de hilo caliente, en concreto el modelo "revisión C"de "Modern Device". Para realizar la calibración, su utilizó un anemómetro más fiable, modelo "Windsonic"de Gill Instruments Ltd, como *ground truth* (valores verdad o de referencia). Este último es un anemómetro ultrasónico, con un rango de medición de 0 a 60 m/s y una precisión de $\pm 2\,\%$. Además, la temperatura del aire se mide mediante una sonda PT100 para mejorar la precisión de las mediciones de temperatura propias del anemómetro de hilo caliente.

Para lograr la calibración del sensor de viento, es necesario encontrar la relación (si existe) entre las entradas y salidas, de modo que el modelo calibrado sea capaz de predecir los valores de salida y sean lo más cerca posible de los valores reales. Se consideran como entradas del sistema la lectura de voltaje sin procesar del anemómetro de hilo caliente y la temperatura de aire del sensor PT100, mientras que la salida del sistema es la velocidad del viento medida desde el anemómetro ultrasónico. Los datos de estos tres sensores (voltaje del anemómetro de alambre caliente en voltios, temperatura del aire en grados Celsius y viento del anemómetro ultrasónico en metros por segundo) se midieron cada 2 segundos, mientras que la velocidad del viento varió entre 0 y 21 m/s. El controlador permite cambiar la velocidad continuamente (por ejemplo, una rampa de velocidad), pero la velocidad se incrementó paso a paso, para permitir que el flujo dentro del túnel se estabilizase. Se esperó durante 20 segundos después de cada cambio de velocidad de viento para asegurar que ambos sensores y el flujo fueran estables antes de registrar medidas. Se realizaron varias campañas de mediciones a diferentes temperaturas de aire entre 19 y 30°C.

El método de medición fue similar para las diferentes campañas de medida a diferente temperatura de aire: se comenzó a 0 m/s, la velocidad de viento fue incrementada en pequeños saltos, al mismo tiempo que se intentaba obtener un buen muestreo de velocidades de viento bajas a medias, donde los anemómetros de hilo caliente son más fiables y sus condiciones de trabajo son más comunes. Por lo tanto, el experimento se centra principalmente en valores de velocidad de viento de hasta 10-15 m/s, aproximadamente. Por otro lado, la velocidad de viento se incrementó modulando la frecuencia manualmente, esperando un tiempo determinado de estabilización y luego durante otro período de tiempo para permitir que se capturen suficientes registros de datos. Se obtuvieron más de 4000 puntos de datos de entrada-salida.

El método de validación experimental para predecir la velocidad de viento basado en el modelo de GPR propuesto se describe en un diagrama de flujo en la Figura 1.

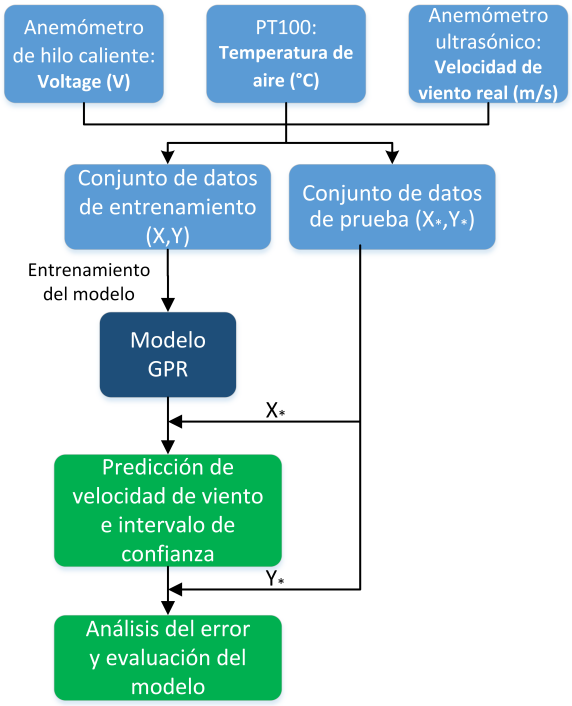

Figura 1. Diagrama de flujo que describe el proceso de calibración y validación propuesto.

Como se puede observar, todo el conjunto de datos de entrenamiento se utiliza para entrenar el modelo GPR: tanto la matriz X, que corresponde al voltaje del anemómetro de hilo caliente y la temperatura de aire, como el vector Y que corresponde a la velocidad real del viento medida con el anemómetro ultrasónico. Una vez que el modelo ha sido entrenado, la matriz X_* del conjunto de prueba (voltaje del anemómetro de hilo caliente y temperatura de aire) se usa para predecir la velocidad del viento y obtener el intervalo de confianza correspondiente. Finalmente, el vector Y_* (velocidad del viento real) del conjunto de prueba se usa para analizar el error cometido y evaluar el modelo GPR. Se incluyen diferentes tamaños de datos en los conjuntos de entrenamiento y prueba.

Para garantizar una estimación correcta de los intervalos de confianza (o también denominados intervalos creíbles), el modelo GPR debe tener en cuenta el ruido gaussiano aditivo empleado en el modelo [50]. La "Toolbox" de MATLAB para los modelos GPR optimiza la desviación estándar de ese rui-

do, denotada como "Sigma", mientras entrena el modelo para un conjunto de datos de entrada dado. Finalmente, cuando el modelo GPR hace una predicción, también genera un intervalo de predicción al considerar la incertidumbre de ambos, el ruido aditivo (el valor "Sigma"), y el valor de incertidumbre de los parámetros aprendidos de los datos.

En primer lugar se evalúa si el modelo GPR es el que es capaz de lograr mejores predicciones de acuerdo a los datos obtenidos. Para verificar este hecho, se evalúa el desempeño de diferentes modelos de calibración calculando sus errores de validación, todo ello mediante el uso varias métricas: el error medio absoluto (o MAE, por sus siglas en inglés, Mean Absolute Error), la raíz del error cuadrático medio (o RMSE, por Root Mean Square Error) y el coeficiente de determinación o R^2. Este proceso se llevó a cabo con la aplicación "MATLAB's regression Learner App", incluida en "Statistics and Machine Learning Toolbox". El conjunto de datos completo se empleó para entrenar los modelos, y se utilizó validación cruzada con 6 particiones o intervalos. La validación cruzada divide los datos en particiones, entrena el modelo utilizando las observaciones fuera de la partición, evalúa el rendimiento del modelo utilizando datos en la partición y finalmente calcula el error de prueba promedio de todas las particiones. Este método hace un uso eficiente de todos los datos y permite obtener una buena estimación de la precisión predictiva del modelo final. Los resultados confirman que el GPR es el modelo de regresión que mejor se ajusta a los datos. En particular, el modelo GPR con función de covarianza exponencial produce el MAE y RMSE más bajos, y un buen valor de R^2.

Por otro lado, se utiliza el Criterio de Información Bayesiano (BIC, por sus siglas en inglés, Bayesian Information Criterion) [61, 62] para comparar los modelos GPR. BIC es una métrica basada en calcular la probabilidad más alta a posteriori para encontrar el mejor modelo para hacer predicciones. El modelo se ajusta mejor a los datos cuando se obtiene un valor más bajo de BIC. La probabilidad tiene en cuenta tanto la proximidad de los valores predichos a los *ground truth* como la magnitud de la incertidumbre predicha. Con esta métrica también se confirma que el modelo GPR con función de covarianza exponencial es el modelo que es capaz de lograr mejores predicciones.

A continuación, se aplica el GPR con función de covarianza exponencial a los datos, seleccionándose al azar los puntos de entrenamiento y prueba, y constituyendo el 70 % y 30 % de los datos respectivamente. Los conjuntos de entrenamiento y prueba se normalizan en [0,1] y los hiperparámetros óptimos se obtienen mediante el método de gradiente conjugado. Las predicciones y la varianza se calculan con los conjuntos de entrenamiento y prueba usando Matlab2017b. Se obtienen un MAE y RMSE para puntos de prueba

de 0.1620 m/s y 0.2833 m/s, respectivamente, mientras que R^2 para estos puntos de prueba también es alto (0.99563), de forma que se observa que los errores en la predicción son pequeños y los valores predichos en la mayoría de las ocasiones se encuentran dentro del intervalo de confianza. Los resultados están obviamente influenciados por los datos de entrenamiento, que se seleccionan al azar. Se podría pensar que con otros datos de entrenamiento, se obtendrían peores resultados. Para evaluarlo, se realizan 100 iteraciones seleccionando aleatoriamente diferentes conjuntos de entrenamiento y, en consecuencia, conjuntos de prueba, siempre cumpliendo que el 70 % de los datos se utilizan para el entrenamiento y el 30 % restante para la prueba. Se obtienen MAE, RMSE y R^2 similares, lo que indica que el modelo proporciona una buena aproximación del viento real en función del voltaje del anemómetro de hilo caliente y la temperatura del aire.

Como alternativa, se aplica la validación cruzada (o cross validation) al modelo GPR para predecir la velocidad de viento, con el objetivo de garantizar que son independientes de la partición entre datos de entrenamiento y prueba. Ahora se seleccionan conjuntos de datos completos para el entrenamiento y se validarán en otros conjuntos de datos de prueba, por tanto, no entrenados. Es decir, en este caso el modelo GPR se entrena sin una sola observación de la respuesta del sensor para una temperatura específica, y evaluaremos su rendimiento al inferir ("interpolar") su comportamiento a partir de la respuesta a otras temperaturas. En este caso, el RMSE promedio de todos los casos es 0.024 m/s para los conjuntos de datos de entrenamiento y 1.734 m/s para los conjuntos de datos de prueba. El MAE promedio es de 0.012 m/s y 1.373 m/s para los conjuntos de datos de entrenamiento y prueba, respectivamente. Como se esperaba, estos valores son similares a los resultados del método anterior para los datos de entrenamiento, pero mucho más altos para los conjuntos de datos de prueba. Esto podría explicarse por la falta de información que el GPR tiene para hacer predicciones sobre el comportamiento del sensor en condiciones de las que no ha podido aprender. Sin embargo, gracias a la naturaleza probabilística del GPR, permite tener una incertidumbre pronosticada para cada predicción, y en la mayoría de los casos donde el error es grande, la incertidumbre también es alta. En particular, el modelo GPR tiene mayores errores al estimar la velocidad del viento para los conjuntos de los extremos (los conjuntos de datos con temperaturas de aire en los extremos), ya que en esos caso las estimaciones se realizan extrapolando (no interpolando como en el resto de casos) el comportamiento del sensor para esas condiciones. Para cuantificar y demostrar este hecho, se evalúa el promedio RMSE (1.51 m/s) y MAE (1.13 m/s) cuando las predicciones son "interpoladas". Por otro lado, los valores promedio de RMSE y MAE de los dos conjuntos de datos en los que las predicciones son "extrapo-

ladas"son 2.305 m/s y 1.968 m/s, respectivamente, validando la hipótesis de que las predicciones son menos precisas cuando necesitan extrapolarse.

Finalmente, dado que el método propuesto propone usar la temperatura de aire real como una entrada al modelo de estimación de la velocidad de viento, es necesario conocer cuanto afecta la medición de la temperatura de aire a los resultados. La configuración experimental empleada en este estudio consiste en una sonda PT100 para medir la temperatura del aire, con una precisión de ± 0.06°C a 0°C. Para evaluar su influencia en el rendimiento del modelo GPR, se han introducido diferentes errores en la medición de la temperatura ambiente, que son los siguientes:

- Errores aleatorios: Consisten en ruido aleatorio y se han considerado $\pm 0.1°C$, $\pm 0.2°C$, $\pm 0.5°C$, and $\pm 1°C$, respectivamente.
- Errores sistemáticos: Son aquellos que se producen de igual modo en todas las mediciones que se realizan de una magnitud y un ejemplo de el caso evaluado puede ser no proteger el sensor de temperatura de la radiación solar directa, lo que afecta a sus mediciones. En este caso se han considerado $+0.25°C$, $+0.5°C$, $+1°C$, and $+1.5°C$, con respecto al valor real.

Los resultados para estos errores se comparan con los resultados obtenidos en el experimento con la sonda PT100. Se observa que para errores aleatorios de temperatura de aire de $\pm 0.1°C$ y $\pm 0.2°C$, los resultados de MAE, RMSE y R^2 para los puntos de prueba son similares. Para una precisión de la temperatura del aire de $\pm 0.5°C$, la variación es más notable, aunque aún puede ser aceptable, mientras que para $\pm 1°C$ el error es, como se esperaba, mucho mayor. Según los resultados de los errores sistemáticos, el modelo GPR es más sensible a ellos y, en consecuencia, produce predicciones más erróneas. Se aceptan errores sistemáticos de hasta $+0.25°C$. Resumiendo, atendiendo a los resultados obtenidos, podemos concluir que el modelo GPR funciona con una precisión razonable con errores aleatorios de hasta $\pm 0.5°C$ o con errores sistemáticos de hasta $+0.25°C$.

3.3. Publicación científica 3

" **Ultraviolet Index (UVI) inside an Almería-Type Greenhouse (Southeastern Spain)**"

La radiación ultravioleta (UV) es una parte de la radiación óptica que cubre las longitudes de onda entre 100 y 400 nm. Al mismo tiempo, la radiación

UV se divide en tres bandas diferentes: UVA (315-400 nm), UVB (280-315 nm) y UVC (100-280 nm). La intensidad de la radiación UV aumenta con la elevación del sol, menor latitud, mayor altitud y reflexión del suelo, y disminuye con la presencia de nubes y ciertos gases en la atmósfera como el ozono, el oxígeno y el dióxido de carbono. Precisamente, estos gases absorben toda la radiación UVC y el 90 % de la radiación UVB [63]. Por lo tanto, solo la radiación UVA y una pequeña cantidad de radiación UVB proveniente del sol llega a la superficie de la Tierra.

El Índice UV (UVI de aquí en adelante) fue introducido en Canadá en 1992 por Kerr et al [64] para informar sobre el aumento de los niveles de UV debido al agotamiento de la capa de ozono. Posteriormente, fue adoptado y recomendado como un estándar global por la Organización Mundial de la Salud et al. [65], ya que además de cuantificar la irradiación UV, indica su efecto potencial sobre los seres humanos. El UVI se basa en el eritema inducido por el espectro de acción de referencia en la piel humana [66]. El UVI es un índice adimensional con valores desde cero hacia adelante e indica el daño potencial de los rayos UV sobre los seres humanos, de modo que mientras UVI es mayor, el daño potencial es mayor y es necesario menos tiempo para producirlo. Para una mejor comprensión y conciencia pública, la Organización Mundial de la Salud et al. [65] recomienda el uso de códigos de colores según la categoría de exposición y establece un UVI igual a 3 como el umbral a partir del cual existe riesgo de daño causados por la radiación UV y, por lo tanto, es necesaria la protección solar. Cada color está estandarizado por el *Pantone Matching System* (PMS). Sin embargo, según [67], también existe riesgo para las personas con piel clara (piel tipo I y II, según Fitzpatrick [68, 69]) cuando están expuestas a un UVI entre 2 y 3 durante más de 1.5 h.

Aunque la radiación UV representa solo alrededor del 5 % de la radiación solar total [70, 71], tiene efectos nocivos considerables en los seres humanos, dependiendo de la intensidad de su exposición a los rayos UV. A corto plazo, los rayos UV producen eritema (o quemaduras solares) que podrían empeorar y provocar edema, dolor, formación de ampollas y, finalmente, descamación o pelado de la piel [70]. A largo plazo, la radiación UV produce envejecimiento de la piel (como consecuencia de cambios degenerativos en las células, tejidos fibrosos y vasos sanguíneos) [65], cáncer de piel (melanoma cutáneo maligno y cáncer de piel no melanoma) [72], lesiones oculares (cataratas, pterigium, fotoqueratitis, daño y deterioro de la retina) [73] y daño al sistema inmunitario [65]. El envejecimiento de la piel produce sequedad, flacidez, pérdida de elasticidad, arrugas, surcos en la piel, pigmentación moteada y telangiectasia [70]. La incidencia y mortalidad debido a cáncer de piel han aumentado en los últimos años [74, 75, 76]. Especialmente, el melanoma maligno cutáneo (CMM), que representa entre el 5 y 10 % de todos los cánceres de piel [77, 78]

pero tiene una tasa de mortalidad mucho más alta que el cáncer de piel no melanoma (NMSC), ya que este último progresa más lentamente y aparece en zonas del cuerpo expuestas al sol, facilitando la detección temprana [78]. Cabe destacar que los rayos UV también tienen beneficios para la salud. El 90 % de la vitamina D que necesitan los seres humanos proviene de la radiación UV [79], aunque una exposición diaria de 10 a 15 minutos en la cara, brazos y manos con radiación de baja intensidad podría ser suficiente para obtenerla [80]. Sin embargo, dependiendo de la dosis diaria recomendada de vitamina D y otros factores como nubes, contaminación del aire, pigmentación intensiva de la piel, edad avanzada o uso excesivo de cosméticos de protección solar [81], puede ser necesario aumentar el tiempo o la intensidad de la exposición, siempre tomando medidas preventivas y precauciones para evitar correr riesgos. Sin embargo, en algunos países en latitudes medias o altas no hay suficiente radiación UV durante el invierno [82], lo que causa deficiencia de vitamina D y, en consecuencia, problemas de pigmentación de la piel [83]. Además, varias enfermedades como el raquitismo, la psoriasis y el eccema se tratan con radiación UV, siempre bajo supervisión médica y considerando el riesgo potencial [65].

Los efectos de los rayos UV son mayores en personas con colores más claros de piel, cabello y ojos, y también con la presencia de pecas [70]. Respecto al color de la piel, Fitzpatrick definió diferentes tipos de piel [68, 69]. Aunque la mayoría de los cánceres de piel se producen en personas con piel tipo I o II, las personas de piel oscura también son sensibles a los efectos UV, especialmente aquellos que afectan los ojos y el sistema inmunitario. Además, cuando los cánceres de piel afectan a personas de piel oscura, generalmente se detectan en etapas más avanzadas y peligrosas. Por otro lado, la dosis de radiación UV [84, 85] y la susceptibilidad a las quemaduras solares [70] es igual entre los sexos. Sin embargo, la incidencia y mortalidad del cáncer de piel es mayor en los hombres [75, 76]. Esto podría deberse al hecho de que las mujeres pueden ser más cuidadosas con respecto a la protección solar [86, 87] y son más conscientes del riesgo de UV [88] en comparación con los hombres.

Los trabajadores al aire libre reciben entre 2 y 8 veces más de exposición a los rayos UV que los trabajadores en interior según diferentes autores [89, 90]. Este hecho hace a los trabajadores al aire libre más vulnerables a los efectos negativos de los rayos UV sobre la salud. Varios trabajos han reportado riesgos para la salud por exposición prolongada a los rayos UV en trabajadores al aire libre en todo el mundo: Serrano et al. en España [91], Milon et al. en Suiza [78], Gies et al. en Australia [92], Thieden et al. en Dinamarca [84], Stepanski et al. en los Estados Unidos [85] y Hammond et al. en Nueva Zelanda [93], entre otros. Estos riesgos para la salud también existen en días nublados porque, aunque las nubes reducen la intensidad de

la radiación UV, la intensidad de la radiación infrarroja se reduce aún más. Esto reduce la sensación de calor (que generalmente ayuda a advertir sobre el riesgo por radiación UV) y aumenta el riesgo de sobreexposición al sol [70]. Además, se produce mayor daño ocular cuando el UVI es más alto y hay nubosidad, ya que la radiación UV se dispersa y golpea los ojos en diferentes ángulos donde las defensas naturales del ojo como cejas, párpados y cuencas no ofrecen protección [94].

En los últimos tiempos, el agotamiento de la capa de ozono [95, 77] ha estado causando un aumento de los niveles de UVI. Además, el UVI en zonas rurales es más alto que en las ciudades debido a la claridad de la atmósfera y a la menor contaminación del aire (que bloquea una parte de la radiación UV) [77, 96]. En Almería, unas 55.000 personas trabajan en invernaderos [3], que son edificios agrícolas destinados a mantener condiciones climáticas adecuadas para los cultivos. Los invernaderos están compuestos de cubiertas de plástico transparentes sostenidas por estructuras metálicas ligeras, con ventilación a través de ventanas en el techo y las paredes, y radiación solar difusa [97]. Los trabajadores de invernaderos pueden considerarse trabajadores al aire libre, ya que están expuestos al viento y a la radiación UV. El principal período de trabajo en invernaderos dura desde finales de julio hasta mediados de junio; sin embargo, se extiende a casi todo el año ya que las tareas de mantenimiento también se llevan a cabo en períodos sin cultivos [7, 6, 98, 99]. Aunque solo la radiación solar difusa llega al interior de un invernadero, la radiación UV también puede ser alta [79]. Además, el suelo de los invernaderos está cubierto de arena, que refleja hasta el 15 % de la radiación UV y aumenta el UVI. Sin embargo, a pesar de todos estos factores, la radiación UV generalmente no se mide en invernaderos y los trabajadores no son conscientes de la posibilidad de que exista riesgo de daño por radiación UV en el interior de los invernaderos.

El estudio se realizó en un invernadero ubicado a 15 km al este de Almería (36°51'54"N – 2°17'02"W y 98 m sobre el nivel del mar), en España. El tipo de invernadero es el más común en la provincia de Almería: "raspa y amagado". Tiene un área de 1024 m^2 (32x32 m), con una altura de 3.4 m y 4.1 m en la canal y la cresta, respectivamente. Tiene tres capas de polietileno con un espesor de 200 μm, con una transmitancia de luz visible del 81 % y una transmitancia de luz difusa del 29 % al comienzo de su vida útil, sostenida por una estructura de acero y con ventanas laterales y cenitales automáticas que permiten ventilación natural. El suelo del invernadero está cubierto de grava y arena y la temperatura del aire dentro del invernadero oscila entre 0°C en invierno y 55°C en verano [9]. Vale la pena señalar que la cubierta de plástico de invernadero se instaló en julio de 2016 y tiene una vida útil de 3 campañas (2016-17, 2017-18 y 2018-19) debido a su desgaste y pérdida

de transmisión. Por lo tanto, los datos obtenidos en este estudio comienzan desde el final de la segunda campaña de la cubierta de plástico y se extienden hasta casi el final de la tercera campaña.

Los sensores utilizados para medir la radiación UV tienen una curva de respuesta espectral y un campo de visión que cumple con los requisitos definidos en ISO/CIE 17166 [66]. Cada sensor ha sido calibrado para medir el índice UV de acuerdo con ISO/CIE 17166, y posteriormente se ha verificado comparándolo con los datos ofrecidos por la Agencia Estatal de Meteorología (AEMet), específicamente con la estación ubicada en el aeropuerto de Almería. Además, estos sensores pueden medir la temperatura del aire, utilizándose también estos datos en el estudio.

Doce estaciones de medición se distribuyen uniformemente dentro del invernadero y otra se sitúa en el exterior. La infraestructura de las estaciones de medida se ha reutilizado, como se informó en trabajos anteriores [32], agregando nuevos sensores y software. Esta infraestructura consiste en un poste vertical y tres barras horizontales a diferentes alturas, utilizando la más alta para la instalación de los sensores UVI. Esta altura superior es de 1,56 m sobre el suelo, que corresponde a la cabeza (equivalente a la altura de los ojos) según el percentil 50 de la población española [34]. De esta manera, se analiza la radiación UV que afecta las partes del cuerpo donde puede haber un mayor riesgo para la salud, como los ojos y la cara y el cuello (que normalmente están descubiertos y expuestos a la radiación).

La campaña experimental se llevó a cabo en el invernadero descrito anteriormente durante un año completo, desde el 1 de julio de 2018 hasta el 31 de junio de 2019. El cultivo desde el comienzo de este estudio es el melón, hasta su cosecha entre el 21 y el 23 de junio de 2018. Luego, el 14 de julio de 2018, se retiró la cosecha y el 16 de agosto de 2018, la cubierta de plástico del invernadero fue blanqueada. El blanqueo generalmente se realiza al comienzo de cada cultivo (trasplante) y su objetivo principal es reducir la cantidad de radiación solar que incide en el interior del invernadero y, por lo tanto, disminuir la temperatura de aire interior, evitando el estrés en las plántulas. El producto utilizado fue "Blanco España" (un producto compuesto a base de carbonato de calcio), con dosis de 50 kg de Blanco España por 1000 m^2 de cubierta de plástico. Posteriormente, el 21 de agosto de 2018, se cultivó tomate pera durante un ciclo largo. El 6 de marzo de 2019, se realizó un nuevo blanqueo de la cubierta de plástico con dosis similares a las anteriores. La cosecha de tomate se retiró el 25 de abril de 2019 y desde entonces, tareas de mantenimiento y preparación del próximo ciclo de cosecha se llevaron a cabo hasta el final del estudio.

Durante el tiempo que se llevó a cabo este estudio, los agricultores realizaron sus labores en el invernadero, especialmente para el cultivo de tomate,

ya que el cultivo de melón solo coincidió durante un corto período al comienzo del estudio. Estas labores son: trasplante, poda de formación, aporcado (cubrir la parte inferior de la planta con arena), escardar (remover la tierra con una azada), binas/escardas, tutorado (atar el tallo de la planta con un hilo, en de tal manera que un extremo del hilo esté ubicado en la parte basal de la planta y el otro extremo esté unido a una malla horizontal de alambres ubicada dentro del invernadero a cierta altura sobre el suelo), fertirrigación, aplicación de productos fitosanitarios, polinización con abejas, despuntar ramos (eliminar los ramos axilares para mejorar el desarrollo del tallo principal), liar y destallar (eliminar hojas senescentes e infectadas), inflorescencias y adelgazamiento de frutos (eliminar los frutos deformados, dañados, de pequeño tamaño y mal posicionados), cosecha y eliminación de la planta. Por lo tanto, los agricultores han trabajado dentro del invernadero realizando estas tareas durante el estudio, siendo susceptibles a daños por los efectos de la radiación UV.

En primer lugar se presentan los resultados de la campaña de medición de UVI en el interior y exterior del invernadero y su distribución espacial, junto con una representación 3D de los datos de UVI en vídeo para cada instante de tiempo. También se analiza la relación UVI entre el interior y exterior, y la variación estacional de UVI. El valor máximo de UVI fue de 4.69 y se midió el 5 de julio de 2019 a las 12:44 a.m. en la estación de medida 5, mientras que en el exterior el UVI máximo de ese mismo día fue de 9.48 y se midió a las 12:16 a.m.. Se observa que el UVI supera el límite de riesgo hasta en cinco meses: julio, agosto, septiembre, mayo y junio. Se ha observado que la mayoría de los UVI máximos se registran en las estaciones de medida 7, 10, 11 y 12, es decir, la mayoría de los UVI máximos se registran en la esquina suroeste del invernadero. Es notable una caída significativa en UVI entre el 16 de agosto y el 8 de septiembre, lo que resulta en que el límite de riesgo no se exceda en este período. Esto se debe a que la cubierta plástica del invernadero fue blanqueada el 16 de agosto, lo que provocó el bloqueo de parte de la radiación UV mientras duró el efecto. Este efecto generalmente dura hasta la llegada de las primeras lluvias. Desde noviembre de 2018 y hasta su eliminación el 25 de abril de 2019, el cultivo de tomate alcanzó alrededor de 2,20 m de altura. Esto ha podido producir sombra, reduciendo la radiación UV y el riesgo potencial de daños a los trabajadores por radiación UV. Sin embargo, esto solo ocurre en cultivos altos (tomate de ciclo largo, pepino y berenjena, entre otros). Por otro lado, al analizar la relación UVI entre el interior y exterior, se esta analizando la capacidad de la cubierta plástica del invernadero para bloquear la radiación UV. Se observa que al blanquear la cubierta plástica del invernadero, lógicamente esta relación disminuye, al disminuir el UVI interior. El blanqueo de invernaderos generalmente se realiza en períodos de

alta radiación o temperatura para evitar el estrés en el cultivo, principalmente en su etapa inicial. Sin embargo, se ha demostrado que la radiación UV que llega al interior del invernadero se reduce considerablemente, por lo que puede usarse no solo para el cultivo, sino también como un método eficaz para proteger a los trabajadores contra la radiación UV. Podría aplicarse tanto en los meses de verano, donde se realizan trabajos de mantenimiento, como en algunos períodos de primavera (desde febrero o marzo). En ciertos cultivos de primavera no sería posible, ya que sería perjudicial para ellos (especialmente para el melón y la sandía, aunque no es descartable).

Posteriormente, se compara el UVI entre las 12 estaciones del interior del invernadero, obteniéndose mayores diferencias de UVI en periodos de verano y primavera, donde el UVI es mayor, y alcanzándose unas diferencia máxima de 2.54 en julio de 2018. Estas diferencias UVI pueden haberse acrecentado debido a la heterogeneidad del blanqueo, el desgaste de la cubierta plástica y la acumulación de suciedad en dicha cubierta. Se comparan dos días consecutivos con la particularidad de que entre ellos se produjo el blanqueo de la cubierta plástica del invernadero. Se observa que la heterogeneidad del blanqueo es una de las causas de las mayores diferencias en UVI dentro del invernadero. Además, se demuestra que el blanqueo de la cubierta plástica del invernadero es un método eficaz para reducir la radiación UV y evitar así el riesgo de daños a los trabajadores.

A continuación, se hace un análisis estacional de los valores UVI obtenidos, tanto en el interior como en el exterior del invernadero. Para ello, se calcula un día promedio, que en el caso del interior del invernadero corresponde al promedio entre las 12 estaciones de medición durante el período estacional considerado, y además se obtiene la desviación estándar asociada. Para el interior del invernadero, el límite de riesgo por radiación UV no se supera en el día promedio de ninguna estación, aunque sí lo supera la desviación estándar en verano. Sin embargo, en muchos días de primavera y verano si que se excede el límite de riesgo, y también se debe tener en cuenta que el blanqueo de la cubierta del invernadero ha contribuido a la reducción del UVI promedio. Por esa razón, se considera en el análisis el periodo de verano sin tener en cuenta el período de blanqueo. En este caso, la media está muy cerca del límite de riesgo y se reduce la desviación típica. Además, se observa que la mayor parte de la radiación UV se concentra lógicamente entre 10 y 14 horas, obteniendo el máximo UVI alrededor de las 12 horas. La desviación estándar lógicamente es más alta en mitad del día que durante la noche, donde es nula. Estos comportamientos también ocurren para el UVI medido en el exterior del invernadero, donde los días promedio de todas las estaciones, excepto el invierno, superan el límite de riesgo. Ciertas tareas como el blanqueo de la cubierta o la construcción de invernaderos se llevan a

cabo al aire libre. Por lo tanto, y en base a los datos obtenidos, es evidente la necesidad de tomar precauciones extremas contra la radiación UV.

Por otro lado, en analogía al climograma de Péguy [100], se introduce un nuevo gráfico, denominado "UVIgrama", para relacionar las temperaturas promedio mensuales y el valor máximo del UVI. Este gráfico establece diferentes categorías en el espacio cartesiano que permiten explicar el comportamiento de la radiación UV y la temperatura de aire mensual y anual, haciendo posible realizar comparativas para diferentes localizaciones y prever comportamientos futuros. Para ello, se establecen 3 límites en el espacio cartesiano: una línea horizontal en UVI igual a 3 que define el límite de riesgo para la radiación UV, una línea vertical en 20°C de temperatura de aire promedio que es el límite de frío a templado y otra línea vertical en 35°C de temperatura de aire promedio que es el límite de templado a cálido. Los límites de temperatura se han definido teniendo en cuenta el estudio climático realizado por Callejón Ferre et al. [14]. De esta forma, se establecen 6 categorías: frío sin riesgo UV, frío con riesgo UV, templado sin riesgo UV, templado con riesgo UV, cálido sin riesgo UV y cálido con riesgo UV, lo que permite enmarcar cada mes en una categoría y obtener información de temperatura y radiación UV relevante para el interior de un invernadero, especialmente útil para la prevención de riesgos en la salud de los trabajadores. En el *UVIgrama* de este estudio, se observa que los meses fríos no siempre producen UVI más bajos, ya que también influyen diversos factores como la salida del sol (dependiendo de la estación), la presencia de nubes o contaminación del aire, entre otros. Por otro lado, lógicamente, los UVI más altos se registran en verano (junio y julio), mientras que los UVI más bajos se registran en invierno (diciembre y enero). Se observa que el otoño registra UVI más bajos que los obtenidos en la primavera.

Finalmente, se observa que existe un riesgo de daño a las personas debido a la radiación UV, ya que se obtiene un UVI mayor al umbral de riesgo definido en 3. Por tanto, motivadas por los resultados obtenidos, se proponen las siguientes recomendaciones y medidas de prevención para reducir el riesgo de daño por radiación UV en trabajadores de invernaderos:

- De forma análoga al Factor de Protección Solar de los protectores solares (SPF, por sus siglas en inglés, Sun Protection Factor), se desarrolló un factor de protección para la ropa frente a la radiación UV denominado Factor de Protección Ultravioleta (UPF, por Ultraviolet Protection Factor) [101]. Factores de 15–24 ofrecen buena protección, 25–39 muy buena y más de 40 excelente protección. Se deben usar prendas con un factor UPF de 30 o más. Las prendas deben cubrir completamente las piernas y usar mangas largas cuando sea posible, siempre adaptadas al

entorno de trabajo y a la aceptación de los trabajadores, para que sean respetadas y permitan la realización de las tareas con comodidad.

- Se recomiendan sombreros de ala ancha, ya que proporcionan sombra a una gran parte de la cabeza y cuello, protegiéndolos de la radiación UV. Si los sombreros de ala ancha no están disponibles o son incómodos para cualquiera de las tareas a realizar, sería aconsejable usar gafas de sol con alta protección contra la radiación UV y diseño envolvente o con paneles laterales [71].

- Para áreas de difícil protección contra el sol, se recomienda usar protector solar con SPF de 30 o más, similar al UPF. El protector solar debe aplicarse 15 minutos antes de la exposición al sol y renovarse cada dos horas. El protector solar puede ser inútil si la transpiración es alta, y la aplicación debe renovarse con más frecuencia. La cantidad de crema utilizada debe ser alrededor de 2 mg/cm^2, ya que es bajo estas condiciones cuando el protector solar protege de acuerdo con su SPF especificado [102].

- Los tiempos de trabajo deben gestionarse para evitar las horas centrales del día. Las sombras también deben usarse cuando sea posible, especialmente durante los descansos. Aunque la presencia de sombras no es habitual en los invernaderos, se pueden instalar pequeños toldos o carpas con protección frente a la radiación UV.

- Se recomienda que el trabajador examine su piel regularmente. Si se observa una nueva mancha, peca o un cambio en la forma, tamaño o color de cualquiera de sus lunares, debe consultar a un dermatólogo para un examen de piel lo antes posible.

- Como alternativa a las medidas de protección individual anteriores, se recomienda como medida de protección colectiva, realizar el blanqueo de la cubierta del invernadero en períodos de mayor radiación UV. Esto se haría siempre que sea posible y no dañe el cultivo.

- Finalmente, se ha diseñado un sistema de alarma para alertar a los trabajadores sobre el riesgo de daño por radiación UV dentro del invernadero. Este sistema consiste en un dispositivo conectado al ordenador de placa reducida o SBC (por sus siglas en inglés, Single Board Computer) de la estación de medida y que alerta a los trabajadores mediante una señal acústica y luminosa cuando se alcanzan valores cercanos al umbral de riesgo.

Capítulo 4

Conclusiones generales

La presente Tesis Doctoral se presenta por la modalidad de compendio de publicaciones y ha sido desarrollada en el periodo comprendido entre 2017 y 2020. El Plan de Investigación planteado originalmente se ha llevado a cabo con éxito, y ello se ha plasmado en las publicaciones científicas resultantes de esta Tesis Doctoral [9, 10, 11]. A continuación, se detallan las conclusiones obtenidas en el trabajo de investigación desarrollado, divididas por la publicación de la que se derivan.

4.1. Publicación científica 1: On air temperature distribution and ISO 7726-defined heterogeneity inside a typical greenhouse in Almería

Los resultados obtenidos proporcionan medidas experimentales en un invernadero típico en Almería ("raspa y amagado") durante un año completo. Las campaña de medición, así como los instrumentos de medida usados, cumplen con los requerimientos y métodos definidos en la ISO 7726 para estudiar el ambiente térmico. Hasta este momento, no existía un estudio profundo sobre las condiciones térmicas y el riesgo de estrés por calor de los trabajadores de invernaderos que cumpliera con los requerimientos de la norma ISO 7726. Por tanto, los resultados obtenidos de la distribución de temperatura y condiciones de heterogeneidad pueden ser útiles para futuros estudios del estrés térmico de los trabajadores.

La heterogeneidad térmica de la temperatura de aire en el invernadero ha sido confirmada para largos periodos de tiempo, tanto en dirección horizontal como en dirección vertical. El estudio revela que el ambiente es más hete-

rogéneo y durante más tiempo horizontalmente que verticalmente. Además, invierno y verano son más heterogéneos que otoño y primavera, mientras que la heterogeneidad vertical esta concentrada principalmente en estaciones frías. También se ha observado una gran influencia de la nubosidad en los días homogéneos horizontales y verticales, coincidiendo la mayoría de los días nublados con días homogéneos. La heterogeneidad de la temperatura del aire depende principalmente del sol, ya que la heterogeneidad se produce casi exclusivamente en las horas centrales del día y nunca por la noche. Además, se observan diferencias de temperatura de aire a lo largo del invernadero en direcciones Este-Oeste y Norte-Sur de acuerdo al movimiento del sol.

La cubierta plástica de los invernaderos permite la incidencia de la radiación difusa hacia su interior. Esto es un factor a tener en cuenta a la hora de evaluar las condiciones térmicas de los trabajadores, ya que se producen diferencias de hasta 12°C entre temperatura de globo y temperatura de aire.

Finalmente, en base a los resultados obtenidos, se han presentado algunas recomendaciones para evaluar el ambiente térmico en el interior de los invernaderos.

4.2. Publicación científica 2: Uncertainty-Aware Calibration of a Hot-Wire Anemometer With Gaussian Process Regression

La velocidad del viento es un parámetro difícil de medir con precisión y con dispositivos de bajo coste. En este estudio, se propone la calibración de un anemómetro de hilo caliente de bajo coste mediante técnicas de aprendizaje automático (ML), intentando resolver su principal inconveniente, que es la pérdida de precisión cuando varía la temperatura de aire. Tras comparar el desempeño de diferentes modelos de regresión, el Proceso de Regresión Gaussiana (GPR) es el modelo que mejor se ajusta a los datos y ofrece estimaciones más precisas. Por lo tanto, el problema se ha abordado utilizando el modelo GPR para estimar una distribución a posteriori sobre la velocidad del viento, dada la respuesta de un anemómetro de hilo caliente y mediciones de temperatura de aire, al mismo tiempo que se utiliza un anemómetro ultrasónico para entrenar el modelo y como valor de *ground truth* para evaluar rigurosamente el error cometido en la predicción. Según los resultados, es posible emplear un anemómetro de hilo caliente de bajo coste utilizando el proceso de calibración propuesto en diferentes aplicaciones, con una precisión razonable y en un rango típico de temperatura.

4.3. Publicación científica 3: Ultraviolet Index (UVI) inside an Almería-Type Greenhouse (Southeastern Spain)

Este trabajo ha analizado el riesgo de exposición a la radiación UV de los trabajadores de invernadero durante un año completo, en un invernadero "raspa y amagado" ubicado en Almería. Aunque se puede pensar que no hay riesgo debido a estar bajo la cubierta plástica del invernadero, se muestra que el límite establecido por la Organización Mundial de la Salud et al. [65] es excedido, existiendo riesgo de daño por radiación UV. Esto ha sido evaluado por medio de una red de sensores de radiación UV ubicados en el interior y exterior del invernadero.

Los UVI superan el límite de riesgo hasta en cinco meses en el invernadero estudiado, estando los períodos de riesgo de UVI distribuidos en primavera y verano y concentrados entre las 10 a 14 horas, obteniendo los valores máximos de UVI muy cerca de las 12:00 am. En el exterior, lógicamente, el riesgo es aún mayor, el límite de riesgo se supera prácticamente todo el año, excepto en los meses de invierno. Los trabajadores de invernaderos también realizan ciertas tareas en el exterior, por lo que es necesario tomar aún más precauciones.

En el interior del invernadero se ha demostrado que existen diferencias de UVI debido a diversos factores como la heterogeneidad del blanqueo, el desgaste de la cubierta plástica y la acumulación de suciedad en dicha cubierta. Estas diferencias de UVI son mayores en períodos donde dicho UVI es mayor, como verano y primavera. Además, se observa que los valores más altos de UVI generalmente se encuentran en la esquina suroeste del invernadero.

Por otro lado, se ha creado un diagrama llamado "UVIgrama"que ofrece información climatológica y de radiación UV sobre una ubicación para cada mes y global para todo el año. Relaciona las temperaturas medias mensuales y el valor máximo de UVI.

Finalmente, se ofrecen algunas recomendaciones y medidas de prevención para reducir el riesgo de daño por radiación UV en trabajadores de invernaderos. Una de ellas es especialmente interesante y su efectividad se ha observado en este estudio. Se trata de blanquear la cubierta plástica del invernadero, se recomienda siempre que sea posible y no tenga efectos negativos en el cultivo. Además, se ha diseñado un sistema de alarma para alertar a los trabajadores mediante una señal acústica y luminosa cuando se alcanzan valores UVI cercanos al límite de riesgo.

Abreviaturas

$AEMet$	—	Agencia Estatal de Meteorología.
AH	—	Humedad Absoluta de aire (Absolute air Humidity).
ANN	—	Redes Neuronales Artificiales (Artificial Neural Networks).
BIC	—	Criterio de Información Bayesiano (Bayesian Information Criterion).
CCA	—	Anemómetro de Corriente Constante (Constant-Current Anemometer).
CET	—	Hora de Europa Central (Central European Time).
CFD	—	Dinámica de Fluidos Computacional (Computational Fluids Dynamics).
CMM	—	Melanoma Maligno Cutáneo (Cutaneous malignant melanoma).
CTA	—	Anemómetro de Temperatura Constante (Constant-Temperature Anemometer).
CVA	—	Anemómetro de Voltaje Constante (Constant-Voltage Anemometer).
$CPD{-}UAL$	—	Centro de Proceso de Datos de la Universidad de Almería (Data Processing Centre of the University of Almería).
BIC	—	Criterio de Información Bayesiano (Bayesian Information Criterion).
GP	—	Proceso Gaussiano (Gaussian Process).
GPR	—	Regresión de Procesos Gaussianos (Gaussian Process Regression).
$HTTP$	—	Protocolo de Transferencia de Hipertexto (Hypertext Transfer Protocol).
MAE	—	Error Medio Absoluto (Mean Absolute Error).
ML	—	Aprendizaje Automático (Machine Learning).
MRV	—	Campo aleatorio de Markov (Markov Random Fields).
NAT	—	Traducción de Direcciones de Red (Network Address Translation).
$NMSC$	—	Cáncer de Piel No Melanoma (Non-melanoma Skin Cancer).
OSH	—	Seguridad y Salud Ocupacional (Occupational Safety and Health).

PMS	—	Pantone Matching System.
RH	—	Humedad Relativa de aire (Relative air Humidity).
$RMSE$	—	Raíz del Error Cuadrático Medio (Root Mean Square Error).
SBC	—	Ordenador de Placa Reducida (Single Board Computer).
$SMLT$	—	Statistics and Machine Learning Toolbox (de Matlab).
SPF	—	Factor de Protección Solar (Sun Protection Factor).
SSH	—	Secure SHell.
SVM	—	Máquinas de Soporte Vectorial (Support Vector Machines).
ta	—	Temperatura de aire (Air temperature).
tg	—	Temperatura de globo (Globe temperature).
t_{nw}	—	Temperatura natural de bulbo húmedo (Natural wet-bulb temperature).
$\overline{tr}$	—	Temperatura radiante media (Mean radiant temperature).
to	—	Operative temperature (Operative temperature).
UPF	—	Factor de Protección Ultravioleta (Ultraviolet Protection Factor).
UPS	—	Sistemas de Alimentación Ininterrumpida (Uninterruptible Power Supply).
UTC	—	Tiempo Universal Coordinado (Coordinated Universal Time).
UV	—	Ultravioleta.
UVI	—	Índice Ultravioleta.
va	—	Velocidad de aire.
WHO/OMS	—	Organización Mundial de la Salud (World Health Organization).
WSN	—	Redes Inalámbricas de sensores (Wireless Sensor Networks).

Bibliografía

Bibliografía

[1] D. W. Lotter, "Organic Agriculture," *Journal of Sustainable Agriculture*, vol. 21, no. 4, pp. 59–128, 2003. doi::10.1300/J064v21n04_06.

[2] J. Hernández, S. Bonachela, M. R. Granados, J. C. López, J. J. Magán, and J. I. Montero, "Microclimate and agronomical effects of internal impermeable screens in an unheated Mediterranean greenhouse," *Biosystems Engineering*, vol. 163, pp. 66–77, 2017. doi:10.1016/j.biosystemseng.2017.08.012.

[3] A. Cabrera, D. Uclés, and T. Agüera, *Informes y Monografías / Análisis de la campaña hortofrutícola de Almería 2015/2016*. Almería, España. Fundación Cajamar, 2016. http://www.publicacionescajamar.es/pdf/series-tematicas/informes-coyuntura-analisis-de-campana/analisis-de-la-campana-hortofruticola-17.pdf (Disponible el 26/02/2018).

[4] UNE-EN-13031-1, *Invernaderos, proyecto y construcción. Parte 1: invernaderos para producción comercial*. AENOR. Madrid, España, 2002.

[5] N. Castilla and N. C. Prados, *Invernaderos de plástico: tecnología y manejo*. Mundi-Prensa Libros, 2007.

[6] J. Pérez-Alonso, A. J. Callejón-Ferre, A. Carreño-Ortega, and J. Sánchez-Hermosilla, "Approach to the evaluation of the thermal work environment in the greenhouse-construction industry of SE Spain," *Building and Environment*, vol. 46, no. 8, pp. 1725–1734, 2011. doi:10.1016/j.buildenv.2011.02.014.

[7] A. J. Callejón-Ferre, J. Pérez-Alonso, J. Sánchez-Hermosilla, and A. Carreño-Ortega, "Ergonomics and psycho-sociological quality indexes in greenhouses, Almería (Spain)," *Spanish Journal of Agricultural Research*, vol. 7, no. 1, pp. 50–58, 2009. doi:10.5424/sjar/2009071-397.

[8] A. J. Callejón-Ferre, J. Pérez-Alonso, A. Carreño-Ortega, and B. Velázquez-Martí, "Indices of ergonomic-psycholsociological workplace quality in the greenhouses of Almería (Spain): Crops of cucumbers, peppers, aubergines and melons," *Safety Science*, vol. 49, no. 5, pp. 746–750, 2011. doi:. doi:10.1016/j.ssci.2010.12.009.

[9] R. A. García-Ruiz, J. López-Martínez, J. L. Blanco-Claraco, J. Pérez-Alonso, and n. J. Callejón-Ferre, "On air temperature distribution and ISO 7726-defined heterogeneity inside a typical greenhouse in Almería," *Computers and electronics in agriculture*, vol. 151, pp. 264–275, 2018. doi:10.1016/j.compag.2018.06.001.

[10] R. A. García-Ruiz, J. L. Blanco-Claraco, J. López-Martínez, and n. J. Callejón-Ferre, "Uncertainty-aware Calibration of a Hot-Wire Anemometer with Gaussian Process Regression," *IEEE Sensors Journal*, vol. 151, no. 17, pp. 7515–7524, 2019. doi:10.1109/JSEN.2019.2915093.

[11] R. A. García-Ruiz, J. López-Martínez, J. L. Blanco-Claraco, J. Pérez-Alonso, and Á. J. Callejón-Ferre, "Ultraviolet index (UVI) inside an Almería-type greenhouse (Southeastern Spain)," *Agronomy*, vol. 10, no. 1, p. 145, 2020. doi:10.3390/agronomy10010145.

[12] G. Vox, P. Losito, F. Valente, R. Consoletti, G. Scarascia-Mugnozza, E. Schettini, C. Marzocca, and F. Corsi, "A wireless telecommunications network for real-time monitoring of greenhouse microclimate," *Journal of Agricultural Engineering*, vol. 45, no. 2, pp. 70–79, 2014. doi:10.4081/jae.2014.237.

[13] Y. Zhao, M. Teitel, and M. Barak, "SE—Structures and Environment: Vertical temperature and humidity gradients in a naturally ventilated greenhouse," *Journal of Agricultural Engineering Research*, vol. 78, no. 4, pp. 431–436, 2001. doi:10.1006/jaer.2000.0649.

[14] A. J. Callejón-Ferre, F. Manzano-Agugliaro, M. Díaz-Pérez, and J. Carreño-Sánchez, "Improving the climate safety of workers in Almería-type greenhouses in Spain by predicting the periods when they are most likely to suffer thermal stress," *Applied ergonomics*, vol. 42, no. 2, pp. 391–396, 2011. doi:10.1016/j.apergo.2010.08.014.

[15] R. Riemer and A. Bechar, "Investigation of productivity enhancement and biomechanical risks in greenhouse crops," *Biosystems Engineering*, vol. 147, pp. 39–50, 2016. doi:10.1016/j.biosystemseng.2016.03.009.

[16] M. Cecchini, A. Colantoni, R. Massantini, and D. Monarca, "Estimation of the risks of thermal stress due to the microclimate for manual fruit and vegetable harvesters in central Italy," *Journal of agricultural safety and health*, vol. 16, no. 3, pp. 141–159, 2010. doi:10.13031/2013.32040.

[17] A. Marucci, B. Pagniello, D. Monarca, M. Cecchini, A. Colantoni, and P. Biondi, "Heat stress suffered by workers employed in vegetable grafting in greenhouses," *J. Food, Agric. Environ*, vol. 10, pp. 1117–21, 2012. http://refhub.elsevier.com/S0168-1699(17)30818-9/h0205 (Disponible el 26/02/2018).

[18] M. Diano, M. Valentini, P. Samele, and I. Di Gesu, "Exposure to hot environments of horticultural greenhouses workers of the center of Calabria: evaluative comparison methods," *Italian Journal of Occupational and Environmental Hygiene*, vol. 7, no. 2, pp. 56–114, 2016. http://refhub.elsevier.com/S0168-1699(17)30818-9/h0075 (Disponible el 26/02/2018).

[19] L. Okushima, S. Sase, I.-B. Lee, and B. Bailey, "Thermal environment and stress of workers in naturally ventilated greenhouses under mild climate," *Acta Horticulturae*, vol. 559, pp. 793–798, 2001. doi:10.17660/ActaHortic.2001.559.118.

[20] K. E. Chad and J. M. M. Brown, "Climatic stress in the workplace: its effect on thermoregulatory responses and muscle fatigue in female workers," *Applied ergonomics*, vol. 26, no. 1, pp. 29–34, 1995. doi:10.1016/0003-6870(95)95749-P.

[21] J. Zhao, N. Zhu, and S. Lu, "Productivity model in hot and humid environment based on heat tolerance time analysis," *Building and environment*, vol. 44, no. 11, pp. 2202–2207, 2009. doi:10.1016/j.buildenv.2009.01.003.

[22] K. Parsons, "Occupational health impacts of climate change: Current and future ISO Standards for the assessment of heat stress," *Industrial health*, vol. 51, no. 1, pp. 86–100, 2013. doi:10.2486/indhealth.2012-0165.

[23] ISO 8996:2004, *Ergonomics of the thermal environment: Determination of metabolic rate.* International Organization for Standardization. Geneva, Switzerland, 2004.

[24] ISO 9920:2007, *Ergonomics of the thermal environment: Estimation of thermal insulation and water vapour resistance of a clothing ensemble.* International Organization for Standardization. Geneva, Switzerland, 2007.

[25] ISO 7726:1998, *Ergonomics of the thermal environment e instruments for measuring physical quantities.* International Organization for Standardization. Geneva, Switzerland, 1998.

[26] A. López, D. L. Valera, F. D. Molina-Aiz, and A. Peña, "Effectiveness of horizontal air flow fans supporting natural ventilation in a mediterranean multi-span greenhouse," *Scientia Agricola*, vol. 70, no. 4, pp. 219–228, 2013. doi:10.1590/S0103-90162013000400001.

[27] C. Kittas, T. Bartzanas, and A. Jaffrin, "Temperature gradients in a partially shaded large greenhouse equipped with evaporative cooling pads," *Biosystems Engineering*, vol. 85, no. 1, pp. 87–94, 2003. doi:10.1016/S1537-5110(03)00018-7.

[28] P. Soni, V. M. Salokhe, and H. J. Tantau, "Effect of screen mesh size on vertical temperature distribution in naturally ventilated tropical greenhouses," *Biosystems Engineering*, vol. 92, no. 4, pp. 469–482, 2005. doi:10.1016/j.biosystemseng.2005.08.005.

[29] T. Q. Zorzeto and P. A. M. Leal, "Wireless sensor network to map the meteorological variability in a greenhouse with evaporative cooling," *Acta Horticulturae*, vol. 1154, pp. 213–220, 2017. doi:10.17660/ActaHortic.2017.1154.28.

[30] F. D. Molina-Aiz, D. L. Valera, and A. J. Álvarez, "Measurement and simulation of climate inside Almería-type greenhouses using computational fluid dynamics," *Agricultural and Forest Meteorology*, vol. 125, no. 1-2, pp. 33–51, 2004. doi:10.1016/j.agrformet.2004.03.009.

[31] G. Tong, D. Christopher, and B. Li, "Numerical modelling of temperature variations in a chinese solar greenhouse," *Computers and electronics in agriculture*, vol. 68, no. 1, pp. 129–139, 2009. doi:10.1016/j.compag.2009.05.004.

[32] J. López-Martínez, J. L. Blanco-Claraco, J. Pérez-Alonso, and A. J. Callejón-Ferre, "Distributed network for measuring climatic parameters in heterogeneous environments: Application in a greenhouse," *Computers and Electronics in Agriculture*, vol. 145, pp. 105–121, 2018. doi:10.1016/j.compag.2017.12.028.

[33] K. P. Ferentinos, N. Katsoulas, A. Tzounis, T. Bartzanas, and C. Kittas, "Wireless sensor networks for greenhouse climate and plant condition assessment," *Biosystems Engineering*, vol. 153, pp. 70–81, 2017. doi:10.1016/j.biosystemseng.2016.11.005.

[34] A. Carmona-Benjumea, "Datos antropométricos de la población laboral española," *Prevención, trabajo y salud: Revista del Instituto Nacional de Seguridad e Higiene en el Trabajo*, vol. 14, pp. 22–35, 2001. http://www.insht.es/InshtWeb/Contenidos/Documentacion/TextosOnline/Rev_INSHT/2001/14/artFondoTextCompl.pdf (Disponible el 26/02/2018).

[35] H. H. Bruun, *Hot-wire anemometry: Principles and signal analysis.* Oxford University Press, 1995.

[36] P. Bradshaw, *An introduction to turbulence and its measurement.* Pergamon Press, Oxford, 1971.

[37] J. Hinze, *Turbulence*, vol. 218. McGraw-Hill, New York, 1975.

[38] N. P. Cheremisinoff and P. N. Cheremisinoff, *Flow measurement for engineers and scientists.*, vol. 2. Marcel Dekker, New York, 1988.

[39] A. Al-Salaymeh, "Flow velocity and volume flow rate sensors with a wide band width," *Ph.D. Dissertation, Technischen Fakultät der Universität Erlangen-Nürnberg*, Germany, 2001.

[40] A. Perry, *Hot-wire Anemometry.* New York, NY, USA: Oxford University Press, 1982.

[41] C. Lomas, *Fundamentals of hot wire anemometry.* Cambridge, U.K.: Cambridge University Press, 1986.

[42] M. Hultmark and A. J. Smits, "Temperature corrections for constant temperature and constant current hot-wire anemometers," *Measurement Science and Technology*, vol. 21, no. 10, 2010.

[43] P. Bearman, "Corrections for the effect of ambient temperature drift on hot-wire measurements in incompressible flow," *DISA Information*, no. 11, pp. 25–30, 1971.

[44] N. Khamshah, A. N. Abdalla, S. P. Koh, and H. F. Rashag, "Issues and temperature compensation techniques for hot wire thermal flow sensor: A review," *International Journal of Physical Sciences*, vol. 6, no. 14, pp. 3270–3278, 2011.

[45] R. K. Pandit and D. Infield, "Comparative analysis of Gaussian Process (GP) power curve models based on different stationary covariance functions for the purpose of improving model accuracy," *Renewable Energy*, vol. 140, pp. 190–202, 2019. doi:10.1016/j.renene.2019.03.047.

[46] R. K. Pandit, D. Infield, and J. Carroll, "Incorporating air density into a Gaussian process wind turbine power curve model for improving fitting accuracy," *Wind Energy*, vol. 22, no. 2, pp. 302–315, 2019. doi:10.1002/we.2285.

[47] C. E. Rasmussen and C. K. Williams, *Gaussian Processes for Machine Learning*, vol. 1. Cambridge, MA, USA: MIT Press, 2006.

[48] F. di Sciascio and A. N. Amicarelli, "Biomass estimation in batch biotechnological processes by Bayesian Gaussian process regression," *Computers & Chemical Engineering*, vol. 32, no. 12, pp. 3264–3273, 2008. doi:10.1016/j.compchemeng.2008.05.015.

[49] L. JingDong, H. Li, and Z. HongBo, "Forming defects prediction for sheet metal forming using Gaussian process regression," in *29th Chinese Control And Decision Conference (CCDC)*, pp. 472–476, IEEE, 2017. doi:10.1109/CCDC.2017.7978140.

[50] R. K. Pandit and D. Infield, "Using Gaussian process theory for wind turbine power curve analysis with emphasis on the confidence intervals," in *6th International Conference on Clean Electrical Power (ICCEP)*, pp. 744–749, IEEE, 2017. doi:10.1109/ICCEP.2017.8004774.

[51] W.-Z. Lu and W.-J. Wang, "Potential assessment of the "support vector machine" method in forecasting ambient air pollutant trends," *Chemosphere*, vol. 59, no. 5, pp. 693–701. doi:10.1016/j.chemosphere.2004.10.032.

[52] Y. Chuan and L. Chen, "The application of support vector machine in the hysteresis modeling of silicon pressure sensor," *IEEE Sensors Journal*, vol. 11, no. 9, pp. 2022–2026, 2011. doi:10.1109/JSEN.2011.2109706.

[53] J. Alonso, A. R. Castañon, and A. Bahamonde, "Support Vector Regression to predict carcass weight in beef cattle in advance of the slaughter," *Computers and electronics in agriculture*, vol. 91, pp. 116–120, 2013. doi:10.1016/j.compag.2012.08.009.

[54] R. Pandit and D. Infield, "Comparative analysis of binning and support vector regression for wind turbine rotor speed based power curve use in condition monitoring," in *53rd International Universities Power Engineering Conference (UPEC)*, pp. 1–6, IEEE, 2018. doi:10.1109/UPEC.2018.8542057.

[55] L. Hadjiiski, P. Geladi, and P. Hopke, "A comparison of modeling nonlinear systems with artificial neural networks and partial least squares," *Chemometrics and intelligent laboratory systems*, vol. 49, no. 1, pp. 91–103, 1999. doi:10.1016/S0169-7439(99)00030-1.

[56] F. Gebben, S. Bader, and B. Oelmann, "Configuring artificial neural networks for the prediction of available energy in solar-powered sensor nodes," in *2015 IEEE SENSORS*, pp. 1–4, IEEE, 2015. doi:10.1109/ICSENS.2015.7370253.

[57] A. Al-Salaymeh *et al.*, "Optimization of hot-wire thermal flow sensor based on a neural net model," *Applied thermal engineering*, vol. 26, no. 8, pp. 948–955, 2006. doi:10.1016/j.applthermaleng.2005.08.004.

[58] J. Hu and J. Wang, "Short-term wind speed prediction using empirical wavelet transform and Gaussian process regression," *Energy*, vol. 93, pp. 1456–1466, 2015. doi:10.1016/j.energy.2015.10.041.

[59] D. L. Valera, A. J. Álvarez, and F. D. Molina, "Aerodynamic analysis of several insect-proof screens used in greenhouses," *Spanish Journal of Agricultural Research*, vol. 4, no. 4, pp. 273–279, 2006. doi:10.5424/sjar/2006044-204.

[60] A. Lopez-Martinez, D. L. Valera-Martínez, F. Molina-Aiz, A. Peña-Fernandez, and P. Marín-Membrive, "Microclimate evaluation of a new design of insect-proof screens in a Mediterranean greenhouse," *Spanish Journal of Agricultural Research*, vol. 12, no. 2, pp. 338–352, 2014.

[61] G. Schwarz, "Estimating the dimension of a model," *The Annals of Statistics*, vol. 6, no. 2, pp. 461–464, 1978.

[62] J. R. Lloyd, D. K. Duvenaud, R. B. Grosse, J. B. Tenenbaum, and Z. Ghahramani, "Automatic Construction and Natural-Language Description of Nonparametric Regression Models," in *Twenty-eighth AAAI conference on artificial intelligence*, pp. 1242–1250, 2014.

[63] S. K. Amar, S. Goyal, A. K. Srivastav, D. Chopra, and R. S. Ray, "Combined effect of benzophenone-2 and ultraviolet radiation promote photogenotoxicity and photocytotoxicity in human keratinocytes," *Regulatory Toxicology and Pharmacology*, vol. 95, pp. 298–306, 2018. doi:10.1016/j.yrtph.2018.04.003.

[64] J. Kerr, C. McElroy, D. Tarasick, and D. Wardle, "The Canadian ozone watch and UV-B advisory programs," *Ozone in the Troposphere and Stratosphere, NASA Conf. Publ.*, vol. 3266, pp. 794–797, 1994. https://ntrs.nasa.gov/archive/nasa/casi.ntrs.nasa.gov/19950004680.pdf (Disponible el 21/06/2019).

[65] World Health Organization(WHO), World Meteorological Organization (WMO), United Nations Environment Programme (UNEP), and International Commission on Non-Ionizing Radiation Protection (ICNIRP), "Global solar UV index: A practical guide," *Geneva, Switzerland*, 2002. http://apps.who.int/iris/bitstream/handle/10665/42459/9241590076.pdf;jsessionid=8DC73AAAF5258232AC8854BA2D2EDF0C?sequence=1 (Disponible el 21/06/2019).

[66] ISO/CIE 17166:2019, *Erythema reference action spectrum and standard erythema dose*. International Organization for Standardization. Geneva, Switzerland, 2019.

[67] M. Lehmann, A. B. Pfahlberg, H. Sandmann, W. Uter, and O. Gefeller, "Public Health Messages Associated with Low UV Index Values Need Reconsideration," *International journal of environmental research and public health*, vol. 16, no. 12, p. 2067, 2019. doi:10.3390/ijerph16122067.

[68] T. B. Fitzpatrick, "The validity and practicality of sun-reactive skin types I through VI," *Archives of Dermatology*, vol. 124, no. 6, pp. 869–871, 1988. doi:10.1001/archderm.1988.01670060015008.

[69] T. B. Fitzpatrick, "Soleil et peau," *Journal de Médecine Esthétique*, vol. 2, pp. 33–34, 1992.

[70] B. L. Diffey, "Ultraviolet radiation and human health," *Clinics in Dermatology*, vol. 16, no. 1, pp. 83–89, 1998. doi:10.1016/S0738-081X(97)00172-7.

[71] P. Vecchia, M. Hietanen, B. E. Stuck, E. van Deventer, and S. Niu, *Protecting workers from ultraviolet radiation*, vol. 14. International Commission on Non-Ionizing

Radiation Protection. Oberschleißheim, Germany, 2007. https://www.icnirp.org/cms/upload/publications/ICNIRPUVWorkers.pdf (Disponible el 21/06/2019).

[72] International Agency for Research on Cancer, "Solar and ultraviolet radiation," *Monographs on the evaluation of carcinogenic risks to humans. Lyon, France*, vol. 55, 1992.

[73] R. W. Young, "The family of sunlight-related eye diseases," *Optometry and Vision Science: Official publication of the American Academy of Optometry*, vol. 71, no. 2, pp. 125–144, 1994. doi:10.1097/00006324-199402000-00013.

[74] A. Jemal, F. Bray, M. M. Center, J. Ferlay, E. Ward, and D. Forman, "Global Cancer Statistics," *CA: A Cancer Journal for Clinicians*, vol. 61, no. 2, pp. 69–90, 2011. doi:10.3322/caac.20107.

[75] L. A. Torre, F. Bray, R. L. Siegel, J. Ferlay, J. Lortet-Tieulent, and A. Jemal, "Global Cancer Statistics, 2012," *CA: A Cancer Journal for Clinicians*, vol. 65, no. 2, pp. 87–108, 2015. doi:10.3322/caac.21262.

[76] M. Radespiel-Tröger, M. Meyer, A. Pfahlberg, B. Lausen, W. Uter, and O. Gefeller, "Outdoor work and skin cancer incidence: a registry-based study in Bavaria," *International Archives of Occupational and Environmental Health*, vol. 82, no. 3, p. 357, 2009. doi:10.1007/s00420-008-0342-0.

[77] B. M. Coldiron, "The UV index: A weather report for skin," *Clinics in Dermatology*, vol. 16, no. 4, pp. 441–446, 1998. doi:10.1016/S0738-081X(98)00017-0.

[78] A. Milon, P.-E. Sottas, J.-L. Bulliard, and D. Vernez, "Effective exposure to solar UV in building workers: influence of local and individual factors," *Journal of Exposure Science and Environmental Epidemiology*, vol. 17, no. 1, p. 58, 2007. doi:10.1038/sj.jes.7500521.

[79] A. A. Silva, "The diffuse component of erythemal ultraviolet radiation," *Photochemical & Photobiological Sciences*, vol. 14, no. 11, pp. 1941–1951, 2015. doi:10.1039/c5pp00131e.

[80] J. Cañada, A. Esteve, M. Marin, M. Utrillas, F. Tena, and J. Martínez-Lozano, "Study of erythemal, UV (A+B) and global solar radiation in Valencia (Spain)," *International Journal of Climatology*, vol. 28, no. 5, pp. 693–702, 2008. doi:10.1002/joc.1569.

[81] A. Rusińska, P. Pludowski, M. Walczak, M. K. Borszewska-Kornacka, A. Bossowski, D. Chlebna-Sokół, J. Czech-Kowalska, A. Dobrzańska, E. Franek, E. Helwich, and Others, "Vitamin D supplementation guidelines for general population and groups at risk of vitamin D deficiency in Poland–recommendations of the Polish Society of Pediatric Endocrinology and Diabetes and the Expert Panel with participation of National Specialist Consultants and Representatives of Scientific Societies–2018 update.," *Frontiers in Endocrinology*, vol. 9, p. 246, 2018. doi:10.3389/fendo.2018.00246.

[82] J. W. Krzyścin, A. Lesiak, J. Narbutt, P. Sobolewski, and J. Guzikowski, "Perspectives of UV nowcasting to monitor personal pro-health outdoor activities," *Journal of Photochemistry and Photobiology B: Biology*, vol. 184, pp. 27–33, 2018. doi:10.1016/j.jphotobiol.2018.05.012.

[83] A. R. Webb and M. F. Holick, "The role of sunlight in the cutaneous production of vitamin D3," *Annual Review of Nutrition*, vol. 8, no. 1, pp. 375–399, 1988. doi:10.1146/annurev.nu.08.070188.002111.

[84] E. Thieden, P. A. Philipsen, J. Heydenreich, and H. C. Wulf, "UV radiation exposure related to age, sex, occupation, and sun behavior based on time-stamped personal dosimeter readings," *Archives of Dermatology*, vol. 140, no. 2, pp. 197–203, 2004. doi:10.1001/archderm.140.2.197.

[85] B. M. Stepanski and J. A. Mayer, "Solar protection behaviors among outdoor workers," *Journal of Occupational and Environmental Medicine*, vol. 40, no. 1, pp. 43–48, 1998. doi:10.1097/00043764-199801000-00009.

[86] N. A. Kasparian, J. K. McLoone, and B. Meiser, "Skin cancer-related prevention and screening behaviors: a review of the literature," *Journal of Behavioral Medicine*, vol. 32, no. 5, pp. 406–428, 2009. doi:10.1007/s10865-009-9219-2.

[87] D. B. Buller, V. Cokkinides, H. I. Hall, A. M. Hartman, M. Saraiya, E. Miller, L. Paddock, and K. Glanz, "Prevalence of sunburn, sun protection, and indoor tanning behaviors among Americans: Review from national surveys and case studies of 3 states," *Journal of the American Academy of Dermatology*, vol. 65, no. 5, pp. S114.e1–S114.e11, 2011. doi:10.1016/j.jaad.2011.05.033.

[88] K. Hault, H. Rönsch, S. Beissert, P. Knuschke, and A. Bauer, "Knowledge of outdoor workers on the effects of natural UV radiation and methods of protection against exposure," *Journal of the European Academy of Dermatology and Venereology*, vol. 30, no. S3, pp. 34–37, 2016. doi:10.1111/jdv.13631.

[89] O. Larkö and B. L. Diffey, "Natural UV-B radiation received by people with outdoor, indoor, and mixed occupations and UV-B treatment of psoriasis," *Clinical and Experimental Dermatology*, vol. 8, no. 3, pp. 279–285, 1983. doi:10.1111/j.1365-2230.1983.tb01780.x.

[90] C. D. J. Holman, I. M. Gibson, M. Stephenson, and B. K. Armstrong, "Ultraviolet irradiation of human body sites in relation to occupation and outdoor activity: Field studies using personal UVR dosimeters," *Clinical and Experimental Dermatology*, vol. 8, no. 3, pp. 269–277, 1983. doi:10.1111/j.1365-2230.1983.tb01779.x.

[91] M. A. Serrano, J. Cañada, and J. C. Moreno, "Erythemal Ultraviolet exposure in two groups of outdoor workers in Valencia, Spain," *Photochemistry and Photobiology*, vol. 85, no. 6, pp. 1468–1473, 2009. doi:10.1111/j.1751-1097.2009.00609.x.

[92] P. Gies and J. Wright, "Measured solar ultraviolet radiation exposures of outdoor workers in Queensland in the building and construction industry," *Photochemistry and Photobiology*, vol. 78, no. 4, pp. 342–348, 2003. doi:10.1562/0031-8655(2003)0780342MSUREO2.0.CO2.

[93] V. Hammond, A. Reeder, and A. Gray, "Patterns of real-time occupational ultraviolet radiation exposure among a sample of outdoor workers in New Zealand," *Public Health*, vol. 123, no. 2, pp. 182–187, 2009. doi:10.1016/j.puhe.2008.12.007.

[94] D. H. Sliney, "UV radiation ocular exposure dosimetry," *Journal of Photochemistry and Photobiology B: Biology*, vol. 31, no. 1-2, pp. 69–77, 1995. doi:10.1016/1011-1344(95)07171-5.

[95] World Meteorological Organization (WMO), "Scientific Assessment of Ozone Depletion: 2014, Global Ozone Research and Monitoring Project—Report," *Geneva, Switzerland*, vol. 55, p. 416, 2014. https://www.wmo.int/pages/prog/arep/gaw/ozone_2014/documents/Full_report_2014_Ozone_Assessment.pdf (Disponible el 21/06/2019).

[96] S. Robaa, "A study of ultraviolet solar radiation at Cairo urban area, Egypt," *Solar Energy*, vol. 77, no. 2, pp. 251–259, 2004. doi:10.1016/j.solener.2004.01.008.

[97] D. Statuto, P. Picuno, A. M. Abdel-Ghany, *et al.*, "Shading methods for crop protection under greenhouse in Mediterranean areas.," in *Proceedings of the 47th International Symposium, Actual Tasks on Agricultural Engineering, 5-7 March 2019, Opatija, Croatia*, pp. 297–306, University of Zagreb, Faculty of Agriculture, 2019.

[98] M. Gómez-Galán, J. Pérez-Alonso, Á.-J. Callejón-Ferre, and J. Sánchez-Hermosilla-López, "Assessment of postural load during melon cultivation in Mediterranean greenhouses," *Sustainability*, vol. 10, no. 8, p. 2729, 2018. doi:10.3390/su10082729.

[99] M. Gómez-Galán, J.-M. González-Parra, J. Pérez-Alonso, I. Golasi, and Á.-J. Callejón-Ferre, "Forced Postures in Courgette Greenhouse Workers," *Agronomy*, vol. 9, no. 5, p. 253, 2019. doi:10.3390/agronomy9050253.

[100] A. Scordo, A. Maltese, G. Ciraolo, and G. La Loggia, "Estimation of the time lag occurring between vegetation indices and aridity indices in a Sicilian semi-arid catchment," *Italian Journal of Remote Sensing*, vol. 41, no. 2, pp. 33–46, 2009.

[101] T. Gambichler, J. Laperre, and K. Hoffmann, "The european standard for sun-protective clothing: En 13758," *Journal of the European Academy of Dermatology and Venereology*, vol. 20, no. 2, pp. 125–130, 2006.

[102] CIE, *Sunscreen Testing (UVB)*. Report cie 90; CIE: Vienna, Austria, 1991; ISBN 3900734275. doi:10.1111/j.1468-3083.2006.01401.x.